UNIVERSITÀ
DEGLI STUDI
DI PADOVA

Sede Amministrativa: Università degli Studi di Padova

Centro Interdipartimentale Studi e Attività Spaziali (CISAS) “G.Colombo”

SCUOLA DI DOTTORATO DI RICERCA IN : SCIENZE TECNOLOGIE E MISURE SPAZIALI
INDIRIZZO: ASTRONAUTICA E SCIENZE DA SATELLITE
CICLO: XXV

NUMERICAL AND EXPERIMENTAL METHODS FOR THE CALIBRATION OF ELECTRONIC INSTRUMENTATION ON BEPICOLOMBO MISSION

Direttore della Scuola: Ch.mo Prof. Giampiero Naletto
Coordinatore d’indirizzo: Ch.mo Prof. Giampiero Naletto
Supervisore: Ch.mo Prof. Enrico Lorenzini
Co-supervisori: Dott. Ing. Alessio Aboudan
Dott.sa Vania Da Deppo

Dottorando: Michele Cesaro

Abstract

The SIMBIO-SYS instrument suite of the BepiColombo ESA mission to Mercury is equipped with the Stereo Imaging Channel (STC) stereo telescope, based on an innovative and compact design, in which two independent optical channels oriented at ±20° with respect to Nadir collect light on a common detector. The stereo acquisition mode is based on the push frame concept, which has never been adopted on space missions before.

To demonstrate and characterize the capability of the instrument to reconstruct a tridimensional surface with the desired accuracy by means of the stereo push-frame concept, an innovative experimental setup has been realized. The problem of working at an essentially infinite object distance over hundreds km baselines has been overcome by means of a simple collimator lens and two precision rotation stages, scaling down the stereo reconstruction problem in terms of baseline and accuracy requirements. The stereo validation has been performed by comparing the shape of a target object accurately measured by laser scanning, with the shape reconstructed by applying classical stereo algorithms to the acquired image pairs.

The reconstruction of depth information from stereo images of an observed surface requires the characterization of the imaging system in terms of camera calibration process. The particular application required a preliminary analysis of the most suited camera model by verifying the calibration procedure performance. To this end, an innovative method has been developed for the simulation of the calibration data and for the evaluation of calibration algorithms.

A preliminary test of the stereo validation procedure has been performed with an evaluation model of STC. The obtained results show the goodness of this innovative technique, that will be applied also for validating the stereo capabilities of STC flight model.

Sommario

La ricostruzione tridimensionale della superficie dei pianeti riveste un ruolo sempre più importante nell'ambito dell'esplorazione spaziale, dal momento che facilita l'analisi delle caratteristiche geologiche del terreno come la conformazione tettonica, la distribuzione dei crateri da impatto, o eventuali costruzioni vulcaniche, e costituisce una fonte di dati importanti sia per la missione stessa, dando indicazioni utili per la strategia di osservazione, che per la pianificazione missioni future, ad esempio per la ricerca di siti di interesse adatti a missioni di landing.

La missione BepiColombo, il cui lancio è previsto per l'anno 2015, è frutto di una collaborazione tra Agenzia Spaziale Europea (ESA) e Agenzia Spaziale Giapponese (JAXA), e ha per scopo l'esplorazione del pianeta Mercurio, difficilmente analizzabile dalla terra, il cui studio tramite una missione di orbiting potrebbe dare informazioni importanti circa l'origine del sistema solare. La sonda, che secondo le stime raggiungerà il pianeta nel gennaio del 2022, porterà in orbita due satelliti:

- MPO (Mercury Planet Orbiter): progettato e realizzato da ESA è costituito da strumentazione per remote sensing e radioscienza.
- MMO (Mercury Magnetospheric Orbiter): sviluppato da JAXA, il cui compito sarà principalmente lo studio della magnetosfera.

MPO ha come obiettivo lo studio del pianeta dal punto di vista geologico, della conformazione e della composizione: uno degli strumenti che consentirà queste analisi è SIMBIO-SYS (Spectrometer and Imagers for MPO Bepi Colombo – Integrated Observatory SYStem), dedicato all'investigazione spettroscopica, all'imaging ad alta risoluzione e alla ricostruzione tridimensionale della superficie di Mercurio.

SIMBIO-SYS, il cui sviluppo è coordinato dall'Agenzia Spaziale Italiana (ASI), è costituito da un gruppo di tre strumenti che condividono una struttura comune e parte dell'elettronica di controllo, al fine di garantire un'ottimizzazione delle risorse disponibili.

In particolare STC (Stereo Imaging Channel) è un telescopio costituito da due teste ottiche che convogliano i raggi catturati su di un elemento sensibile comune. Le teste ottiche sono disposte entrambe con asse inclinato a 20° rispetto alla direzione del Nadir, una orientata nel verso del moto della sonda e l'altra nella direzione opposta. Il telescopio fornirà una mappatura della superficie del pianeta con una risoluzione spaziale compresa tra 110 e 50 m per pixel. Coppie o insiemi di più di

due immagini di una stessa area, catturate dalle due teste ottiche con inclinazioni diverse, serviranno a ricavare informazioni circa la distanza dei punti osservati e una conseguente ricostruzione tridimensionale del terreno.

La misurazione indiretta della posizione di un punto in un sistema di riferimento a tre dimensioni richiede, oltre alla conoscenza della posizione dell'immagine del punto osservato sull'elemento sensibile, la conoscenza dei parametri intrinseci di ogni camera (lunghezza focale, posizione del centro ottico, rapporti tra dimensioni e numero di pixel, distorsioni ottiche) e dei parametri estrinseci (posizione della camera rispetto ad un sistema di riferimento scelto).

All'incertezza sulla conoscenza dei parametri sopra elencati è dunque legata l'incertezza nella ricostruzione della posizione dei punti osservati: per questo motivo assume particolare importanza la precisione con cui viene effettuata la procedura di calibrazione, attraverso cui viene data una stima di questi valori.

Scopo del lavoro di ricerca è stato sviluppare una procedura per la validazione stereo di STC in laboratorio, necessaria al fine di verificare il rispetto delle specifiche di STC in termini di accuratezza nella ricostruzione di superfici 3D.

L'idea di base per l'attività di validazione stereo in laboratorio di STC è, attraverso l'impiego di elementi ottici e meccanici aggiuntivi, di ridurre la distanza di osservazione dello strumento da grandezze dell'ordine di centinaia di chilometri a circa un metro, rendendo possibile l'acquisizione di immagini di una superficie di prova a distanza ravvicinata e di riprodurre la geometria di osservazione agendo sull'orientamento dell'oggetto osservato e dei due canali ottici. L'accuratezza nella ricostruzione stereo della superficie di prova da parte di STC viene valutata confrontando i risultati ottenuti con una scansione 3D della superficie stessa, effettuata con un laser scanner con precisione più elevata rispetto a quanto richiesto dalle specifiche.

E' stato dunque progettato e realizzato un setup sperimentale per la validazione stereo, le cui prestazioni sono state valutate con un sistema ottico, realizzato con componenti commerciali, che riproduce le caratteristiche geometriche di STC. Utilizzando un software di Ray-Tracing ottico, è stato sviluppato un modello che ha portato alla selezione dei componenti necessari per la realizzazione del sistema con le caratteristiche desiderate in termini di performance ottiche.

Dopo una verifica con analisi interferometrica del rispetto delle prestazioni ottiche delle componenti scelte rispetto a quanto previsto teoricamente, i vari elementi sono stati assemblati e allineati utilizzando strumenti ad alta precisione. Terminata l'integrazione dell'hardware e dei software dedicati al controllo del setup e all'acquisizione delle immagini, sono stati effettuati alcuni test preliminari di calibrazione.

Si è inoltre sviluppato un modello numerico, il cui lo scopo è valutare quale procedura di calibrazione sia più adatta a descrivere la geometria del sistema ottico impiegato sia nel caso dell'apparato costruito con componenti commerciali che nel caso di STC FM.

Il modello numerico ottenuto per la simulazione della procedura di calibrazione è stato validato mettendo a confronto i risultati ottenuti sui dati prodotti in laboratorio sul setup sviluppato e i risultati ottenuti con le simulazioni, e ha fornito indicazioni utili per la simulazione del processo di calibrazione con lo strumento di volo.

I risultati preliminari dell'attività di validazione stereo, ottenuti analizzando le immagini prodotte dal modello funzionale di STC e confrontando le DTM ottenute con le misure di riferimento, rispettano le specifiche in termini di accuratezza della ricostruzione tridimensionale del target osservato, dimostrando che l'apparato e la procedura sviluppati possono essere impiegati per la validazione delle prestazioni stereo di STC.

Contents

Introduction

The tridimensional reconstruction of planetary surfaces is assuming an increasing interest in space exploration; it facilitates the analysis of geologic features such as tectonic conformations, the distribution of impact craters or the conformation of volcanic edifices, providing important data both for the mission itself and for the planning of future missions . In fact 3D reconstruction provides important indication for the selection of interesting areas to be deeply investigated, and helps, as an example, in the selection of suitable areas for landing missions.

The BepiColombo mission is the result of a collaboration between the European Space Agency (ESA) and the Japanese Aerospace Exploration Agency (JAXA). The BepiColombo spacecraft will be launched in 2015, with the aim of exploring the innermost planet of the solar system: Mercury. It's very difficult to observe Mercury with ground-based instruments due to its proximity to the Sun; orbiting missions could provide important information about this poorly explored planet and thus they could help in the understanding of the first phases of solar system formation. The spacecraft will reach the planet in 2022 and it will carry (in polar orbit) two distinct modules:

- The Mercury Planetary Orbiter (MPO): designed and developed by ESA, supporting remote sensing and radioscience instrumentation.
- The Mercury Magnetospheric Orbiter (MMO): developed by JAXA, which will investigate the planet magnetosphere.

The MPO module is a Nadir pointing satellite whose primary objective is the study of Mercury geology, conformation and composition: one of the instruments which will particularly contribute to this analysis is the SIMBIO-SYS (Spectrometer and Imagers for MPO Bepi Colombo – Integrated Observatory SYStem), providing spectrometry, high resolution imaging and 3D reconstruction of the planet surface.

The SIMBIO-SYS Stereo Imaging Channel (STC) in particular, is a stereo telescope, composed by two optical units routing the captured light on a common sensor. The two optical heads are oriented at ± 20° with respect to Nadir, along the spacecraft direction. This particular and innovative geometry will provide a mapping of the planet surface with a spatial resolution ranging from 110 and 50 meters per pixel. Couples (or sets with more than two) of images of a same area, captured with different inclination by the two optical heads will be processed to get surface elevation information, with an accuracy of 80 m.

The main objective of this work has been the development of an innovative method for the pre-flight indoor verification of the stereo capabilities of the STC in terms of target altitude reconstruction accuracy.

The basic concepts of the stereo validation activity are two. The first one is to reduce the observing distance from hundreds of kilometers to about one meter, thus allowing the acquisition of a reference surface at a distance which is compatible with the laboratory available spaces; this is accomplished, thanks to the addition of optical components. The second is to reproduce the Mercury surface observing geometry by rotating both the instrument and the observed target, this is accomplished mounting the target and the camera on two high accuracy motorized rotation stages.

The reduction of the observing distance involves a scaling of the instrument requirements in terms of horizontal resolution and vertical accuracy, which is proportional to the ratio between the on-flight and the indoor target distance. The accuracy of the stereo reconstruction of a reference target achieved with this method is evaluated comparing the obtained digital map with the map derived by a measurement of the target done with a laser scanner, having an accuracy at least 5 times higher than the one required for the stereo reconstruction.

An experimental setup for the stereo validation has been designed and developed. In order to define and test a stereo validation procedure before the integration of the stereo validation set-up with the STC FM, an optical system (functional model) which reproduces the main optical features of the STC has also been designed. Both the functional model of STC and the stereo validation set-up have been realized mainly with commercial components.

The indirect measure of the position of a point in a tridimensional reference frame requires: in addition to the knowledge of the position of the image point of the object on the image planes, the knowledge of a set of intrinsic parameters, which provide an analytical model of the optical systems, and the extrinsic parameters, which define the cameras positions with respect to a desired reference frame. The accuracy of the reconstruction of the position of the observed points is then strictly related to the uncertainty on the knowledge of the parameters described above: the calibration activity, providing an estimation of such parameters, assumes then an important role. For this reason, a numerical model of the setup has been developed in order to perform a preliminary evaluation of the calibration process performance, both in case of stereo validation with the functional model of STC and in case of stereo validation with STC FM.

The experimental data obtained in laboratory have been compared with the simulated data, validating the numerical model for the calibration simulation and providing useful indication for the simulation of the calibration process with the fight model of the instrument.

The parameters estimated have been finally provided as input for the 3D reconstruction of a stereo validation target: the comparison between the digital map obtained from images and the laser scanner map of the target allowed to evaluate the accuracy of the stereo reconstruction.

The preliminary experimental results completely fulfill the requirements, validating the developed innovative method for the indoor evaluation of the stereo telescopes performance.

The first chapter of this thesis is an introduction on the ESA BepiColombo mission to Mercury and on the instrument object of this work, defining the scientific objectives and describing in detail the instrument design.

In order to provide an introduction on the theory fundamental concepts of stereo imaging and camera calibration, the second chapter illustrates the image formation process and the basic algorithms.

The third chapter subject is a detailed view of the developed stereo validation setup, from the main concept and requirements definition to the detailed description of optical design analysis and of the setup components.

The fourth chapter illustrates the simulation activity of the setup calibration process, in which calibration data have been simulated starting from the ray-trace model of the instruments, and provided as input for classical calibration algorithms. Statistical analysis have been applied to evaluate repeatability of the calibration process with respect to the variability of the input noise.

Finally, the fifth chapter describes the experimental results of the calibration activity with the functional model of the STC and the validation of the developed procedure for the simulation of the calibration process, concluding with a description of the preliminary results of stereo validation activity.

List of the acronyms and abbreviations

d.o.f.	degrees of freedom
DTM	Digital Terrain Model
FB	Functional Breadboard
f.o.v.	field of view
LM	Levemberg-Marquardt
pix	pixel
RMS	Root Mean Square
ROC	Rotation stage for the selection of the active Optical Channel
RPV	Rotation stage for the simulation of active channel's Point of View
SC	Spacecraft
SE	Selex ES S.p.A.
STC	Stereo imaging Channel
SVD	Singular Value Decomposition
SVS	Stereo Validation Setup
TVC	Thermal Vacuum Chamber
UPD	University of Padova
w.r.t.	with respect to

1. The Stereo imaging Channel onboard BepiColombo Mission

1.1 **Planet Mercury**

The Mercury planet is the smallest of the four terrestrial planets of the Solar System, and the closest to the Sun. With an orbit period of 88 days, it completes two spin rotation around its axis every three rotations around the Sun. Its surface appears to be highly cratered, mainly due to the absence of atmosphere and to the geological inactivity. During its formation process, it has been subjected to the highest temperature and has experienced the largest diurnal temperature variation of any object in the Solar System. Solar tides have influenced its rotational state. Its surface has been altered during the initial cooling phase and its chemical composition may have been modified by bombardment in its early history. Mercury therefore plays an important role in constraining and testing dynamical and compositional theories of planetary formation.

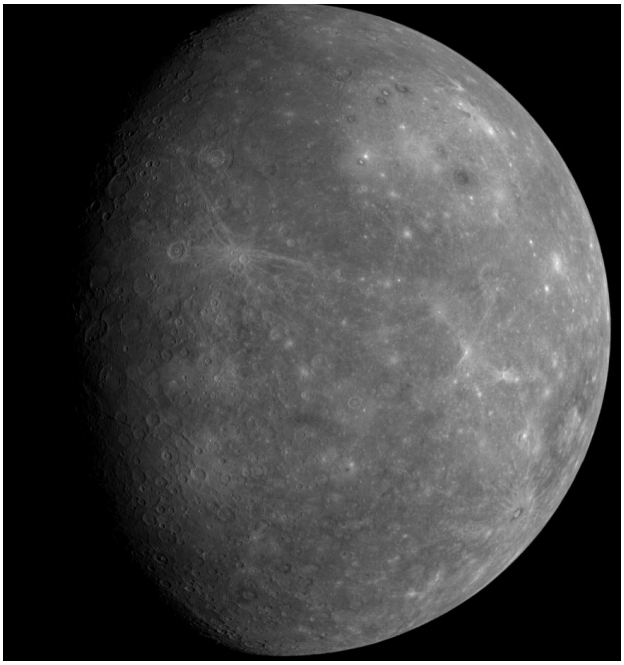

Figure 1-1: Mercury surface imaged by NASA Messenger.

Due to its proximity with the Sun, with a maximum elongation of 28.3°, Earth observations are very difficult and restricted to brief periods, since radiation coming from the Sun could damage the observing telescope.

On the other side, space missions to Mercury are very challenging, due to the intensity of Sun radiations in proximity of the planet. In space investigation history, the first mission which provided very close images, mapping the 40% of the surface in three consecutive flybys, was the NASA Mariner 10, in 1974 [1],[2][3]. The mission revealed also for the first time the presence of a planet magnetic field. In the recent past NASA Messenger [4], launched in 2004, after several flybys between 2008 and 2009, reached its elliptical orbit around the planet on March 18, 2011, providing images of the undiscovered part of planet's surface. The main scientific objectives of the mission are the investigation of the causes of the planet's high density, the study of its geological history, the nature of the magnetic field, the core structure, the study of possible ice formations, and the investigation of the origin of its tenuous atmosphere.

In 2015 an ESA mission, named BepiColombo [5][6] as a tribute to the Italian scientist Giuseppe Colombo (1920-1984), will orbit the planet with two separate spacecrafts for deeper planet investigation .

1.2 BepiColombo mission

With the Rosetta mission, the European Space Agency promoted a research program whose principal objective was the investigation on the origin of the materials composing the most cold and outer layers of Solar System. On the other side the study of Mercury should provide information on the planetary formation process in the innermost and hottest part of the proto-solar nebula. With this intent, starting from 1993, a group of ESA scientists began the discussion of a space mission for the Mercury investigation, which in 1996 was selected as a cornerstone mission for ESA scientific research program. The mission has been developed as a collaboration between ESA and JAXA (Japanese Aerospace Exploration Agency), with the primary scientific objectives of planetary physics and magnetosphere investigation. The instrumentation is divided in two main modules which will be launched on a common spacecraft by an Arianne 5 launcher: the Mercury Planetary Orbiter module (MPO), designed and developed by ESA, and the Mercury Magnetospheric Orbiter (MMO), followed by JAXA.

The final configuration of the mission was approved in November 6, 2003 from ESA's Scientific Program Committee (SPC) and in 2007 started the industrial implementation of the experiment, which will be launched in July 2015.

1.2.1 Mission Objectives

The BepiColombo mission primary objectives were officially defined in 2000 by the BepiColombo Science Advisory Group [7]. The main objectives can be resumed as follows:

- Investigate the origin and evolution of a planet close to the parent star;
- Study Mercury as a planet: its form, interior structure, geology, composition and craters;
- Examine Mercury's vestigial atmosphere (exosphere): its composition and dynamics;
- Probe Mercury's magnetized envelope (magnetosphere): its structure and dynamics;
- Determine the origin of Mercury's magnetic field;
- Investigate polar deposits: their composition and origin;
- Perform a test of Einstein's theory of general relativity.

1.2.2 System Architecture

As previously described, the most efficient way for the reaching of the scientific objectives is the separation of the mission in two separate main modules, with dedicated functions:

- Mercury Planetary Orbiter module (MPO) [8], supporting remote sensing and radio science instrumentation.
- Mercury Magnetospheric Orbiter (MMO), supporting instrumentation for the magnetic field investigation.

The interplanetary cruising phase will be managed by the Mercury Transfer Module (MTM), which is a modular propulsive system on its turn composed by the Solar Electrical Propulsion Module (SEPM) and by the Chemical Propulsion Module (CPM).

The MPO and MMO, together with MTM will be assembled together to form the Mercury Composite Spacecraft (MCS), which will be launched on 2015, approaching to Mercury in January 2022.

The ground segment for the BepiColombo mission will consist in two main elements:

- Mission Operation Center (MOC), at ESOC,
- Science Ground Segment (SGS).

ESA will manage both the launch phase and the MCS and MPO operations, while the MMO module, after MCS separation, will be controlled by the JAXA's Sagamihara Space Operation Center (SSOC).

1.2.3 Mission phases

The BepiColombo mission is divided into five main phases, the first four are considered as non-operative phases, the last one is referred to as the operative phase.

1.2.3.1 Non operative phases

The four non-operative phases are:

- Launch and Early Orbit phase: From the removal of the vehicle umbilical connector until the reaching of a stable SC configuration, including solar arrays deployment. During this phase the satellite is set to minimize power consumption.
- Near Earth Commissioning Phase: after the completion of Launch and Early Orbiting until the end of commissioning. If possible in this phase the payloads will be checked-out, and possible corrections of SC orbit will be evaluated.
- Interplanetary cruise phase: this phase will last about 6 years, until begin of Mercury Approach Phase. In this phase the SC will be subjected to Earth, Venus and Mercury gravity assists, combined with propulsion arcs provided by the MTM module. During this phase MPO and MMO will be nominally switched off sending periodic Health Check data.
- Mercury approach phase: this phase includes the orbit injection and correction maneuvers, the delivery of both MPO and MMO in their desired initial orbits, and all the separation maneuvers.

1.2.3.2 Operative phase

The last phase is the operative phase, named Mercury Orbital Phase, which begins after Mercury orbit injection and after a scientific performance verification phase. Concerning MPO module, the completion of the MPO commissioning will lead to the start of the Routine Operation Phase, which will follow an operation plan elaborated by SGS. This phase is planned to last one Earth year (about four Mercury rotations), but it will possibly be extended of an additional year.

1.2.4 Communications

The MCS and MPO ESA modules will communicate with the MOC residing at ESOC (Germany) which on its turn is connected to its Ground Station located in Cebreros (Spain). The MPO will communicate via X-band (uplink) and via X/Ka-band (downlink) with Ground Station The amount of downlink science data foreseen for the nominal mission life is about over 1.550 Gb, with an average downlink ranging between 30 and 675 kbit/s.

MMO will be controlled by ISAS/JAXA ground station in Usuda (Japan), except during the cruise phase, in which MMO data will be routed through MPO to ground via a military standard 1553 link.

1.3 **MPO**

The Mercury Planetary Orbiter is the ESA's scientific contribution to BepiColombo mission, whose instrumentation will provide radio science and remote sensing for planet conformation and composition investigation. The main scientific objectives of MPO can be resumed as follows:

- Close range studies of the surface
- Investigations of the interior structure of Mercury
- Fundamental planetary science
- Fundamental magnetometric investigation
- Study of exosphere.

The MPO spacecraft is a three-axis stabilized. The Z-axis points in the nadir direction for a continuous observation of the planet.

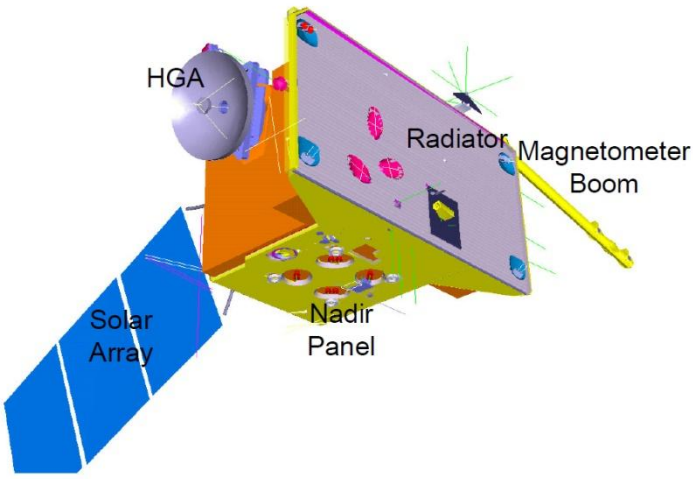

Figure 1-2: MPO satellite.

The orbit is polar to facilitate global mapping and as low as possible to optimize spatial resolution of the imaging channels. The minimum periherm and apoherm altitudes, 400 km and 1500 km, are imposed by the thermal environment.

1.3.1 MPO Payload

The list of instruments, which has been confirmed in November 2005 by the SPC is resumed in the following table.

BELA	BepiColombo Laser Altimeter
ISA	Italian Spring Accelerometer
MERMAG	Mercury Magnetometer
MERTIS-TIS	Mercury Thermal Infrared Spectrometer
MGNS	Mercury Gamma ray and Neutron Spectrometer
MIXS	Mercury Imaging X-ray Spectrometer
MORE	Mercury Orbiter Radio science Experiment
PHEBUS	Probing of Herman Exosphere by Ultraviolet Spectroscopy
SERENA	Search for Exosphere Refilling and Emitted Neutral Abundances (Neutral and ionised particle analyser)
SIMBIO-SYS	Spectrometers and Imagers for MPO BepiColombo Integrated Observatory System (High resolution and stereo cameras, Visual and NIR spectrometer)
SIXIS	Solar Intensity X-ray Spectrometer

Table 1-1: MPO payload, instrument list approved by SPC in November 2005.

1.3.2 MPO Orbital parameters and SC attitude

The MPO orbital parameters are the result of a best match between the scientific requirements fulfill and the minimization of delta V for Mercury in-orbit injection. The result is an eccentric polar orbit characterized by the following parameters, which are illustrated in Figure 1-3:

Parameter	**Symbol**	**Unit**	**Value**
Periherm altitude	h_p	km	400 ± 20
Apoherm altitude	h_a	km	1508 ± 20
Inclination	i	°	90 ± 2
Longitude of the ascending node	Ω	°	67.7
Argument of periherm	ω	°	16
Period	T	hr	2.32
Eclipse duration	t_e	min	< 42

Table 1-2: MPO Orbital parameters at beginning of life (BOL).

a.

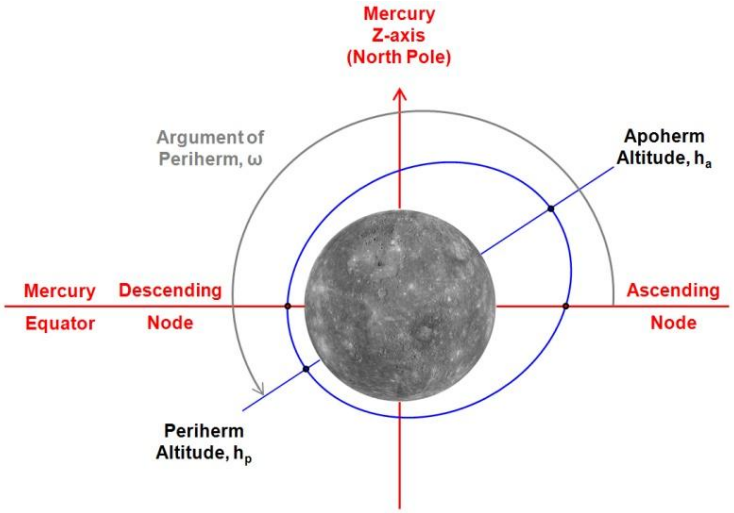

b.

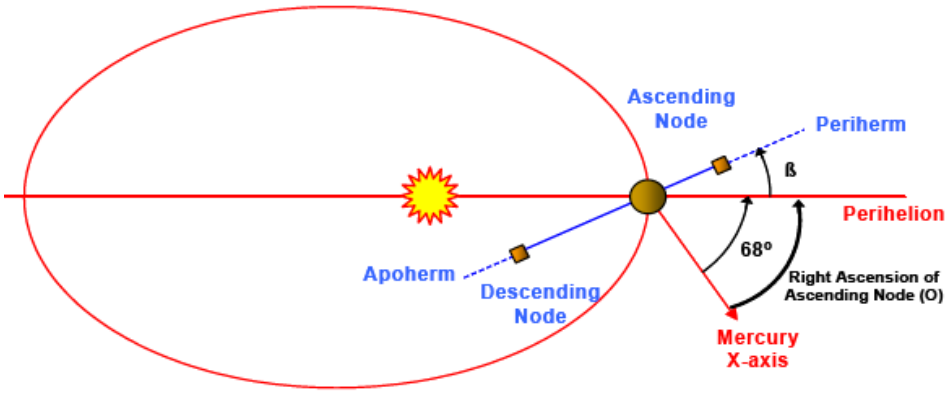

Figure 1-3: (a) Representation of the system Mercury – SC with some characteristic orbits elements. (b) Representation of the system Sun – Mercury – SC with some characteristic orbits elements.

The MPO argument of periherm ω and altitude of periherm h_p values will be subjected to continuous changes during the mission due to the variation of the value of the J^2 – term of Mercury gravity field.

The SC attitude, illustrated in Figure 1-4, shows the *x*-axis defined as pointing towards SC direction, *z*-axis nadir pointing, and the *y*-axis perpendicular to the orbit which completes the right handed reference frame. The roll, pitch and yaw Euler angles are defined as the rotations of the SC w.r.t. the *x*, *y* and *z* axis respectively.

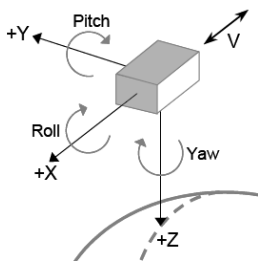

Figure 1-4: MPO nadir pointing reference frame representation.

Since the MPO radiators (-Y axis) faces are designed to be exposed towards cold space, a flip-over maneuver will be performed at aphelion and perihelion to avoid exposure to the Sun of the radiator surfaces, as illustrated in Figure 1-5.

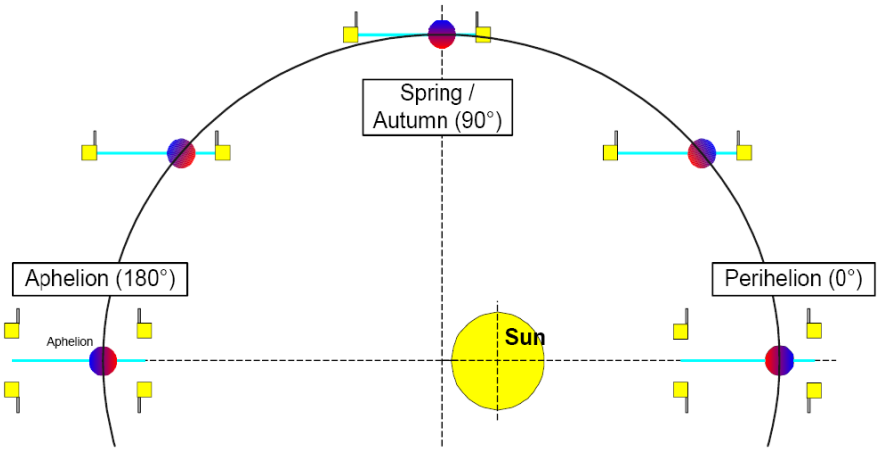

Figure 1-5: MPO flip over during Mercury's orbit illustration.

The MPO flip-over have consequences on the computation of Solar minimum incidence angle for the instruments observing planet's surface, with important consequences on instrument design and observing strategies.

1.4 The SIMBIO-SYS suite

The SIMBIO-SYS suite [9] (Spectrometer and Imagers for MPO BepiColombo – Integrated Observatory System), has been designed as a set of instruments with different functions, investigating on different channels, sharing a common optical bench. Such optical bench represents the only thermal, mechanical and electric interface between the instrument and the SC. The design of the suite is based on the maximum instrument integration: power supply, data handling and software operations are shared, in order to optimize the scientific results during each phase of the mission.

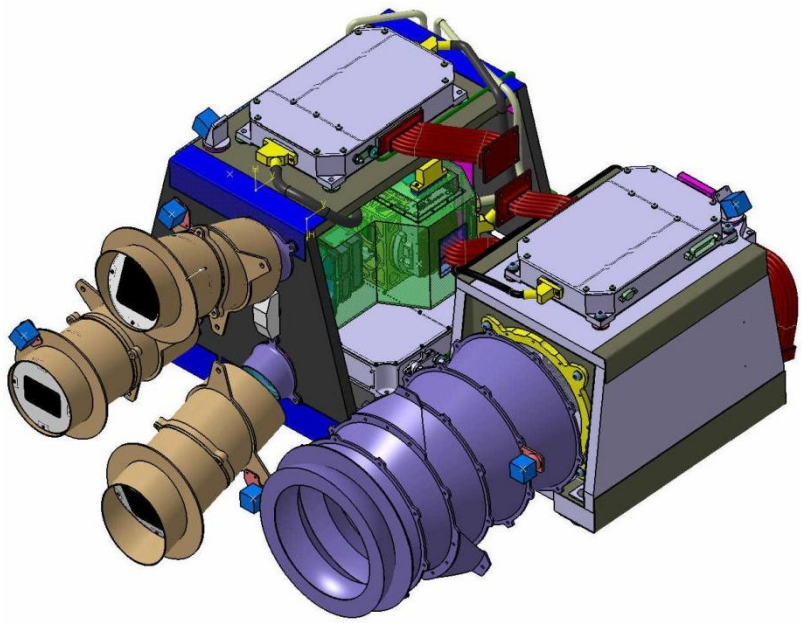

Figure 1-6: Representation of the SIMBIO-SYS suite in a recent Structural Thermal Model configuration.

The SIMBIO-SYS is composed by three instruments, referred to also as channels:

- HRIC: High Spatial Resolution Imaging Camera [10],
- STC: Stereo Imaging Channel [11],
- VIHI: Visual and Infrared Hyper – spectral Imager [12].

1.4.1 Scientific objectives

The SIMBIO-SYS channels will allow to obtain images of the surface integrated with information about geology, topography and composition, with a detail level sufficient to help in the reconstruction of the evolution of the planet. The main issues that the SIMBIO-SYS will investigate regard surface geology and stratigraphy, the surface composition, the impact crater population and

degradation, the presence of volcanic deposits, the analysis of past and present crustal dynamics and the interaction between surface and exosphere.

The optical channels have been designed in order to accomplish the following scientific objectives:

- Global mapping with stereo imaging with 50-110 m/pixel spatial scale and 80 m vertical accuracy at periherm over the equator.
- Color mapping of selected regions in 4 broad band filters in the range from 410 to 930 nm.
- Global mapping with spectroscopy in the spectral range from 400 to 2000 nm with a spatial resolution better than 500 m.
- High spatial resolution (5-10 m) imaging of selected areas summing up to at least 20% of planet surface in a panchromatic filter and in 3 different broad band filters, in the range from 400 to 900 nm.
- Hyperspectral imaging of selected areas in the spectral range from 400 to 2000 nm with a spatial sampling down to 100 m.

1.5 The Stereo Imaging channel

STC [13][14] is a wide angle camera designed to image each portion of the Mercury surface from two different perspectives (see Figure 1-7): it is composed by two sub-channels with the orientation of +20° and –20° from the nadir direction and adopts a catadioptric optical design with common detector in order to save mass and power. STC provides panchromatic stereo image pairs in order to reconstruct the Digital Terrain Model (DTM) of the planet surface with 80 m vertical accuracy and color images of selected areas. STC configuration takes into account 5 filters in 400-1000 nm spectral range: a broad-band filter for stereoscopic acquisition is centered at 700 nm with 200 nm bandwidth; 4 narrow-band filters are centered at 420, 550, 700 and 920 nm and have 20 nm bandwidth.

a. 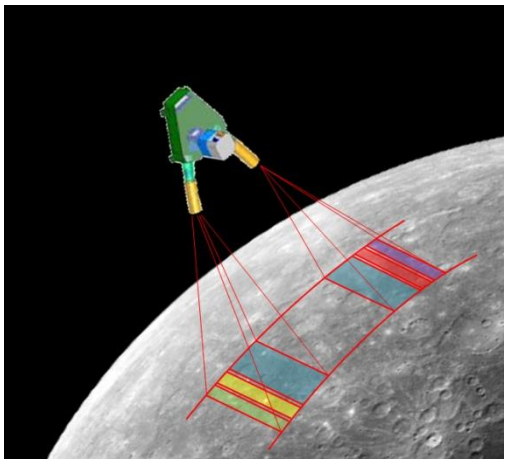 b. 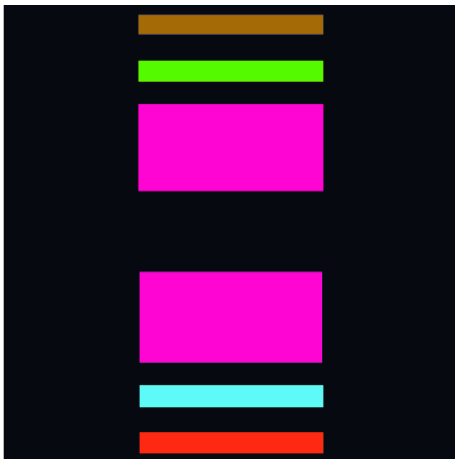

Figure 1-7: SIMBIO-SYS Stereo Imaging Channel (STC) (a) optical concept, (b) detector filter areas disposition (black areas are not illuminated).

STC will allow to analyze key features of the planet surface, such as craters and volcanic edifices, and will provide the context for HRIC acquisitions.

1.5.1 Scientific requirements

The STC main scientific requirement is to perform a global panchromatic 3D mapping of the surface, integrated with a selective study of interest areas in predefined spectral bands [14]. The requirement for the scaling factor means value equals to 110m/px, with a best value of 50 m/px at periherm when observing equator areas. The STC will combine the stereo reconstruction capabilities together with spectral analysis in order to study surface composition and to define the main geological units, such as morphology of the tectonic features, impact craters conformation and volcanic edifices. A series of scientific requirements, reported in Table 1-3, have been implemented in order to satisfy the scientific objectives, regarding the scale factor and the optical performance, in terms of Ensquared Energy (EE) and Modulation Transfer Function (MTF).

Requirement	Value
Scale factor	50 m/px at periherm
Swath	38 km at periherm
Stereoscopic properties	±20° stereo angle with respect to Nadir. Both images on the same detector
Vertical accuracy	80 m
EE MTF	> 70% inside 1 pixel > 60% at Nyquist frequency
Wavelength coverage	410-930 nm (5 filters)
Filters	panchromatic (700 ± 100 nm)
	420 ± 10 nm
	550 ± 10 nm
	750 ± 10 nm
	920 ± 10 nm

Table 1-3: SIMBIO-SYS STC scientific requirements.

1.5.2 Optical design

In order to reach a good balance between optical performance and optimization of resources, such as mass and volume, the camera is based on a catadioptric optical design in which the detector and most of the optical elements are shared by the 2 channels. The design has been chosen to satisfy the required optical performance for all the filters in the whole FoV of each filter and it has been kept as short as possible, compatibly with the need of limiting the cross-talk and to cope with stray-light problems due to the common optical path.

The focal length of the system is 95 mm and allows to reach the 50 m/pixel scale factor at periherm, adopting a 10 μm pixel size SiPIN CMOS as detector, useful in terms of radiation hardness and for the capability of snapshot image acquisition, allowing very short exposure times (< 1 ms).

The global FoV of each channel is 5.3° × 4.8°, subdivided in 3 strips, one for each filter, covering 3 quasi-contiguous strips on Mercury surface: at periherm on the equator each strip corresponds to an area of about 40 × 19 km^2 for the panchromatic filter, 40 × 3 km^2 for the color ones.

The STC optical solution (see Figure 1-8) is composed by two independent elements: a fore-optics, consisting of two folding mirrors per each sub-channel, and a common telescope unit, which is an off-axis portion of a modified Schmidt design. The couple of folding mirrors redirect the ± 20° wide beams along direction much closer to the system optical axis (± 3.75°). A correcting doublet is positioned after the folding mirrors and replaces the classical Schmidt correcting plate, in order to

reduce the telescope length by about a factor 2 respect to the classical configuration. This correcting doublet has a nearly null optical power: it mainly corrects the aberrations induced by the primary mirror.

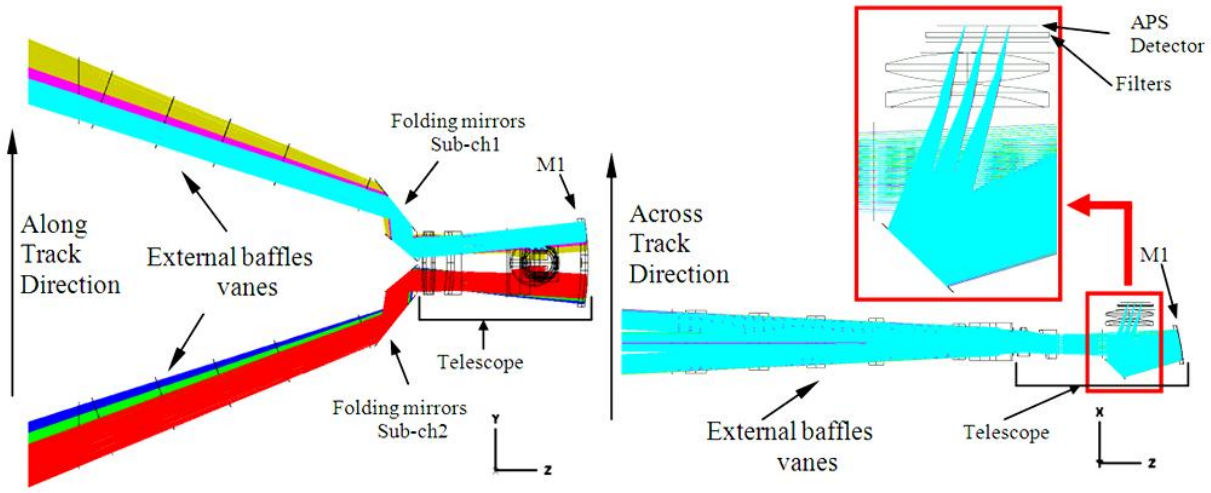

a) b)

Figure 1-8: STC Optical layout: a) the configuration is viewed in the plane defined by the along track and nadir directions; b) the projection in the orthogonal plane, the one including across track and nadir directions. In the inset, an enlarged view of the focal plane region helps to better follow the rays.

Optical concept	Catadioptric: modified Schmidt telescope plus folding mirrors fore-optics
Stereo solution (concept)	2 identical optical channels; detector and most of the optical elements common to both channels
Focal length (on-axis)	95 mm
Pupil size (diameter)	15 mm
Focal ratio	*f*/6.3
Mean image scale	21.7 arcsec/px (105 µrad/px)
FoV (cross track)	5.3°
FoV (along track)	2.4° panchromatic 0.4° color filters
Detector	Si_PIN (format: 2048 × 2048; 10 µm squared pixel); 14 bits dynamic range

Table 1-4: STC main optical features.

The optical design of the STC has been optimized in order to fulfill the requirements [15]. The mean Ensquared Energy (EE) computed by means of ray-trace analysis result to be in the order of 80% for each filter, over the wavelengths of interest. Figure 1-9 (a) shows the optical performance of the actual STC optical design in terms of spot diagram, which is always within pixel size indicated by the black squares for all field values.

Also the MTF displayed in Figure 1-9 (b) results to be within the requirements, with a mean value of 60-70% at Nyquist frequency of 50 cycles/mm for all the filters over the whole f.o.v.

Concerning optical distortions, thanks to the Schmidt design and to the positioning of the aperture stop, the contribution is very limited, with a distortion amount of less than 0.3% over all the filter. In Figure 1-10 the result of distortion analysis for panchromatic filter is reported, in which the difference between the predicted pattern (represented by the regular grid) and the real position of chief rays (×) are amplified of a twenty factor. The distortion contribution over the whole panchromatic f.o.v is about -0.2% [14].

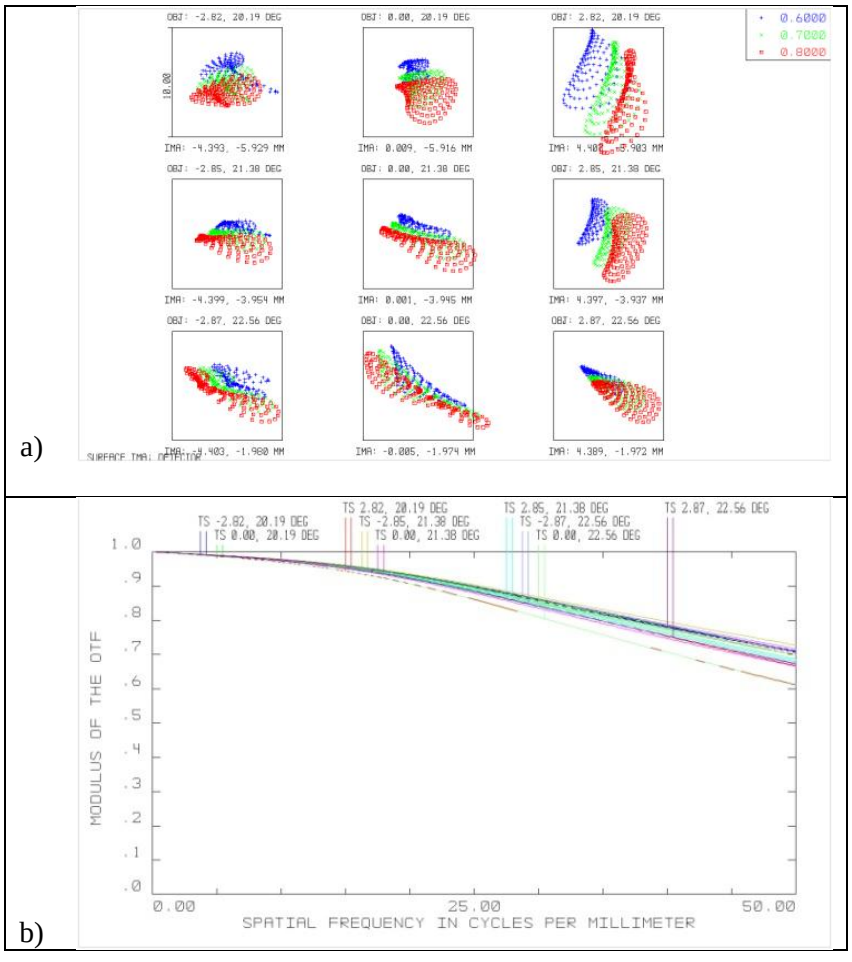

Figure 1-9: STC optical performance: (a) spot diagrams; (b) MTF for the panchromatic filter.

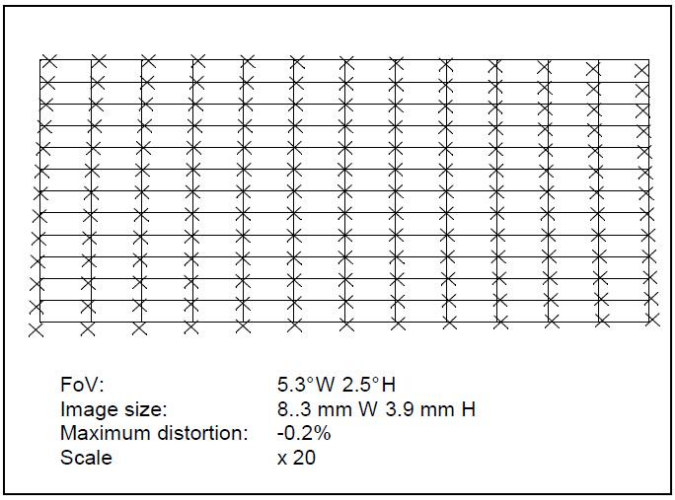

Figure 1-10: Grid distortion for the panchromatic filter. Note that real chief ray displacements from theoretical values are multiplied by a factor of twenty to make the distortion effects clearly visible.

1.5.3 Observation Strategy

The global stereo mapping, which is the main scientific objective of STC, will be completed during the first 6 months of the mission: the instrument will work when the planet will be at aphelion. During the following planned 6 months of the mission it will work on selected targets. In order to map in stereo mode the whole surface, STC shall work with both sub-channels. STC is extremely flexible as regards the operative scenarios: depending on the mission phase, STC will work with one or both sub-channels, using any filter combination, with different window sizes on the filters areas and different compression ratios. STC will be able to produce color mosaics of chosen regions and DTMs of interesting targets with a grid size of 100-250 m depending on the altitude of the spacecraft (SC) with respect to the Mercury surface.

1.5.4 Observing geometry

The geometry of the stereoscopic system composed by the two STC optical channels imaging a same portion of planet's surface depends on the latitude of the observed area, due to the eccentricity of the SC orbit.

Considering the mean orbital parameters of the MPO over the nominal mission lifetime, the angles of incidence of the two optical channels and the stereo baselines have been computed as a function of the latitude observed at Mercury's surface. Figure 1-11: shows the directions of the principal rays of the panchromatic filters of the two STC optical channels for a subset of Mercury surface

latitudes. The two optical channels are named Forward looking channel (FWD, in red) and Backward looking channel (BWD, in blue) for simplicity.

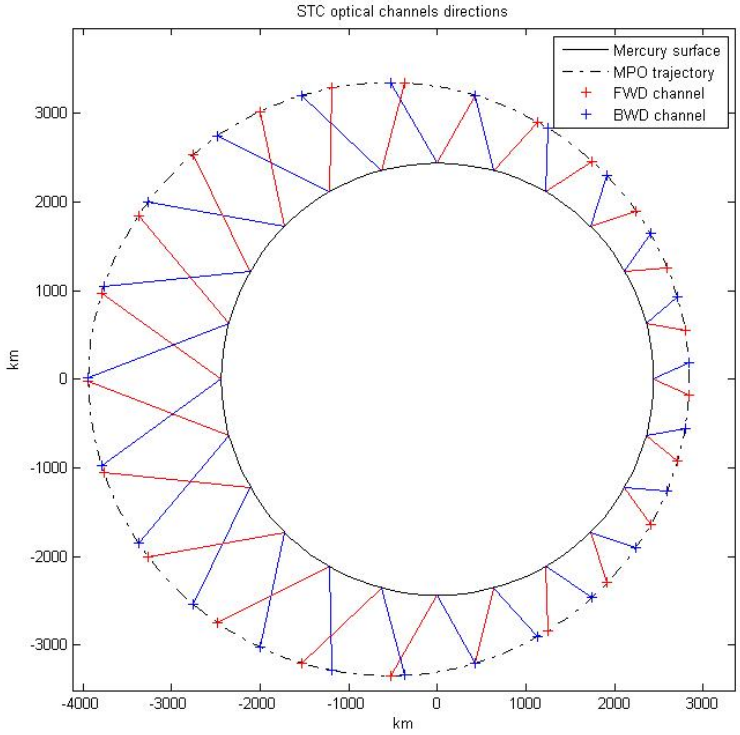

Figure 1-11: STC optical channels directions. The continuous black line represents the Mercury surface. The dotted line represents an orbit of the MPO. The blue and red vectors represent the directions of the panchromatic filters of the STC backward and forward looking channel during the MPO orbit respectively.

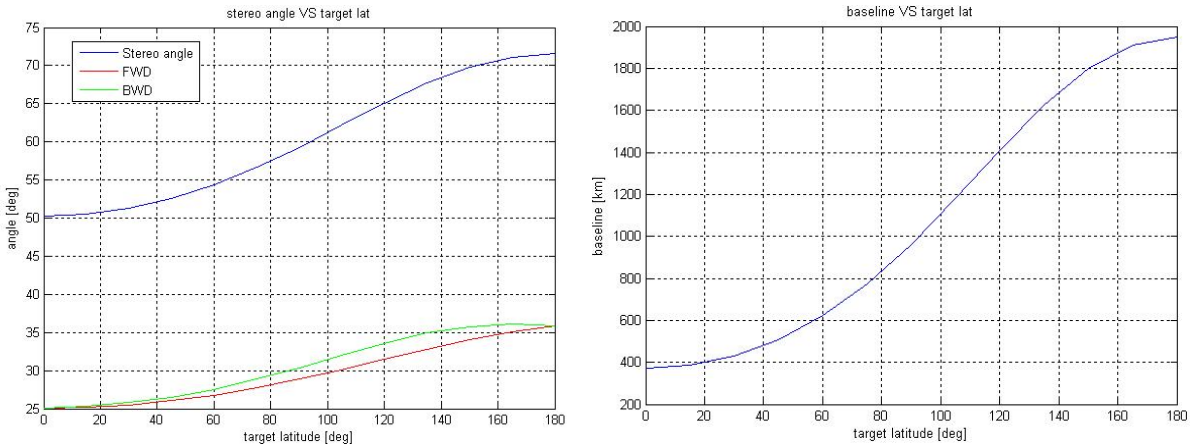

a) b)

Figure 1-12: (a) STC stereo angle in function of observing target latitude. (b) STC stereo baseline in function of observing target latitude.

Figure 1-12 (a) shows the stereo angle values (blue line) for latitudes ranging from 0 to 180 deg. The value ranges between about 50.22° at periherm, and 71.6° at apoherm. The stereo angle has been computed as the sum of the angle of incidence of the two STC channels (red and green lines)

w.r.t. the normal to the planet surface at the observed latitude. In Figure 1-12 (b) the baseline values computed for latitudes ranging from 0 to 180°: the estimated baseline, which can be approximately defined as the distance between the forward looking channel observing point and the backward looking channel observing point, equals to 370.11 Km at periherm, growing to 1951.2 km at apoherm[1].

[1] The baseline and stereo angles concepts will be illustrated in detail in the next chapter.

2. Background and related work

2.1 **Camera model**

The first fundamental step in retrieving depth information from images of a target is to know how light coming from the observed scene is collected by the camera's sensing elements and to give an analytic description of the image formation process.

2.1.1 Notation

In the next sub-sessions a 3D point will be indicated with the following syntax: $P = [X,Y,Z]^T$, and a 2D point q with $= [x, y]^T$. The homogeneous representations of the same vectors, obtained by adding 1 as the last element, will be indicated as: $\tilde{P} = [X, Y, Z, 1]^T$ and $\tilde{q} = [x, y, 1]^T$. The matrices are expressed with bold capital characters (e.g. $\boldsymbol{K}$).

2.1.2 Intrinsic parameters

The most commonly used camera model in computer vision is the so called *pinhole* model. The name is due to the main concept of such model, in which a camera is represented as a hole on a wall: the latter blocks light coming from the scene except for the rays passing through the hole (Figure 2-1). Beyond the wall an image plane can be positioned: the rays coming from the whole will compose a scaled image of the scene, flipped upside-down and left side-right. The distance between the hole and the image plane is referred as *focal length* of the pinhole camera.

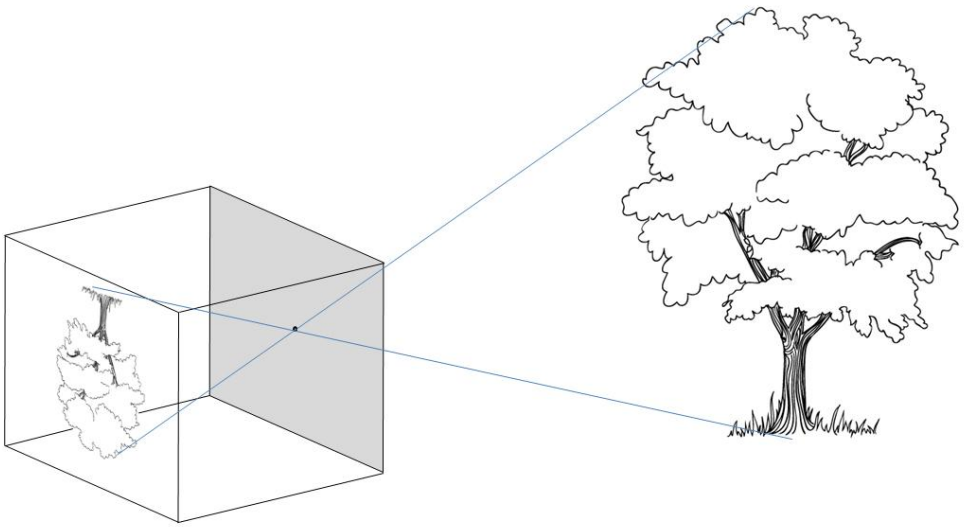

Figure 2-1 Pinhole camera schematic representation. The light rays passing through a hole (center of projection) provide a flipped image on the opposite wall (image plane).

Considering a bi-dimensional example of pinhole camera (see Figure 2-2), the relation between a point with height *X*, laying at a distance *Z* from the pinhole plane, and its coordinates on the image plane *x*, considering a focal length *f*, is given by:

$$-x = f\frac{X}{Z} \qquad 2.1$$

which is derived from a simple relation between similar triangles.

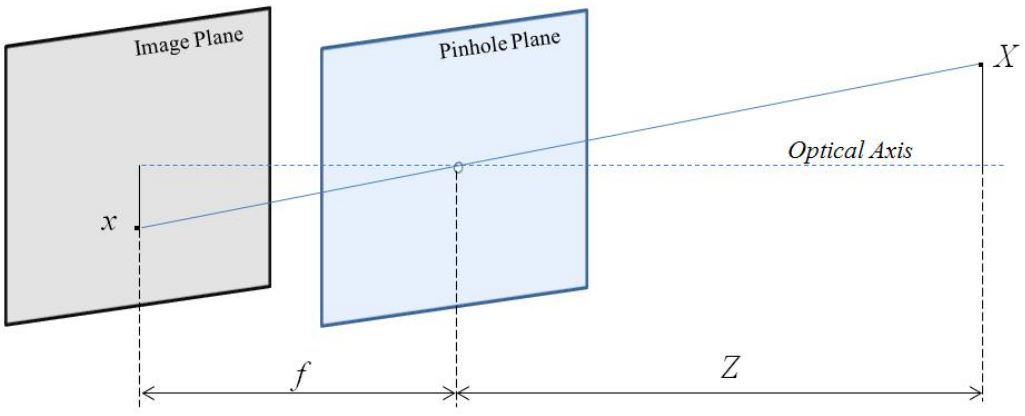

Figure 2-2: Pinhole camera with focal length f

To provide a simpler mathematical model of the camera, the image plane can be considered as positioned between the pinhole projection center and the observed object. This representation, illustrated in Figure 2-3, presents the advantage of removing the minus sign from eq. (2.1).

The *i*, *j* and *k* tensors illustrated in Figure 2-3 define the camera reference frame, with the origin *O* coinciding with the camera center of projection, *i* and *j* perpendicular and aligned with the sensor sides, and *k* corresponding to the optical axis direction.

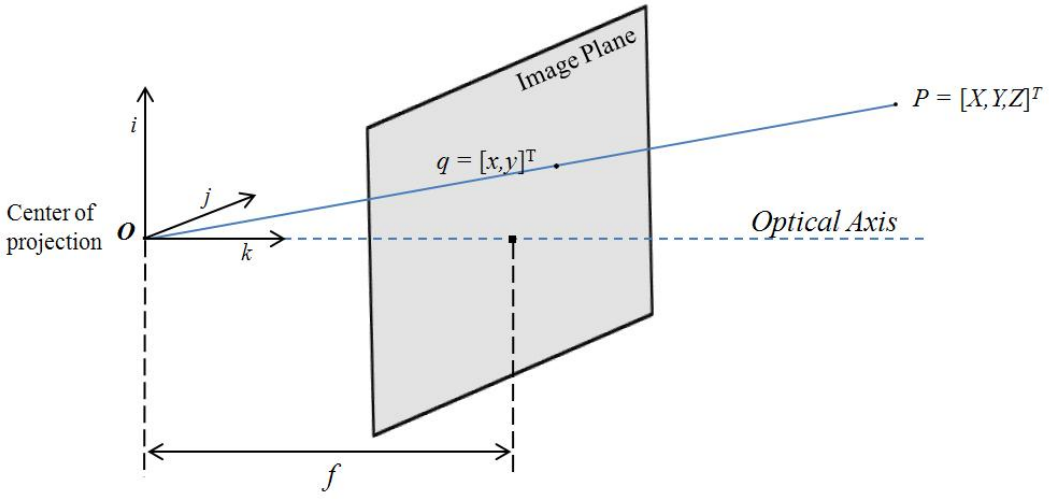

Figure 2-3 Compact representation of pinhole camera with focal length f.

Writing the relation between a 3D point $P = [X,Y,Z]^T$ and its image plane coordinates $q = [x, y]^T$ in matrix form, we obtain the relation:

$$s\tilde{q} = \overline{\mathbf{K}}P, \qquad s\begin{bmatrix} x \\ y \\ 1 \end{bmatrix} = \begin{bmatrix} f & 0 & c_x \\ 0 & f & c_y \\ 0 & 0 & 1 \end{bmatrix} \cdot \begin{bmatrix} X \\ Y \\ Z \end{bmatrix} \tag{2.2}$$

In which $\tilde{p}$ is the image point expressed in homogeneous coordinates, defined up to a scale factor *s*, and c_x and c_y are the image coordinates of the *principal point*, defined as the intersection between the image plane and the optical axis, which in pinhole camera model, is defined as the line passing through the pinhole which is perpendicular to the image plane.

To deal with discrete representation of images and with the possibility of non-square shape of pixel elements (especially in cheap cameras), we have to take into account the pixel dimensions (p_x, p_y), leading to a new equation:

$$s\tilde{q}_p = \mathbf{K}P, \qquad s\begin{bmatrix} u \\ v \\ 1 \end{bmatrix} = \begin{bmatrix} \alpha & \gamma & u_0 \\ 0 & \beta & v_0 \\ 0 & 0 & 1 \end{bmatrix} \cdot \begin{bmatrix} X \\ Y \\ Z \end{bmatrix} \tag{2.3}$$

In which q_p represents the image point coordinates and $[u_0, v_0]$ represent the image coordinates of the camera center both expressed in pixel units. The two focal lengths $\alpha = f/p_x$ and $\beta = f/p_y$ are expressed in pixel units, and the γ parameters is the skew factor, and is obtained with the relation:

$$\gamma = \frac{\tan(\sigma) f}{p_x} \qquad 2.4$$

In which σ is the angle between the y side of a pixel and its ideal direction, normal to the x side.

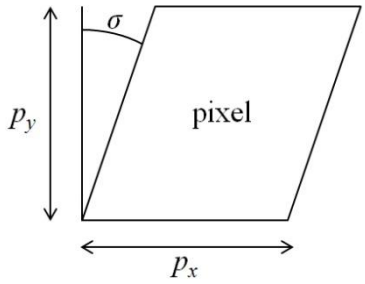

Figure 2-4 Sensor pixel: skew factor

The matrix **K** is referred to as camera matrix, and its entries α, β, γ, u_0, v_0 are known also as the set of the camera *intrinsic* parameters.

Common lens systems introduce a systematic deviation on light rays paths, which typically is resumed in two main distortion contributes: radial distortion and tangential distortion (Figure 2-5).

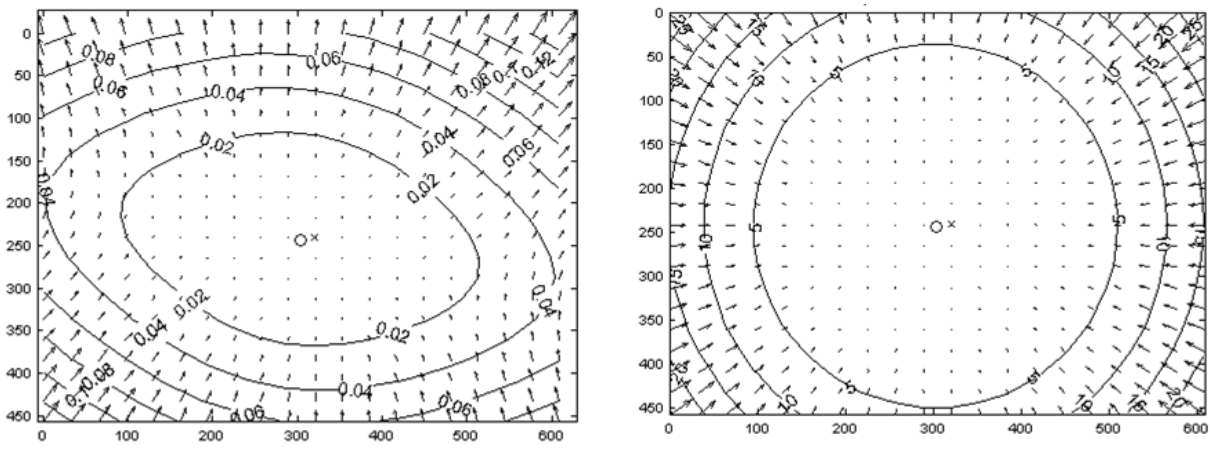

Figure 2-5 Representation of tangential distortion contribution (on the left) and radial distortion contribution (on the right)

The distortion contributions can be analytically described by introducing a vector of distortion coefficients k_i with three coefficients for radial distortion (k_1, k_2, k_5) and two coefficients for tangential distortion (k_3, k_4). Considering a 3D point P with coordinates $[X,Y,Z]^T$ in camera reference frame, its normalized image projection is defined as:

$$q_n = \begin{bmatrix} X/Z \\ Y/Z \end{bmatrix} = \begin{bmatrix} x \\ y \end{bmatrix} \tag{2.5}$$

Introducing the distance from camera center r, $r^2 = x^2 + y^2$, the distortion corrected image coordinates q_d are expressed by:

$$q_d = \begin{bmatrix} x_d \\ y_d \end{bmatrix} = (1 + k_1 r^2 + k_2 r^4 + k_5 r^6) q_n + dq \tag{2.6}$$

In which dq is the tangential distortion vector, computed as follows:

$$dq = \begin{bmatrix} 2k_3 xy + k_4(r^2 + 2x^2) \\ k_3(r^2 + 2y^2) + 2k_4 xy \end{bmatrix} \tag{2.7}$$

The image pixel coordinate q_p and its normalized and distorted coordinates q_d are related by the following equation:

$$\tilde{q}_p = \begin{bmatrix} u \\ v \\ 1 \end{bmatrix} = \mathbf{K} \begin{bmatrix} x_d \\ y_d \\ 1 \end{bmatrix} = \mathbf{K} q_d \tag{2.8}$$

Where **K** is the *camera matrix* defined in eq. (2.3).

2.1.3 Extrinsic Parameters

Generally, space points positions are expressed in an Euclidean reference frame, named *world reference frame*, which doesn't coincide with camera coordinate system. The relation between the two frames can be described by a rotation and a translation.

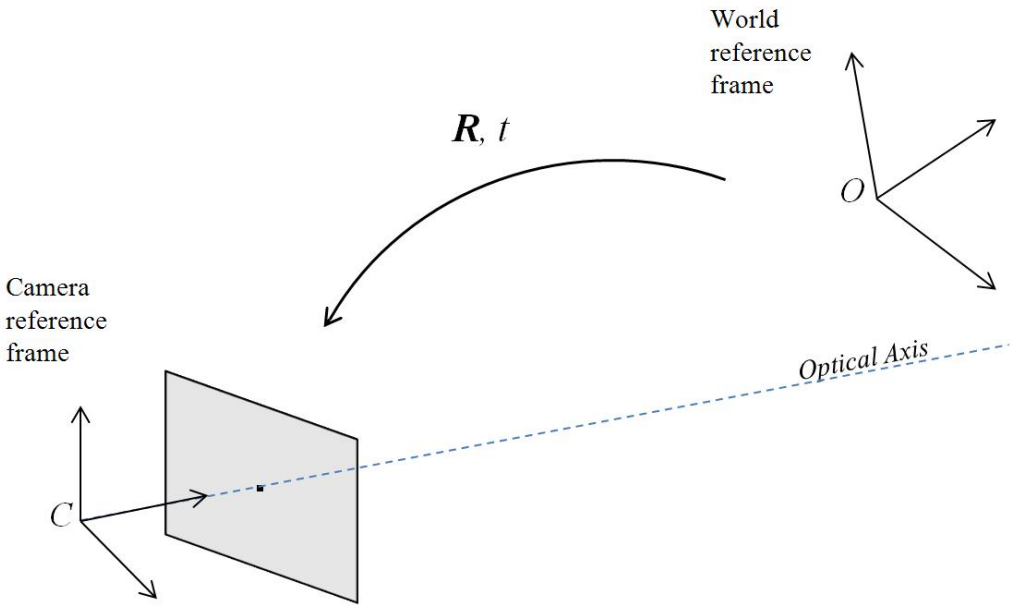

Figure 2-6 Pinhole camera: extrinsic parameters representation

Considering a 3D point P expressed in world reference frame, its representation in camera coordinates equals to $P_{CAM} = \boldsymbol{R}(P - C)$, where C represents the camera center coordinates in world reference frame and $\boldsymbol{R}$ is the rotation between camera and world reference frame. Expressing the relation between P_{CAM} and P in homogeneous coordinates we obtain:

$$\tilde{P}_{CAM} = \begin{bmatrix} \boldsymbol{R} & -\boldsymbol{R}C \\ 0 & 1 \end{bmatrix} \begin{bmatrix} X \\ Y \\ Z \\ 1 \end{bmatrix} = \begin{bmatrix} \boldsymbol{R} & -\boldsymbol{R}C \\ 0 & 1 \end{bmatrix} \tilde{P} \qquad 2.9$$

So the image plane coordinates of a point P in world reference frame can be expressed by the following relation:

$$\tilde{q} = \mathbf{K}[\boldsymbol{R} \mid t]\tilde{P} \qquad 2.10$$

Where **K** is the camera matrix defined in eq. (2.3) and $t = -\boldsymbol{R}C$ and both $\tilde{q}$ and $\tilde{P}$ are expressed in homogeneous coordinates.

2.2 Stereo imaging

The main task of the STC instrument, as described in §1, is to provide a DTM of Mercury surface by means of stereo imaging process: the two optical sub-channels will provide couples of images from two angles of view. Nowadays many literature and algorithms have been developed [16][17] to solve the problem of getting depth information from couples or larger sets of images, in this paragraph a short introduction to the problem is given.

The most evident example of a stereo imaging system is provided by human body: two eyes observing simultaneously the same scene provide our brain with two images from two different observing points. Our brain is able to recognize the same object both on left and right images and to get information on object distance basing on object different position over the two images.

To provide an analytical model of stereo imaging system we shall initially consider the simple case of two cameras with the same intrinsic parameters, with no optical distortions introduced, placed with perfectly parallel optical axis, and with image planes perfectly row-aligned and co-planar, as illustrated in Figure 2-7. This camera configuration is also referred to as *frontal parallel cameras* configuration.

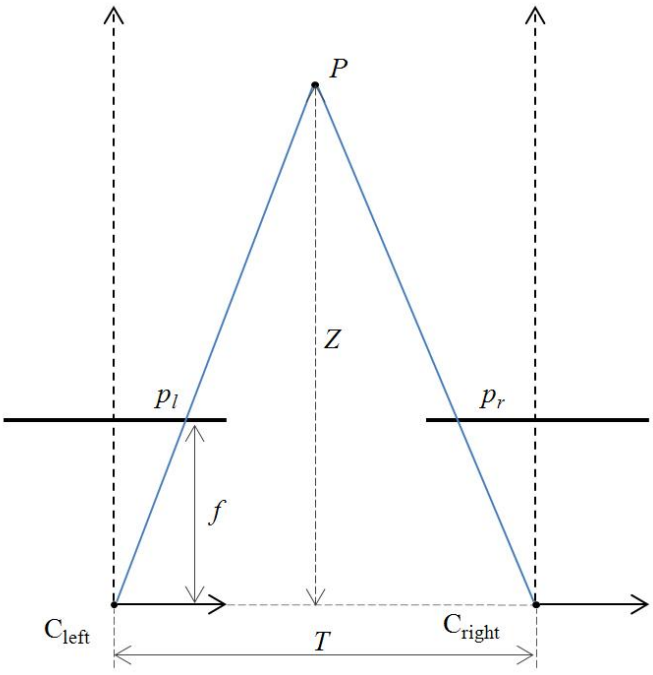

Figure 2-7: Example of stereo imaging system: the two cameras have the same intrinsic parameters and co-planar and aligned image planes.

The distance T between the two camera principal points C_{left} and C_{right} is called *baseline*. Considering the only horizontal image coordinates, a world point P, whose distance from baseline is

Z, is mapped to image coordinates p_l and p_r, the difference between the two image coordinates, referred to as *disparity*, is simply defined as $d = p_l - p_r$. The relation between disparity and point depth, Z, can be simply resumed by the following equation:

$$\frac{T - (p_l - p_r)}{Z - f} = \frac{\mathrm{T}}{\mathrm{Z}} \quad \Rightarrow \quad \mathrm{Z} = \frac{fT}{d} \tag{2.11}$$

From eq. 2.11, which implements the *triangulation* concept, we can notice that depth is inversely proportional to disparity: when disparity is near zero, small disparity variations imply large depth variations, when disparity is large, small disparity variations lead to small depth changes.

As we can see the object depth computation process when cameras are configured in frontal parallel configuration is quite simple: real stereo imaging systems never come up in perfect frontal parallel configuration, with the two cameras reference frames related by a rotation matrix $\boldsymbol{R}$ and a translation 3-vector T (Figure 2-8). To deal with real systems the common approach is to provide transforms which provide a mathematical alignment of the images, to provide this, the introduction of a specific geometry model is needed.

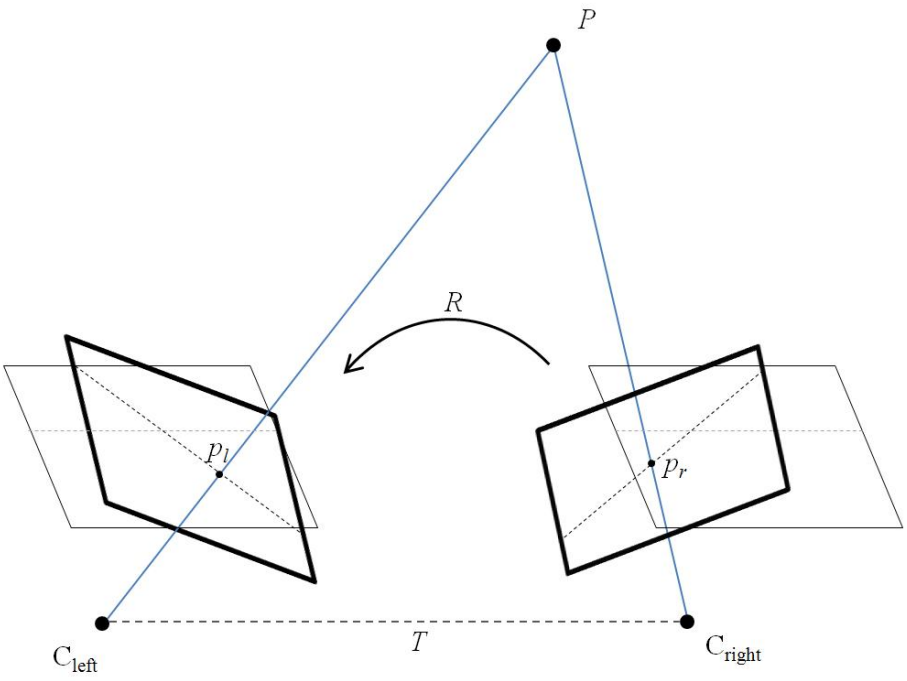

Figure 2-8 Stereo imaging with cameras not in frontal parallel configuration.

2.2.1 Epipolar geometry

The geometry of a generic stereo imaging system is referred to as *epipolar geometry*. This geometry provides a combination between the two cameras pinhole models and introduces a set of points called *epipoles* which are useful for the definition of stereo matching problem.

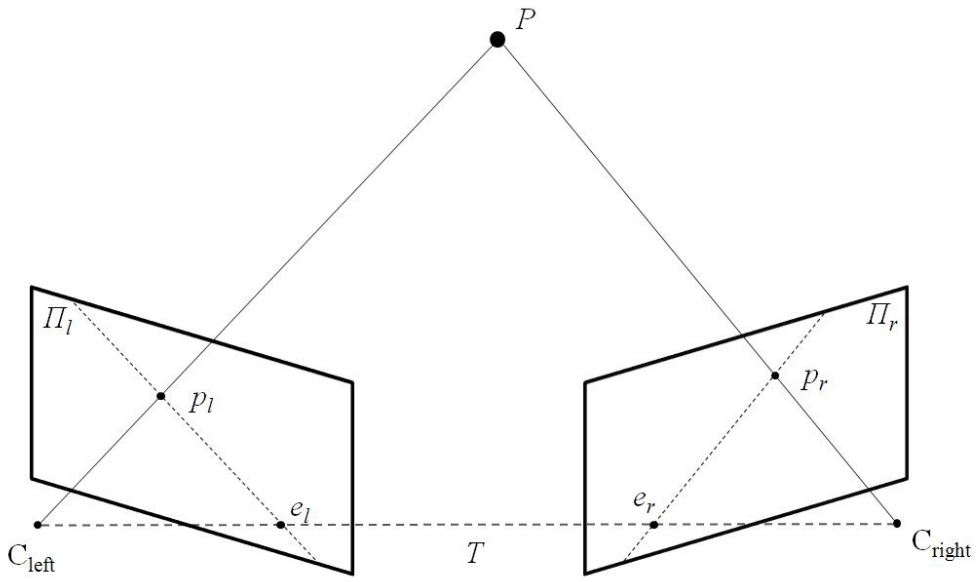

Figure 2-9 Representation of epipolar lines and epipoles.

Given a stereo camera composed by two pinholes with principal points C_{left} and C_{right} and image planes defined as Π_l and Π_r, and given a 3D space point *P* observed by both cameras, we define the *epipolar plane* as the plane defined by the points *P*, C_{left} and C_{right}. The epipolar plane intersects the image planes defining two *epipolar lines*, which contain the image points of *P*: p_l and p_r. The images of C_{left} on Π_r and of C_{right} on Π_l are two points e_r and e_l referred to as *epipoles*.

Epipolar geometry is used to define the problem of identification of homologous points between couples of stereo images. Given an image point p_l, we can observe that it could be generated by any 3D points positioned along the line defined by C_{left} and p_l. It's easy to note that the image of that line over Π_r corresponds to the epipolar line defined by e_r and p_r.

We can summarize epipolar geometry in two main statements:

- Every 3D point *P* together with the two camera centers defines a plane which intersects the image planes in two epipolar lines
- Given an image point in one of the two image planes, the *epipolar constraint* states that the corresponding image point on the other image plane belongs to the relative epipolar line.

From these statements we can observe that given any image point, if epipolar geometry of the stereo imaging system is known, the problem of finding its homologous point on the other image plane can be reduced to a 2D research over the corresponding epipolar line, this implies a reduction of computational costs for the homologous search and a reduction of risk of spurious correspondences.

Epipolar geometry can be applied in homologous points search with two different approaches:

- *Image rectification*: transformation of images which gives a new couple of images with pixels disposed as if acquired by a frontal parallel stereo imaging system.
- *Epipolar line computation*: for each epipolar line in image 1, the corresponding epipolar line on image 2 is computed on which perform homologous point search.

Both approaches require the definition of a matrix which relates the image pixels of the two cameras, which is referred to as *fundamental matrix* $\boldsymbol{F}$. Fundamental matrix contains both cameras internal parameters and extrinsic parameters of the stereo system. The orientation parameters are grouped in a matrix named *essential matrix* ($\boldsymbol{E}$).

The essential matrix expresses the epipolar constraint between the physical image coordinates p_l and p_r of a 3D point P over the left and right image planes of a stereo system. Considering the left camera reference frame centered at C_{left}, we define as P_l the coordinates of the 3D point P in such reference frame, and T as the position of the right camera center. The point P expressed in right camera frame is related to P_l as:

$$P_r = \boldsymbol{R}(P_l - T) \tag{2.12}$$

Considering the epipolar plane composed by the two camera centers and the point P we can express the epipolar constraint as:

$$(P_l - T)^T (T \times P_l) = 0 \tag{2.13}$$

Where $(T \times P_l)$ is a vector perpendicular to epipolar plane. Combining 2.20 with 2.21 we obtain:

$$(\boldsymbol{R}^T P_r)^T (T \times P_l) = 0 \tag{2.14}$$

The cross product can be expressed in form of a matrix multiplication introducing the matrix $\boldsymbol{S}$, with:

$$\boldsymbol{S} = \begin{bmatrix} 0 & -T_z & T_y \\ T_z & 0 & -T_x \\ -T_y & T_x & 0 \end{bmatrix}$$

Obtaining:

$$(P_r)^T \boldsymbol{RS} P_l = 0 \;\Rightarrow\; (P_r)^T \boldsymbol{E} P_l = 0 \qquad 2.15$$

Where the essential matrix is defined as $\boldsymbol{E} = \boldsymbol{RS}$. The constraint which relates the image points is simply obtained by 2.15 applying the projection equations $p = fP/Z$ and scaling the resulting equation, obtaining:

$${p_r}^T \boldsymbol{E} p_l = 0 \qquad 2.16$$

To get a relation between the image coordinates expressed in pixel we have to introduce information about the cameras intrinsic parameters in 2.16, by substituting to the physical coordinates p with the relation $q = \mathbf{K}p$, in which q represents the pixel coordinates and $\mathbf{K}$ is the camera matrix of the system, obtaining:

$${q_r}^T (\mathbf{K}_r^{-1})^T \boldsymbol{E} \mathbf{K}_l^{-1} q_l = 0 \qquad 2.17$$

By defining the Fundamental matrix as $F = (\mathbf{K}_r^{-1})^T \boldsymbol{E} \mathbf{K}_l^{-1}$, we can finally describe the relation between the pixel coordinates of the stereo imaging system as:

$${q_r}^T \boldsymbol{F} q_l = 0 \qquad 2.18$$

Both $\boldsymbol{E}$ and $\boldsymbol{F}$ have rank 2: specified a point q_l in pixel coordinate in left camera, it is possible to determine the equation of the corresponding epipolar line $e_r - p_r$ on the right image by solving 2.18. The parameters composing both matrices can be determined by means of calibration process, described in 2.3.

When the images are in frontal parallel configuration and perfectly row-aligned, the epipolar constraint is simplified, since the epipolar lines $e_r - q_r$ and $e_l - q_l$ coincide and they are parallel to

image rows. Dealing with real stereo imaging systems, the two stereo images can be transformed as if they're acquired by a system in frontal parallel configuration, by means of a process referred to as *stereo rectification*. The homologous search problem is thus reduced to a linear search on the image row corresponding to the one of the detected feature, with advantages in computational efficiency and algorithm reliability and disadvantage caused by the image deformation introduced by rectification process.

Once defined the geometry which relates an image point on one of the two images with all the possible homologous candidates over the second image, we need to define a method to quantify the concept of similarity between two image points.

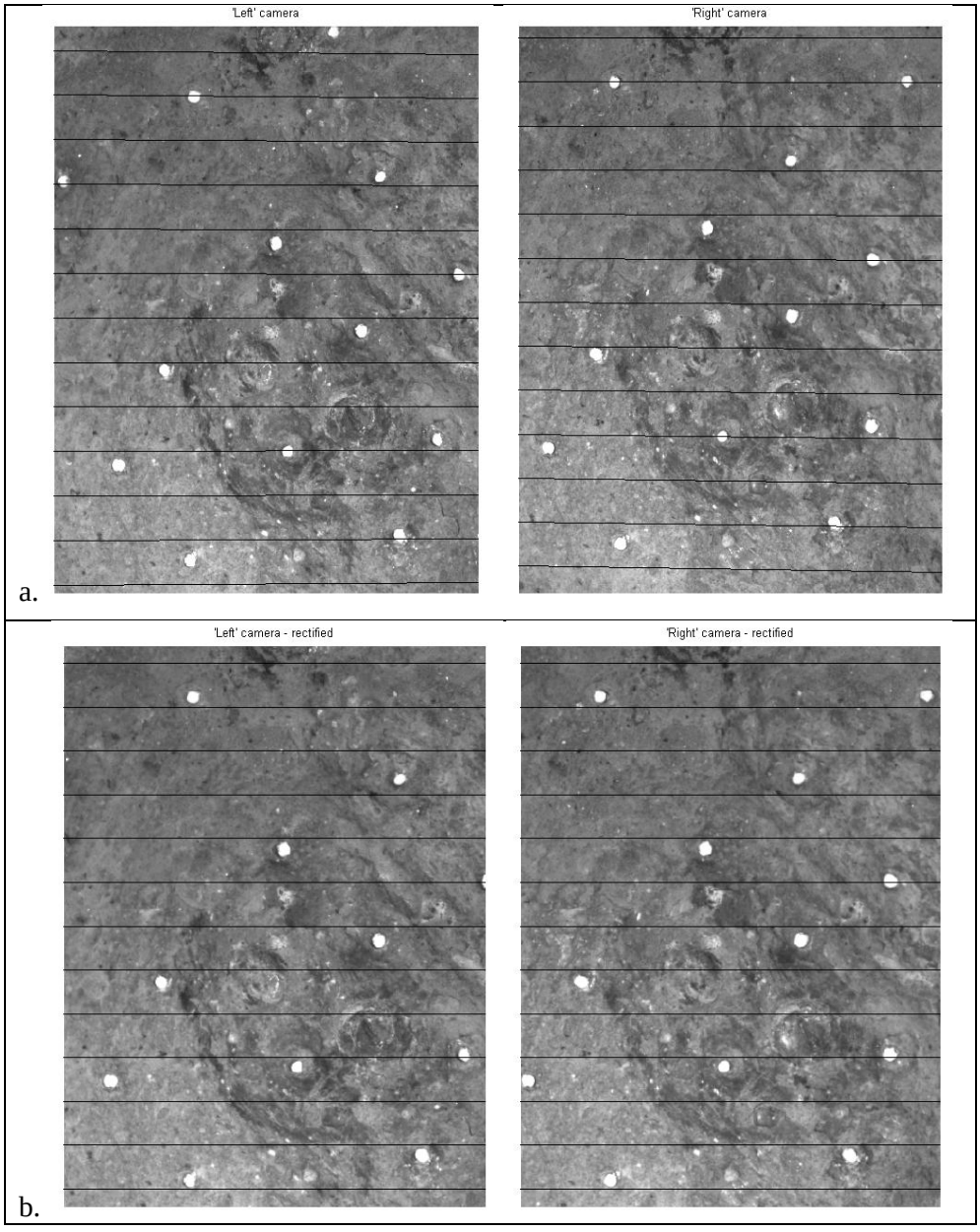

Figure 2-10 (a) Un-rectified stereo couple of images with epipolar lines (black). (b) Rectified stereo couple of images. Note that the black epipolar lines are perfectly horizontal and row-aligned for the rectified stereo couple.

2.2.2 Stereo matching

The stereo matching problem is widely documented in literature: a macroscopic classification of the possible solutions can be done between *feature-based* algorithms [19] and *dense* matching algorithms .

The first category is based on disparity computation for a limited subset of features over the two images: these algorithms are very efficient because of the low number of features and reliable since the features selected are well characterized, avoiding ambiguity problems in homologous search.

Dense stereo matching algorithms objective on the contrary is to generate a disparity map for each point of the common area between the two images, making them heavier in terms of computational cost but more accurate in terms of number of points of generated DTM.

Generally, dense matching is implemented by the use of *area based* algorithms, in which the computation of a similarity function[2] is performed taking into account the image conformation within a correlation window around the evaluated point.

As an example, one of the most common similarity function is the Normalized Cross Correlation (NCC) [20], in which the similarity between a point of coordinates $[i_1, j_1]^T$ on image I_1 and a point $[i_2, j_2]^T$ on image I_2 is evaluated by defining a *reference window* w_1 centered in $[i_1, j_1]^T$ and a *search window* w_2 centered in $[i_2, j_2]^T$. The reference window is shifted over the search window computing the NCC coefficient at each position as follows:

$$NCC = \frac{\sigma_{12}}{\sigma_1 \sigma_2} \frac{\sum_{r=1}^{R} \sum_{c=1}^{C} (w_1(r,c) - \mu_1) \cdot (w_2(r,c) - \mu_2)}{\sqrt{\sum_{r=1}^{R} \sum_{c=1}^{C} (w_1(r,c) - \mu_1)^2 \cdot \sum_{r=1}^{R} \sum_{c=1}^{C} (w_2(r,c) - \mu_2)^2}} \quad 2.19$$

Where *R* and *C* are the window dimensions along the two image frame axis, μ_1 , μ_2, σ_1, σ_2 are the grey values averages and standard deviations in the two windows and σ_{12} is the covariance between the grey values of the two windows.

The value of NCC coefficient ranges ideally between -1, when reference and search window are perfectly complementary, to 1, when the two windows are identical. In practice, due to image noise and to not perfect frontal parallel alignment, a preprocessing of images is needed. The main

[2] Given two image points, the similarity function assigns a numerical value, generally within a predefined range, to the concept of similarity between two image pixels.

advantage of NCC with respect to other well known similarity metrics, such as SAD or SSD [21], is that NCC is less sensitive to image noise and to illumination differences between the two images with the drawback of a higher computational cost.

Sub-pixel accuracy can be achieved by interpolating the correlation coefficients around the maximum region by means of smooth polynomial functions and computing analytically the position of the maximum.

2.3 Camera Calibration

The parameters of camera matrix, the distortion coefficients k_i and the orientation of the camera ($\boldsymbol{R}$, T) can be explicitly evaluated with calibration process, which is typically based on the acquisition of a set of images of a target with known features [22].

The Zhang's algorithm was developed for photogrammetric applications with low cost cameras equipment, and its main advantages are the robustness and the simplicity of calibration rig needed, since it consists of a planar chessboard (or regular grids of easily detectable features) printed on common paper.

The calibration process is based on the detection of chessboard corners (or feature detection) implemented with standard edge detection algorithm [23]: a set of images of calibration target in different positions provides sufficient information to compute a robust estimation of camera parameters. Since the corner coordinates extraction process is affected by error, the calibration algorithm computes a maximum likelihood estimation of camera parameters which minimize the overall back-projection error.

2.3.1 Notation

In the next sub-sessions the 3D points will be referred to as model points $M = [X,Y,Z]^T$ and their relative 2D image coordinates as $m = [u,v]^T$. Their homologous extension notation, according with the previous paragraphs notation, are indicated with $\widetilde{M}$ and $\widetilde{m}$ respectively.

The notation of $(K^{-1})^T$ or $(K^T)^{-1}$ will be abbreviated with K^{-T}.

2.3.2 Homography estimation

The first step in Zhang's algorithm consists in the estimation of the homography transformation which brings from *M* object coordinates to *m* image plane coordinates. The input data are the corner

coordinates extracted from images, and their physical coordinates on calibration chessboard plane. To provide this, we consider as the world reference frame a coordinate system attached to the calibration grid as illustrated in Figure 2-11, with the Z axis orthogonal to the chessboard plane.

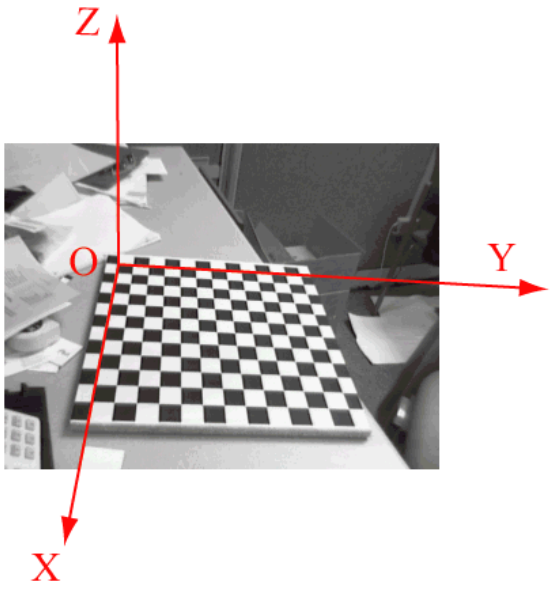

Figure 2-11 Coordinate reference for camera calibration algorithm

The adoption of a planar target and the above illustrated reference frame introduce an important simplification in camera parameter estimation process: since the third coordinate of the object point is always 0, the equation (2.20) can be written as:

$$s\begin{bmatrix} u \\ v \\ 1 \end{bmatrix} = \mathbf{K}[r_1 \;\; r_2 \;\; r_3 \;\; t]\begin{bmatrix} X \\ Y \\ 0 \\ 1 \end{bmatrix} = \mathbf{K}[r_1 \;\; r_2 \;\; t]\begin{bmatrix} X \\ Y \\ 1 \end{bmatrix} \qquad 2.20$$

In which r_i elements represents the columns of the rotation matrix R and the t vector represent the translation vector. The homography to be estimated is the 3 by 3 matrix $\boldsymbol{H} = \mathbf{K}[r_1 \;\; r_2 \;\; t]$.

For each image of the calibration target an homography matrix is estimated. Since corner image coordinates are noisy due to corner extraction process, a maximum likelihood estimation of $\boldsymbol{H}$ is performed basing on Levemberg-Marquard [24] algorithm.

The computed homographies are then combined together to extract the values of intrinsic parameters.

2.3.3 Camera parameters estimation

Writing homography matrix in column form as $\boldsymbol{H} = [h_1\ h_2\ h_3]$, the relation between $\boldsymbol{H}$ and camera parameters is:

$$[h_1\ h_2\ h_3] = \lambda \mathbf{K}[r_1\ \ r_2\ \ t] \tag{2.21}$$

For some scale factor λ. Since rotation matrix columns are forming an orthonormal base, from eq. (2.21) we get the following relations:

$$\begin{aligned} h_1^T \mathbf{K}^{-T}\mathbf{K}^{-1}h_2 &= 0 \\ h_1^T \mathbf{K}^{-T}\mathbf{K}^{-1}h_1 &= h_2^T \mathbf{K}^{-T}\mathbf{K}^{-1}h_2 \end{aligned} \tag{2.22}$$

Since a homography has 8 degrees of freedom (nine entries defined up to a scale factor), and there are 6 camera orientation parameters (three for rotation and three for translation), it provides a constraint for two intrinsic parameters: at least 3 homographies are needed to solve for the five intrinsic parameters: α, β, γ, u_0 and v_0. Since input data are affected by random noise, a larger set of images is needed to improve calibration accuracy.

A first closed form solution of the problem is provided analytically solving an over determined system of homogeneous equations built introducing the matrix:

$$\boldsymbol{B} = \mathbf{K}^{-T}\mathbf{K}^{-1} \equiv \begin{bmatrix} B_{11} & B_{12} & B_{13} \\ B_{21} & B_{22} & B_{23} \\ B_{31} & B_{32} & B_{33} \end{bmatrix}$$

$$= \begin{bmatrix} \frac{1}{\alpha^2} & -\frac{\gamma}{\alpha^2\beta} & \frac{v_0\gamma - u_0\beta}{\alpha^2\beta} \\ -\frac{\gamma}{\alpha^2\beta} & \frac{\gamma^2}{\alpha^2\beta^2} + \frac{1}{\beta^2} & -\frac{\gamma(v_0\gamma - u_0\beta)}{\alpha^2\beta^2} - \frac{v_0}{\beta^2} \\ \frac{v_0\gamma - u_0\beta}{\alpha^2\beta} & -\frac{\gamma(v_0\gamma - u_0\beta)}{\alpha^2\beta^2} - \frac{v_0}{\beta^2} & \frac{(v_0\gamma - u_0\beta)^2}{\alpha^2\beta^2} + \frac{v_0^2}{\beta^2} + 1 \end{bmatrix} \tag{2.23}$$

which is symmetric, and the vector v_{ij}:

$$v_{ij} = [h_{i1}h_{j1},\ h_{i1}h_{j2} + h_{i2}h_{j1},\ h_{i2}h_{j2}, h_{i3}h_{j1} + h_{i1}h_{j3},\ h_{i3}h_{j2} + h_{i2}h_{j3},\ h_{i3}h_{j3}]^T$$

where $h_i = [h_{i1}\ h_{i2}\ h_{i3}]^T$ is the *i*-th column vector of matrix H, such that:

$$h_i^T \mathbf{K}^{-T}\mathbf{K}^{-1}h_j^T = h_i^T \mathbf{B} h_j^T = v_{ij}^T b \tag{2.24}$$

b is a 6 vector built with matrix **B** elements, defined as follows:

$$b = [B_{11}\ B_{12}\ B_{22}\ B_{13}\ B_{23}\ B_{33}\ ]^T$$

The two constraints expressed in (2.22) can be so expressed with the two following homogeneous equations:

$$\begin{bmatrix} v_{12}^T \\ (v_{11} - v_{22})^T \end{bmatrix} b = 0 \qquad 2.25$$

If *n* homographies have been computed from *n* calibration target images, a $2n \times 6$ matrix $\boldsymbol{V}$ can be built stacking the (2.25) equations together. The elements of the vector b can be evaluated solving the homogeneous system:

$$\boldsymbol{V}b = 0 \qquad 2.26$$

If $n \geq 3$, the system is over-determined and has in general a unique solution *b*, obtained as the eigenvector of $\boldsymbol{V}^T\boldsymbol{V}$ associated to its smallest eigenvalue, easily computable by means of SVD decomposition. Once *b* is known, the intrinsic parameters can be easily computed from the $\boldsymbol{B}$ matrix definition (2.23) and the extrinsic for each image from (2.21), as specified in [22].

2.3.4 Maximum likelihood estimation

The solution to (2.26) gives a minimization in algebraic distance between image points and back-projected points, which is not physically meaningful. A better result in camera calibration is given through maximum likelihood estimation obtained minimizing the functional:

$$\sum_{i=1}^{n}\sum_{j=1}^{m}\left\|m_{ij} - \hat{m}(\mathbf{K}, \boldsymbol{R}_i, t_i, M_j)\right\|^2 \qquad 2.27$$

In which m_{ij} is the detected feature of the calibration pattern point M_j on the *i*-th image and $\hat{m}$ is the back projection of calibration pattern feature $M_j$to image *i* through a pinhole camera built with the estimated intrinsic (**K**) and extrinsic ($\boldsymbol{R}_i$, t_i) parameters.

The minimization of eq. 2.27 is a nonlinear minimization problem which can be solved by means of Levemberg-Marquardt algorithm. Such iterative method, which provides a minimization of the geometric distance between the back-projected points and the image points, needs an initial guess which can be provided with the procedure described in the previous paragraph.

The LM algorithm can be also extended to the evaluation of the distortion coefficients simply by introducing them in 2.27, obtaining the functional:

$$\sum_{i=1}^{n}\sum_{j=1}^{m}\left\|m_{ij}-\hat{m}(K,k,R_i,t_i,M_j)\right\|^2 \qquad 2.28$$

Where k is the distortion coefficient vector, containing both the three radial and two tangential distortion coefficients.

The Zhang calibration algorithm provides an estimation of the uncertainties on the extracted values for each camera parameter, computed as the parameter variation corresponding to three times the standard deviation of the re-projection errors.

2.4 Stereo calibration

The calibration procedure described in 2.3 can be easily extended to the estimation of the extrinsic parameters ($\boldsymbol{R}$,T) of a stereo imaging system. If the calibration target is acquired simultaneously by the two cameras, the single camera calibration data can be easily combined to get information about the mutual positioning of the two cameras.

Assuming the calibration target simultaneously imaged by the two cameras, for each stereo couple of images, the single camera calibration procedure computes the extrinsic parameters of the camera referred to the target reference frame: $\boldsymbol{R}_l$ and T_l for the left camera, $\boldsymbol{R}_r$ and T_r for the right camera.

Given a 3D point P in the target reference frame, it will be expressed in the two cameras frames as: $P_l = \boldsymbol{R}_l P + T_l$ and $P_r = \boldsymbol{R}_r P + T_r$, respectively. The coordinates of the point expressed in the two reference frames are related by $P_l = \boldsymbol{R}^T(P_r - T)$. Combining these equation and solving for $\boldsymbol{R}$ and T we obtain:

$$\begin{aligned}\boldsymbol{R} &= \boldsymbol{R}_r(\boldsymbol{R}_l)^T \\ T &= T_r - \boldsymbol{R}T_l\end{aligned} \qquad 2.29$$

Applying the 2.29 to each i-th stereo couple of target images provides a ($\boldsymbol{R}_i$, T_i) couple which differs from the others, due to image noise and rounding errors: stereo calibration procedure assumes the mean values as initial approximation, which is then provided as input for a maximum likelihood iterative procedure which minimize the re-projection error for both camera views.

3. STC experimental setup for stereo validation

3.1 Introduction

The SIMBIO-SYS Stereo Camera (STC) will provide a three-dimensional reconstruction of Mercury surface. The generation of a DTM of the observed features is based on the processing of the acquired images and on the knowledge of the intrinsic and extrinsic parameters of the optical system.

The new stereo concept developed for STC needs a pre-flight verification of the capabilities to obtain elevation information from stereo couples: for this reason, a stereo validation would be helpful to give a much greater confidence with the developed instrument design.

The main idea for STC stereo validation setup is to simulate in laboratory (indoor) the acquisition process that will provide the stereo couples in flight, scaling-down the 3D surface reconstruction problem and applying it to a known target: from the on-flight observation of a planetary surface from an altitude greater than 400 km to the observation of a small stone sample at about 1 meter distance. To simplify the reproduction of the observing geometry of the instrument the case study is limited to the SC operations at periherm, without loss of generality.

In this chapter a description of the design activity of the experimental setup for the preliminary validation of STC stereo reconstruction capabilities is provided.

3.2 Concept design

The main idea for STC stereo validation setup is to simulate in laboratory (indoor) the acquisition process that will be used to acquire the stereo couple in flight. To provide this, the observing geometry has to be scaled down, by shortening the observing distances and by scaling down the observed object features: couples of images of a target with known features have been used to get depth map of the observed surface.

Since in-flight STC have to deal with source/target placed at infinity, in lab an auxiliary optical system, that allows the indoor acquisition of images of a known target, is needed: a lens (collimator) that collimates the light rays coming from the target has been foreseen.

A functional breadboard (FB) of STC, realized mainly with commercial components, was developed and has been used in the setup instead of the STC flight model to make a preliminary analysis of the setup performance.

The set of acquired images have been processed to get a 3D reconstruction of the target [25]: depth information retrieved from stereo reconstruction and the known features of the target allows to get an evaluation of the stereo system's performance both in terms of horizontal resolution and vertical accuracy.

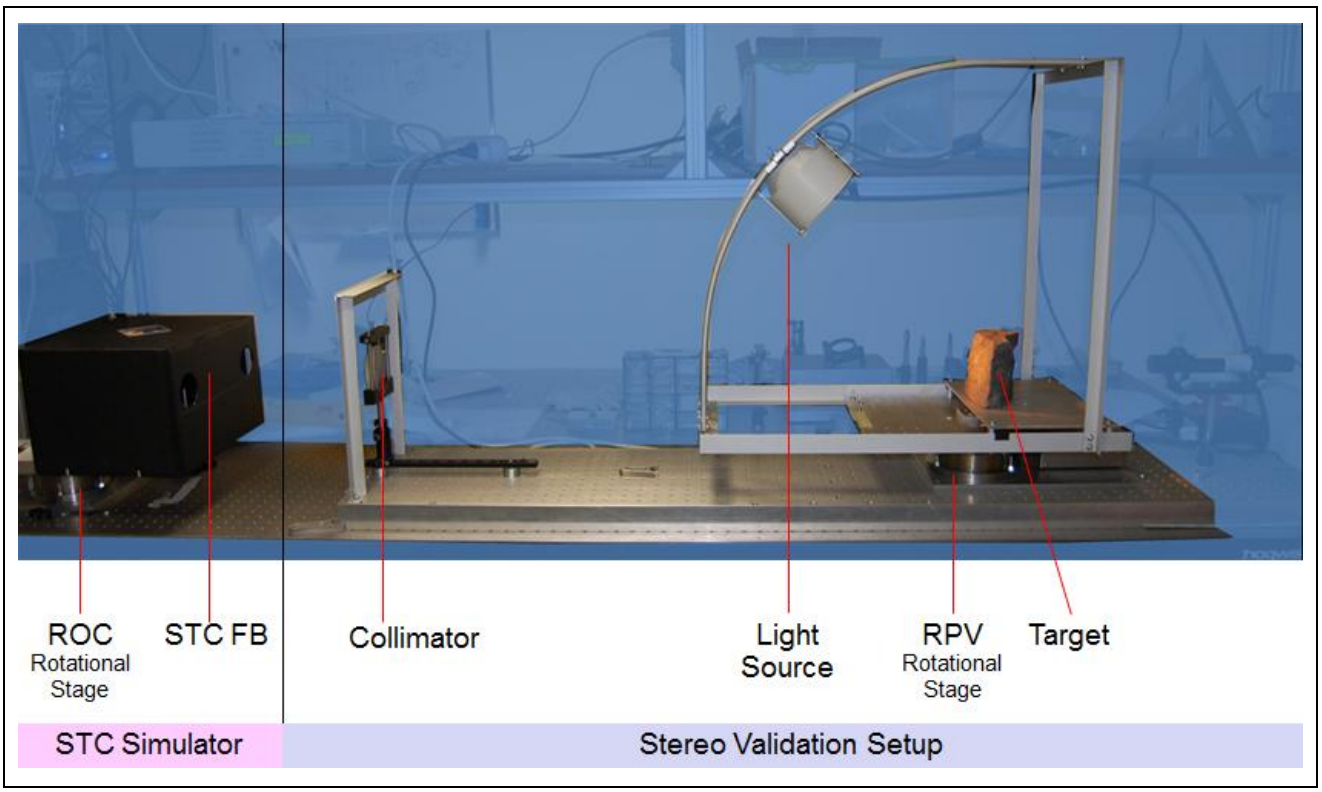

Figure 3-1: STC Stereo Validation Setup assembled and aligned with STC FB in UPD laboratory. The setup main components are illustrated and indicated with red lines.

The experimental setup can be divided in two principal parts:

- The Stereo Validation Setup (SVS), which simulates the observing geometry of the stereo telescope,
- the STC Simulator, which simulates the main STC FM optical and geometrical characteristics.

The stereo validation setup, as illustrated in the right side of Figure 3-1 and in the block diagram at Figure 3-2, is composed by:

- A collimator lens locked to the optical bench,
- a motorized rotation stage which simulates the different STC optical channels points of view (RPV),
- a target positioned on the RPV rotation stage,
- a light source rotating with the target itself, in order to provide constant lighting conditions during the acquisition performed by both the channels.

The STC Simulator is composed by:

- A motorized rotation stage which selects the observing channel (ROC)
- the STC Functional Breadboard (STC FB).

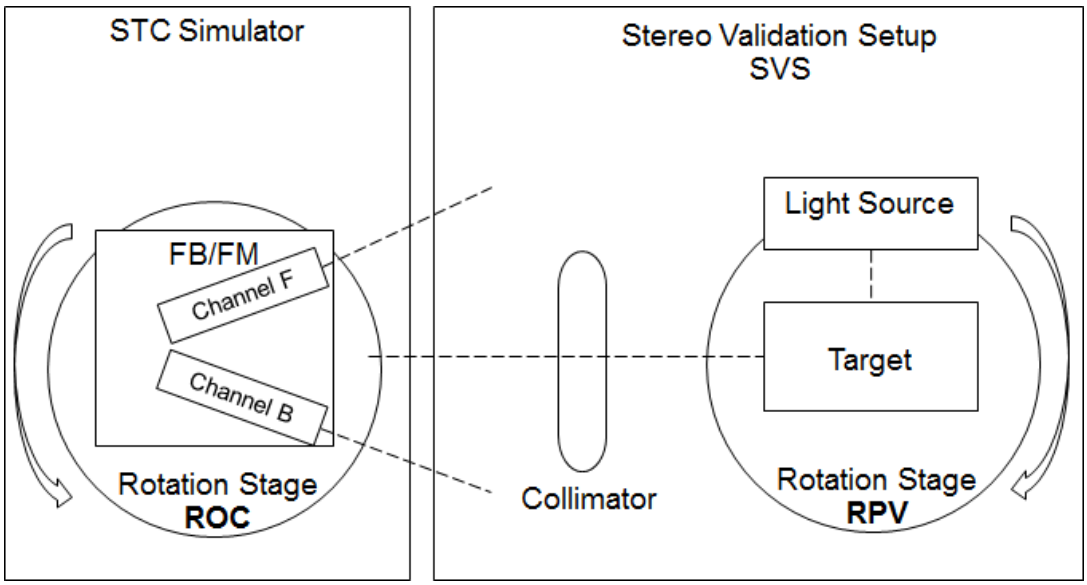

Figure 3-2: STC BB – Stereo Validation Setup: block diagram. On the left side there is the portion relative to the STC simulator; on the right there is the portion relative to the target simulator.

To verify the 3D reconstruction capabilities of the STC FB applied to the stereo validation set-up, the lab target surface has to be known with an accuracy higher than the precision required on the 3D reconstruction itself. For this, the rock samples accurately selected to be used as lab targets have been measured with a suitable accurate 3D laser scanner. The analysis on requirements scaling will be treated in 3.2.4.

To reproduce the observing conditions at periherm and to obtain stereo couples of the target, the samples have been positioned on the RPV rotation stage and rotated by ±20° with respect to the direction of the active camera.

The pair of obtained images have been used as input to a stereo reconstruction pipeline to generate the DEM of the observed area. Depth information obtained with stereo reconstruction has been compared with the laser scanner measurements of the samples to evaluate the system performance. The accuracy of the 3D reconstruction depends on the accuracy of the knowledge of intrinsic and extrinsic parameters of the optical system.

3.2.1 STC Functional breadboard

The STC Functional Breadboard (FB) (see Figure 3-3 and Figure 3-4) is an opto-mechanical system designed to replicate the main STC optical and mechanical features; it is realized mainly with commercial components. The STC FB has been used only in UPD laboratory to perform preliminary tests with the Stereo Validation Setup and to define and test a procedure for stereo validation activity.

STC FB consists of two identical optical heads, each one consisting of an objective with essentially the same optical features and performance of STC and a CCD camera, mounted on a platform. The two heads optical axes are tilted of 40° in the horizontal plane one with respect to the other. The platform and the two mounted optical heads are coupled to a motorized rotation stage (ROC) that can be rotated around a vertical axis. The ROC rotation axis nominally passes through the crossing point of the two optical head axes, as shown in Figure 3-4.

STC optics is simulated by a couple of achromatic doublets. A preliminary optical design has been done choosing only commercial optical components; an improved configuration has also been designed using custom ad-hoc lenses: the latter allows to reach better optical performance. The commercial lens system has been adopted as a preliminary configuration for the first experimental phase, because of faster procurement time.

The main goal of STC FB is to get a functional reproduction of STC, with two separate channels oriented at ±20° with respect to a central axis (corresponding to the SC Nadir direction). The system is equipped with a reference cube, needed to measure with high accuracy instrumentation the cameras orientation and the alignment of the rotation axis.

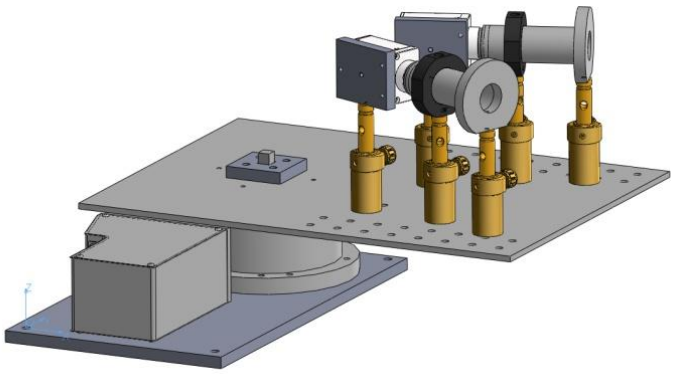

Figure 3-3: STC Functional Breadboard.

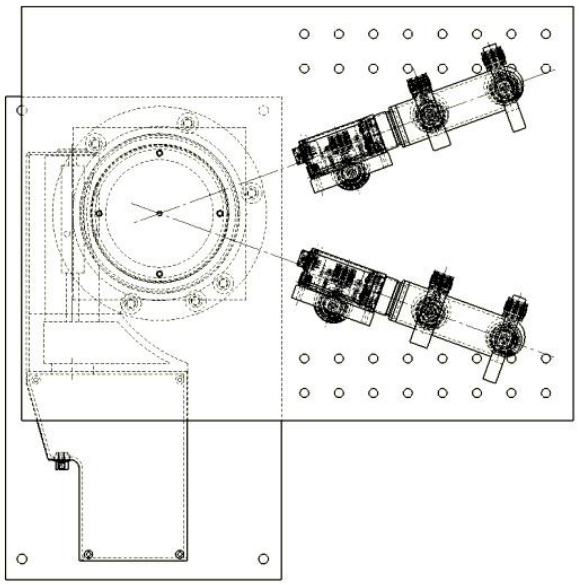

Figure 3-4: STC Functional Breadboard: the two head optical axes cross on the rotation stage axis.

As a naming convention to facilitate the calibration data management, the two optical channels will be referred to as *Forward* looking channel and *Backward* looking channel. Referring to the direction bisecting the two optical axis of the instrument as the Nadir direction, the two channel names are defined as follows: looking at the STC FB from the upside (Figure 3-4), the Forward looking channel is the optical channel disposed at +20 deg clockwise w.r.t. the Nadir direction, and the Backward looking channel is the one disposed at -20 deg clockwise w.r.t. the Nadir direction.

This naming convention is not suitable for on-orbit acquisitions since the SC will be subjected to periodic flip-over exchanging the versus of its trajectory.

3.2.2 Stereo validation setup

The STC stereo validation setup (see Figure 3-5) is a combination of optical and mechanical components that allow the indoor reproduction of the instrument observing conditions.

The experimental setup is composed by a single lens which has the function of bringing at a finite distance the source for illuminating the STC FB, by the lens holder, by a motorized rotation stage, by a stone sample (used as target for the stereo reconstruction) and by a light source.

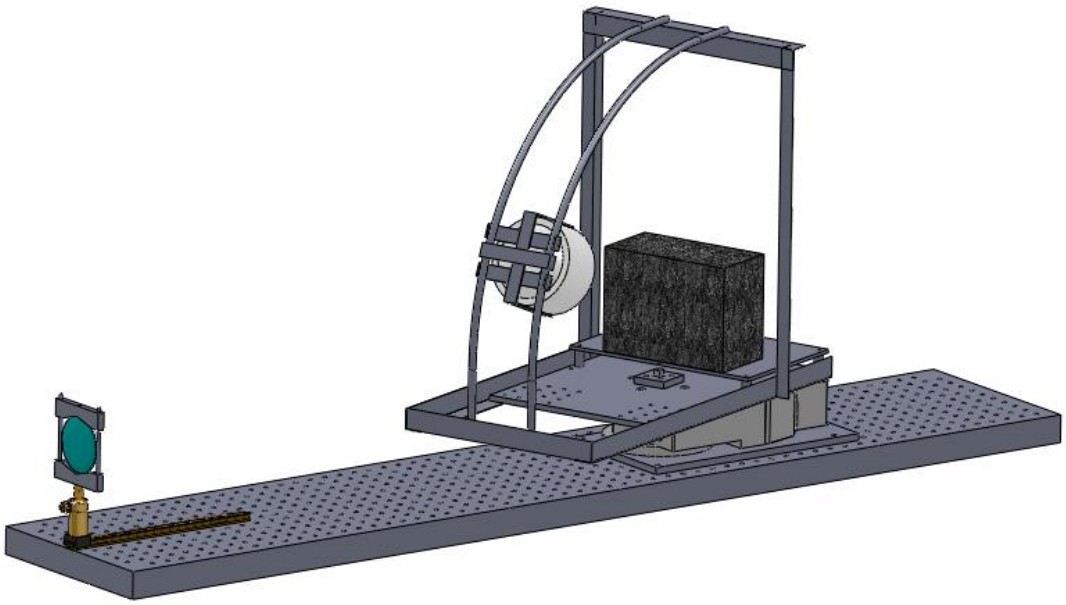

Figure 3-5: Setup for STC indoor stereo validation.

All the STC Stereo Validation Setup components are arranged over a custom, movable, optical bench: this solution facilitate the integration and alignment of the setup with the stereo imaging device that needs to be validated.

The target rotation stage plate is equipped with a custom reference cube, positioned over the rotation axis as showed in Figure 3-5, needed in alignment phase and to check the accuracy and repeatability of target rotation stage.

The light source is a narrow spot halogen lamp mounted over a custom rail system which rotates together with target support plate.

3.2.3 Reproduction of the observing geometry

The main goal for the stereo validation activity is to validate the stereo reconstruction capabilities of the instrument in at least one point of the SC trajectory: for the sake of simplicity the periherm case has been considered.

As described in 1.5, a selected area of the planet surface is imaged from two different points of MPO's trajectory by the two STC optical channels: the first time by the channel looking forward w.r.t. the SC trajectory and the second time by the backward looking one, as illustrated in Figure 3-6.

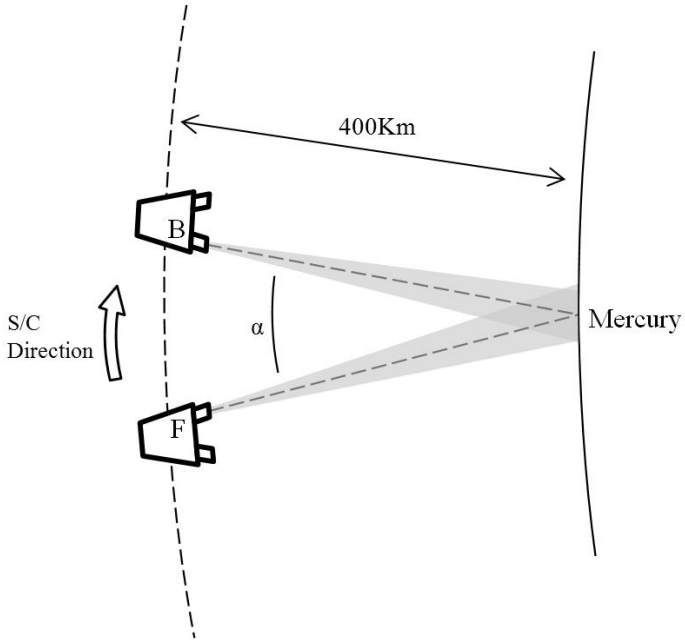

Figure 3-6: STC observing geometry at periherm. The same area of planet surface is imaged before by the Forward looking channel and in a second moment by the backward looking channel.

The stereo imaging system can be thought as a classical two cameras imaging system with the forward looking camera (*F*) related to the backward looking camera (*B*) by a rotation *R* and a translation *T*. The introduction of a collimator lens between the cameras and the target, involves a scaling of the observing geometry: a new imaging system is obtained, composed by the two cameras, combined with the collimator lens, related by the same rotation matrix *R* and by a new translation vector *T'* obtained by scaling *T*.

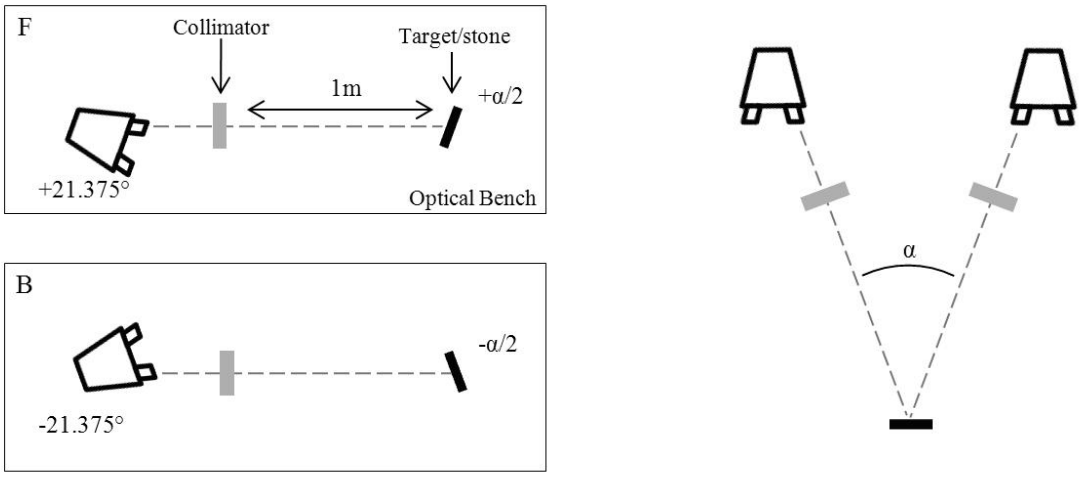

Figure 3-7: Reproduction of the observing geometry at periherm by means of Stereo Validation Setup. (a) Optical bench view, (b) equivalent stereo baseline representation.

Considering the case of observations at periherm, the imaging geometry can be easily reproduced over the optical bench by rotating both the instrument and the observed target as represented in Figure 3-7 (a). Through the coordinated actuation of the two rotation stages: the rotation of the STC FM (or STC FB) provides the alignment of the optical channels with the optical axis of the collimator lens (ROC). The rotation of the target plate (RPV) reproduces the stereo angle α, which is function of the SC attitudes in *F* and *B* positions and of the nominal ±21.375 degrees stereo angle of the two STC's panchromatic filters w.r.t. Nadir direction.

Considering the MPO's mean orbital parameters, the computed stereo angle α at periherm is 50.227 deg: the observing geometry can be reproduced over the optical bench by rotating the target plate (RPV rotation stage) of +25.114 deg and -25.114 deg to simulate the angle of incidence of the panchromatic chief ray w.r.t. Mercury surface of *F* and *B* channels respectively.

3.2.4 Requirements

The scaling of the focusing distance of the target from hundreds of kilometers to about one meter involves a scaling on the footprint of the two cameras and consequently of their horizontal resolution. As a consequence of target scaling the requirement in terms of DTM vertical resolution needs to be scaled down by the same ratio.

The required accuracy on the knowledge of the target (spatial resolution and height) and the size of the area that is imaged by the lab camera are related to the focal length of the collimator. In fact, the

ratio between the observable feature size (vertical accuracy) in the lab images and in the in-flight ones are proportional to the ratio between the collimator focal length and the distance of the spacecraft from the Mercury surface during the acquisition. As an example, when the SC is at periherm the observing distance is about 400 km: considering a collimator focal length of 1 m the scale ratio will be 1:400000. So, considering that the area of the Mercury surface that will be imaged by STC is approximately 40x20 km^2, the corresponding target area that has to be imaged with this setup in the lab is of approximately 10×5 cm^2, referring to the panchromatic filter f.o.v..

In the considered case of 1 m collimator focal length, to obtain the spatial resolution corresponding to that one of STC, it is easy to calculate that it is necessary to know the target surface with an accuracy of 105 μm and 170 μm for the spatial resolution and the height, respectively. This accuracy is within the resolution possibilities of the available laser scanner.

Parameter	**STC**	**SVS/STC**	**SVS/FB**
f (mm)	95 mm	~168 mm	~135 mm
Pixel size (μm)	10	10	9.9
Sensor size (pixel)	880×400	880×400	640×480
f.o.v. (deg)	5.3°×2.4°	3°×1.36°	2.7°×2°
Target distance	400 km	~1600 mm	~1300 mm
Target Footprint	37×17 km^2	92×42 mm^2	67×50 mm^2
Horizontal resolution	50 m/pix	~105 μm/pix	~105 μm/pix
Vertical accuracy	80 m	170 μm	170 μm

Table 3-1: STC and Stereo Validation setup main features and requirements. The first column is referred to STC's features and requirements at periherm, while the second and third column are referred to the SVS applied to STC FM and STC FB respectively. The sensor size and the f.o.v. are referred to the panchromatic channel of the instrument. The target footprint and the target distance are referred to periherm observing conditions.

In Table 3-1 a detailed list of the parameters characterizing the imaging systems is reported: the first column is referring to the on-flight operations with STC at periherm, the second and third column are referring to the SVS applied to the STC FM and to the STC FB respectively. The focal lengths in SVS cases are considered as the nominal focal lengths of the optical system composed by the STC optical sub-channels combined with the collimator lens. The nominal values have been obtained by means of ray-trace software analysis, both in STC FM and in STC FB case (see 3.3).

The target observing distance in SVS case is a nominal mean value of the distance between the image plane of the equivalent pinhole model of the optical systems and the target positioned over the focusing area of the collimator lens.

The vertical accuracy requirement in SVS case has been computed by preserving the ratio between the horizontal resolution and vertical accuracy requirements of STC at periherm.

3.3 Optical design

The optical system was designed by means of a ray-tracing analysis, with the aim of finding the commercial components more suitable to the application. In addition, custom optical elements were considered in order to guarantee higher optical performances.

3.3.1 STC functional Breadboard

The aim in STC Functional Breadboard design was to reproduce the main STC optical features with commercial components.

In order to obtain a system with equivalent focal length of 95mm, basing on ray tracing software analysis results, it was found that the best compromise between design complexity and optical performance could be reached with the combination of two achromatic doublets.

The optical performance has been evaluated in terms of spot radius RMS value and of diffraction ensquared energy (DEE).

A CCD camera with 9.9×9.9 μm pixel was chosen to preserve the same pixel footprint of STC.

The wavelength range considered for the analysis is between 660 and 740 nm, representing the central portion of the bandwidth of the panchromatic filter of STC.

3.3.1.1 Commercial optics

Several commercial lens sets have been tested in order to select the one guaranteeing the best performance: Figure 3-8 shows the index obtained scaling the spot RMS radius by the pixel size for a field placed at the center of the f.o.v. (blue bars), and at the edge (red bars). The best performance is obtained with a couple of EDMUND 32492 achromatic doublets.

Figure 3-9 and Figure 3-10 show the spot radius RMS and diffraction ensquared energy (DEE) values respectively, obtained with a preliminary optical analysis.

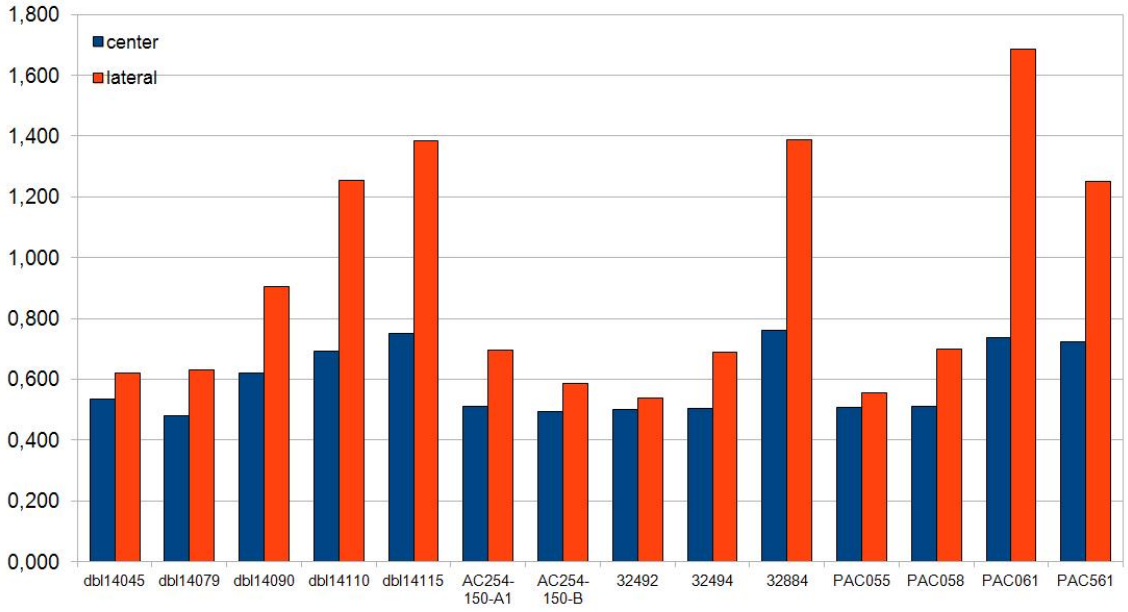

Figure 3-8: RMS Radius over pixel size index for the selected lenses.

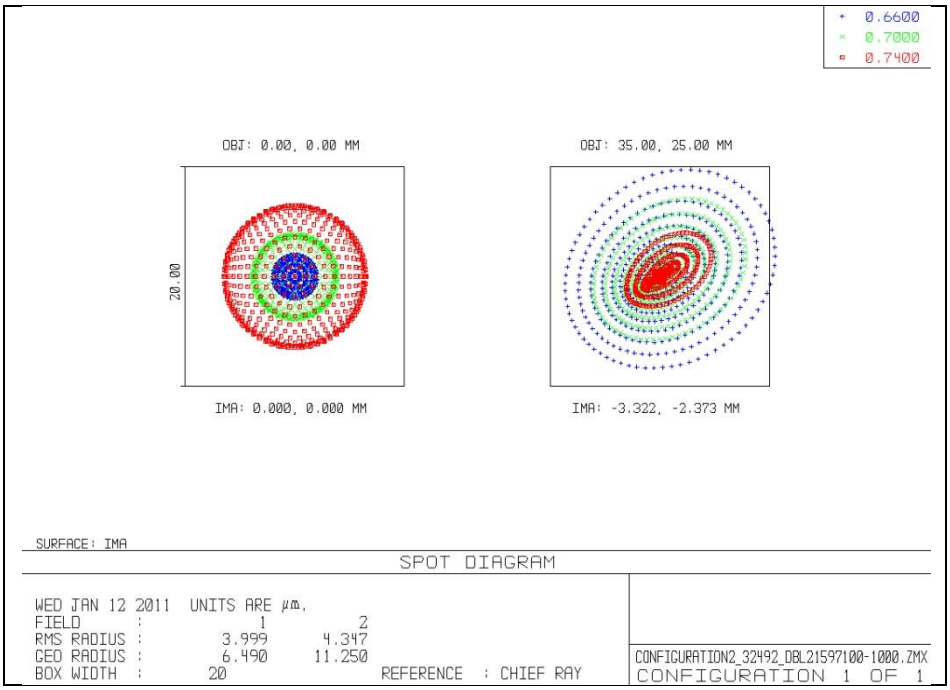

Figure 3-9: STC's functional breadboard: Spot diagram with commercial lenses. The one on the left is the spot diagram at the center of the f.o.v. the one on the right is the spot diagram at the edge of the field. Both spot diagram are compared with a square box of 2×2 pixel size.

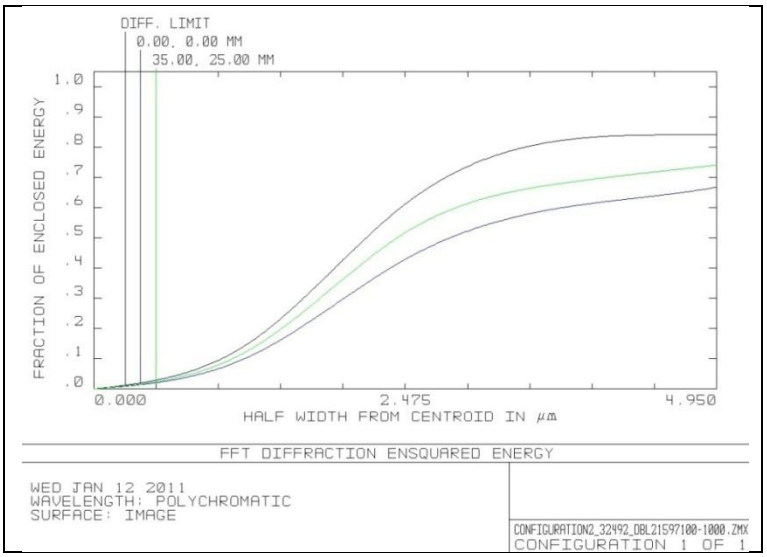

Figure 3-10: STC's functional breadboard: DEE with commercial lenses for the center and the edge of the f.o.v..

3.3.1.2 Custom optics design

Custom optical components were designed for the STC FB to improve the optical performance. The obtained doublets are the result of an optimization both on lenses surface curvatures and glasses. From the RMS radius and from the DEE index analysis shown in Figure 3-11 and Figure 3-12, an improvement of the system performance is noticeable.

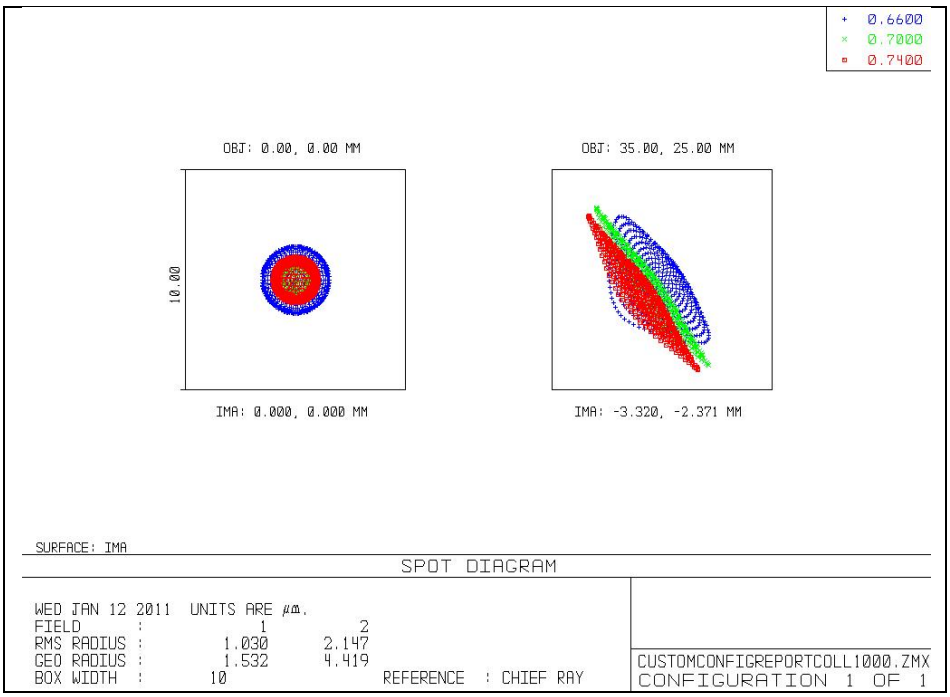

Figure 3-11: STC's functional breadboard: Spot diagram with custom lenses. . On the left the spot diagram at the center of the F.o.v., on the right at the edge. The spot diagrams are compare with a square box having the pixel size dimension.

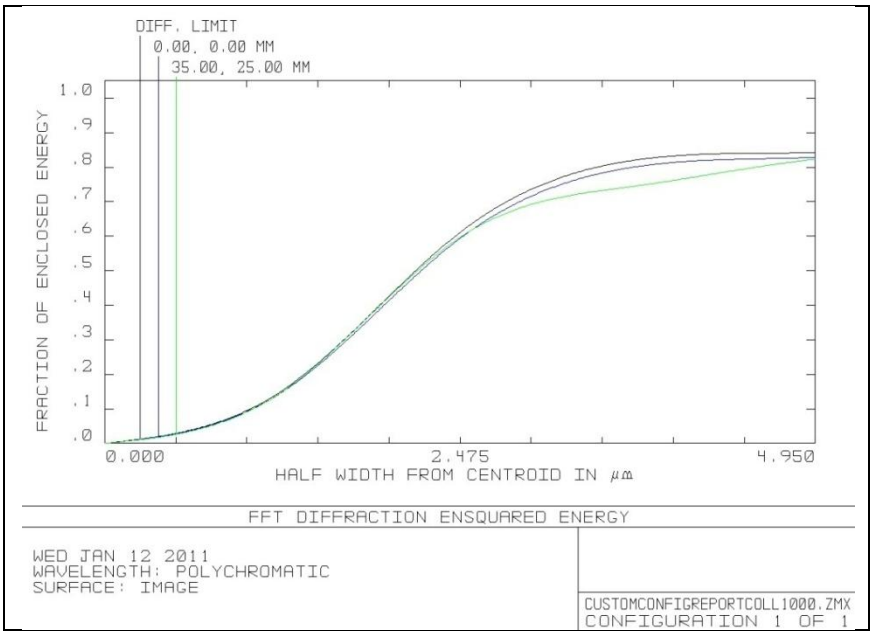

Figure 3-12: STC's functional breadboard: DEE with custom lenses at the center and edge of the f.o.v..

3.3.1.3 Tolerance Analysis

A second phase of the system optical design was dedicated to the analysis of mechanical tolerances for the FB lenses mounting. The two variables considered are the distance between the first lens and the detector (D1), and between the two doublets (D2), shown in Figure 3-13.

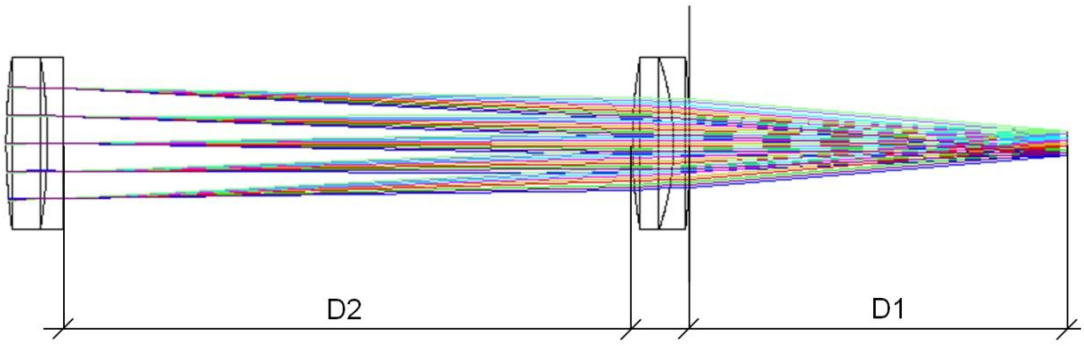

Figure 3-13: STC FB optical layout. The sensor plane is on the right. D1 and D2 are the variables considered for lens mounting tolerance analysis.

The graphs below show the variation of the spot RMS value corresponding to variations of the D1 and D2 distances for a spot centered within in f.o.v. (blue) and at the edge of f.o.v. (red).

Figure 3-14 Spot RMS radius versus CCD-lens 1 (D1) distance variation for the commercial lens set configuration.

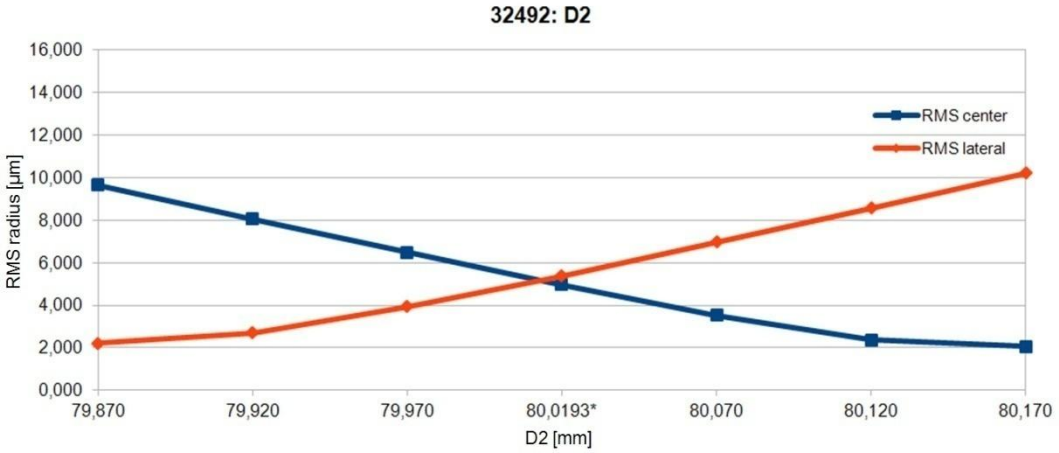

Figure 3-15: Spot RMS radius versus lens1-lens2 (D2) distance variation for the commercial lens set configuration.

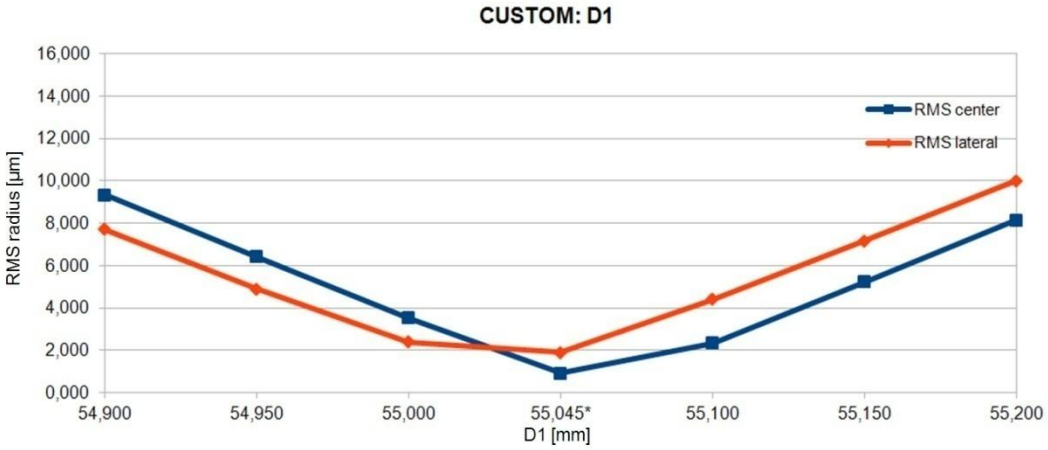

Figure 3-16: Spot RMS radius versus CCD-lens (D1) distance variation for the custom lens set configuration.

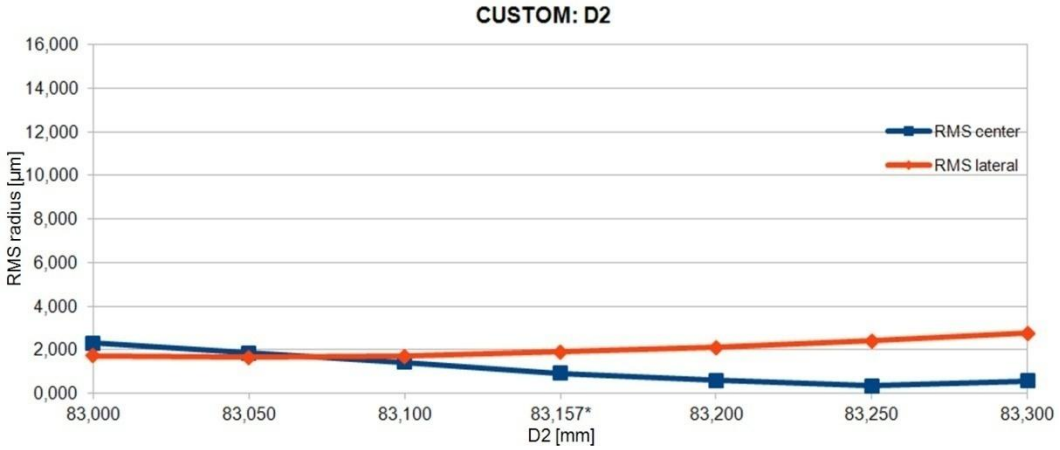

Figure 3-17: Spot RMS radius versus lens1-lens2 (D2) distance variation for the custom lens set configuration.

The graphs show that in order to minimize the optical performance degradation during the alignment of the FB optical elements, a mounting accuracy of 0.1mm is sufficient. In the case of custom lenses the system is still less sensitive to mounting error.

3.3.2 Stereo Validation Setup

The only optical component of the Stereo Validation Setup is the collimator lens, which has the key function of bringing the focusing distance from infinite to a distance compatible with optical bench available dimensions. Optical analysis using ray-trace software proved that a simple achromatic doublet is sufficient to provide collimation of light rays coming from the observed target without affecting sensitively the instrument optical performance. The lens selected for this purpose is a JML DBL21597 achromatic doublet with nominal focal length of 1000 mm.

3.3.3 Optical Analysis

Several optical analyses were made over the whole optical system in order to better understand the system behavior in operating conditions. For the analysis, in order to sample the whole field of view, 9 fields, one at the center and the others at the edges of the f.o.v., have been considered.

To simulate the operative STC condition, i.e. the same target area is viewed by the two sub-channels with an angle of ±20° with respect to the nadir direction, the target will be rotated of ±20° with respect to the optical axis of the camera heads. The optical system has been optimized for the operative case in which the target is rotated by ±20° with respect to the system optical axis. The 9 adopted reference fields are symmetrical in the reference system of the target, since we consider to

view the same target area by two different directions; however they are not symmetrical with respect to the collimator and cameras optical axes because of the different position along the direction of the optical axis. In fact, the reference points closer to the collimator have a greater angle of incidence, and thus bigger aberration, than those far from the collimating lens.

3.3.3.1 SVS with STC FB

Figure 3-18 to Figure 3-23 show the results of the optical analysis in the case of commercial and custom lenses, considering the spot diagram and the RMS error versus field. From the performed analysis, it can be noticed a progressive deterioration of the optical performance moving from the center to the image edges. This is due to the fact that the target is tilted with respect to the plane perpendicular axis, introducing a defocus in the images. It can also be noticed that the spots are not symmetric for the reason previously described The overall performance is better in the case of custom design optics, anyway, in both configurations, it is acceptable for the aim of the tests. In fact the RMS spot radius is far less than 10 µm (which is the size of the detector pixel) over the whole f.o.v..

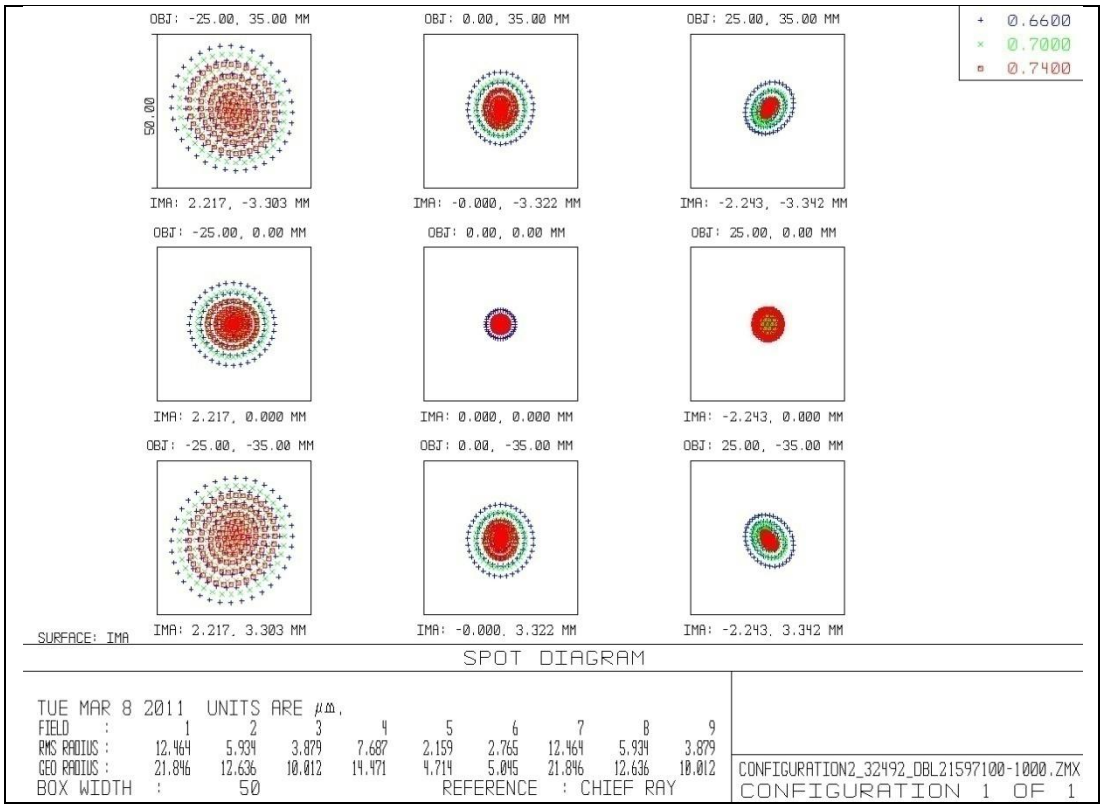

Figure 3-18: STC FB with stereo validation setup. Spot diagrams for the configuration with commercial lenses and target rotated at +20° w.r.t. optical axis of the FB's active channel.

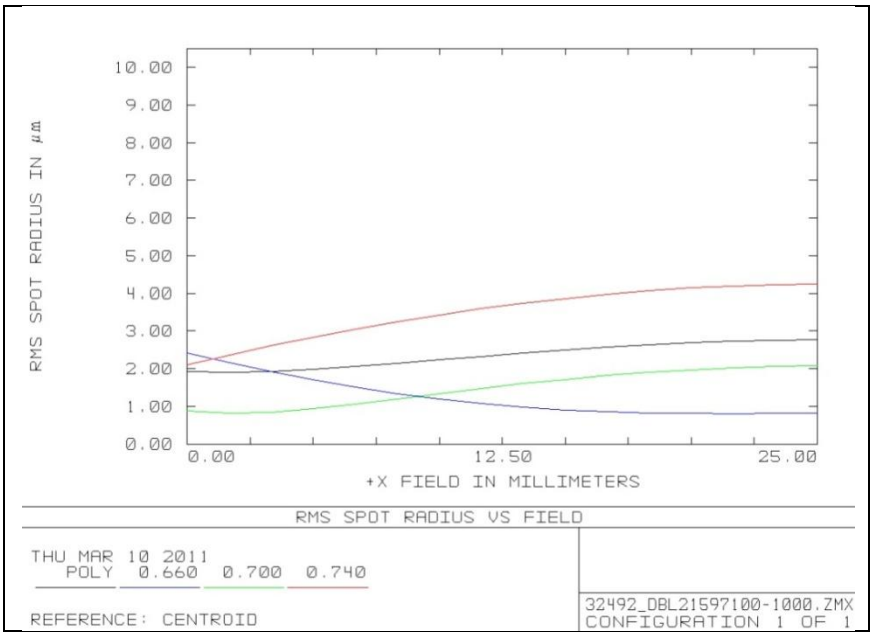

Figure 3-19: STC FB with stereo validation setup. RMS spot radius versus +X field for the configuration with commercial lenses and target rotated at +20° w.r.t. optical axis of the FB's active channel.

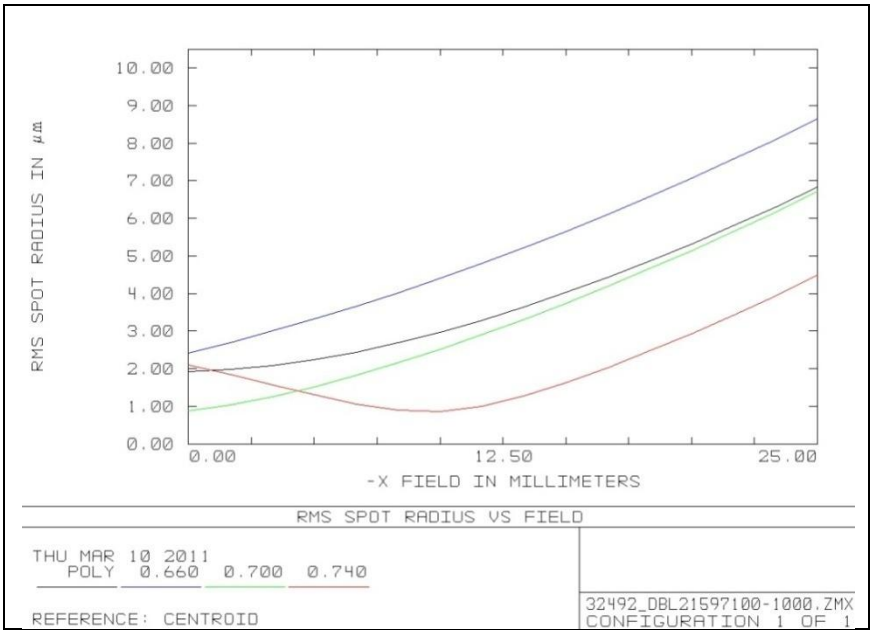

Figure 3-20: STC FB with stereo validation setup. RMS spot radius versus –X field for the configuration with commercial lenses and target rotated at +20° w.r.t. optical axis of the FB's active channel.

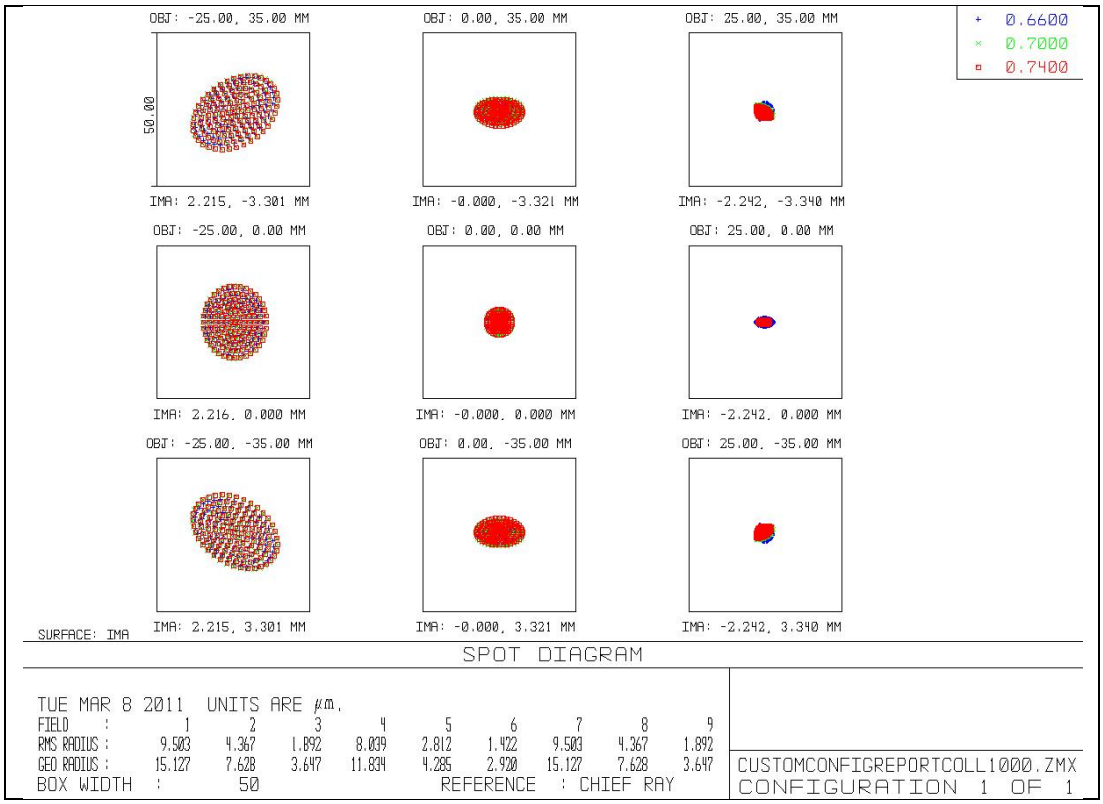

Figure 3-21: STC FB with stereo validation setup. Spot diagrams for the configuration with custom lenses and target rotated at +20° w.r.t. optical axis of the FB's active channel.

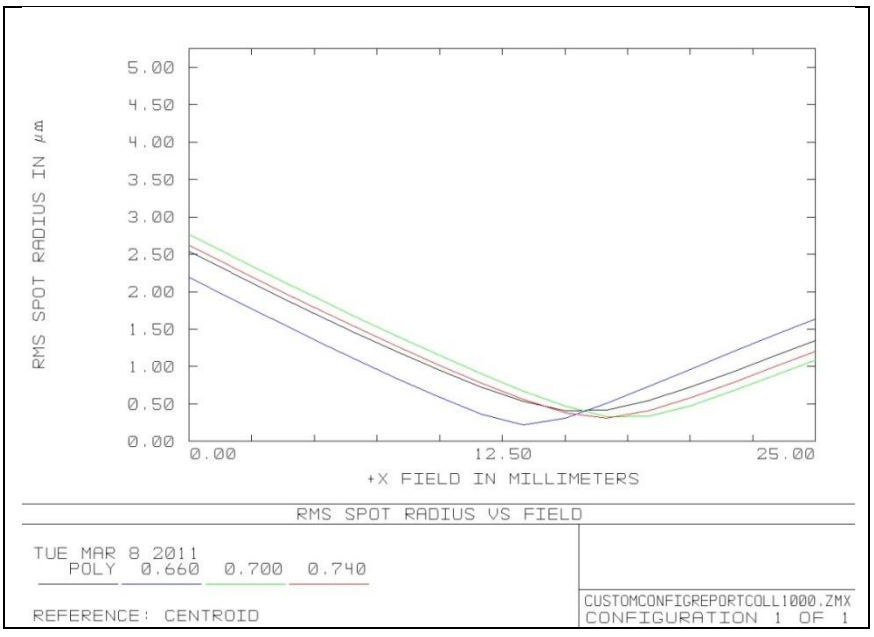

Figure 3-22: STC FB with stereo validation setup. RMS spot radius versus +X field for the configuration with custom lenses and target rotated at +20° w.r.t. optical axis of the FB's active channel.

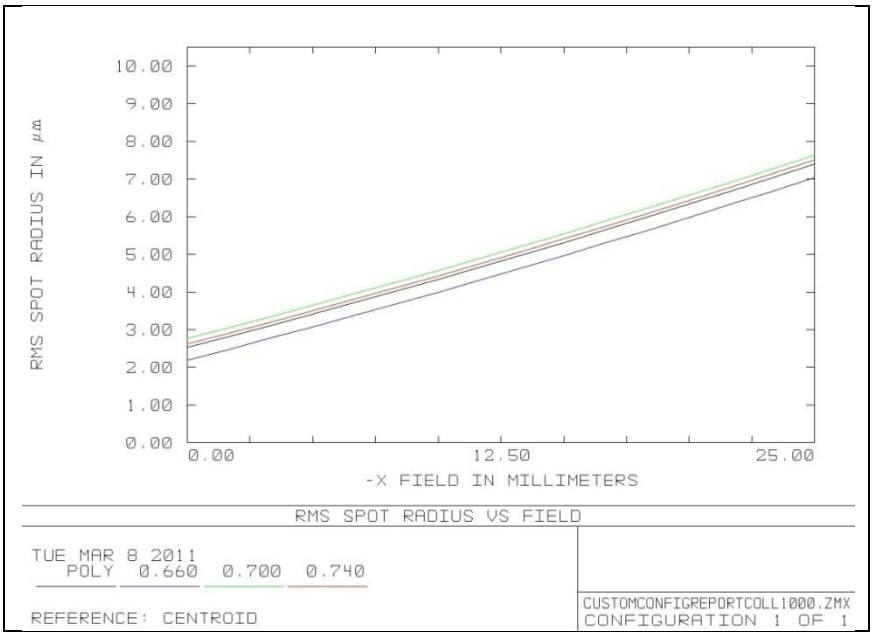

Figure 3-23: STC FB with stereo validation setup. RMS spot radius versus –X field for the configuration with custom lenses and target rotated at +20° w.r.t. optical axis of the FB's active channel.

3.3.3.2 SVS with STC FM

The same analysis have been performed in case of SVS aligned with STC optical channels, obtaining similar results: in Figure 3-24 and Figure 3-25 we can see the spot diagram of STC without collimator lens and aligned with collimator lens respectively. It can be noticed that the spot diagram shape is not significantly affected by collimator lens contribution. The envelope of the spots is always within the 10 µm pixel size.

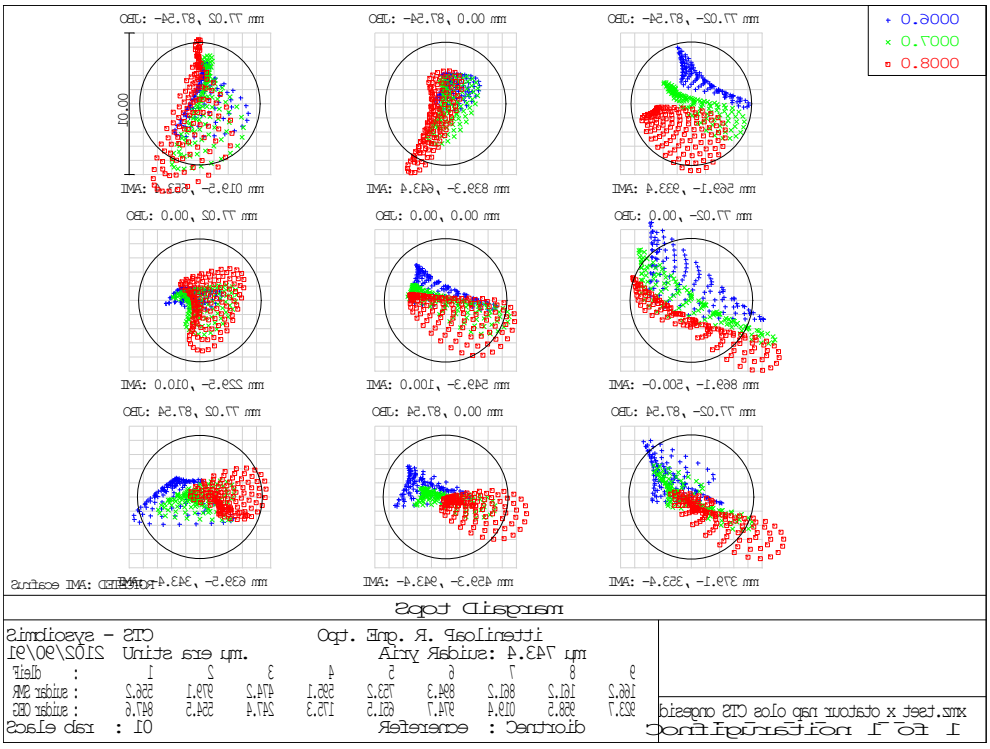

Figure 3-24: STC spot diagram. The spot rms radius is always within 10 µm, corresponding to the instrument pixel size.

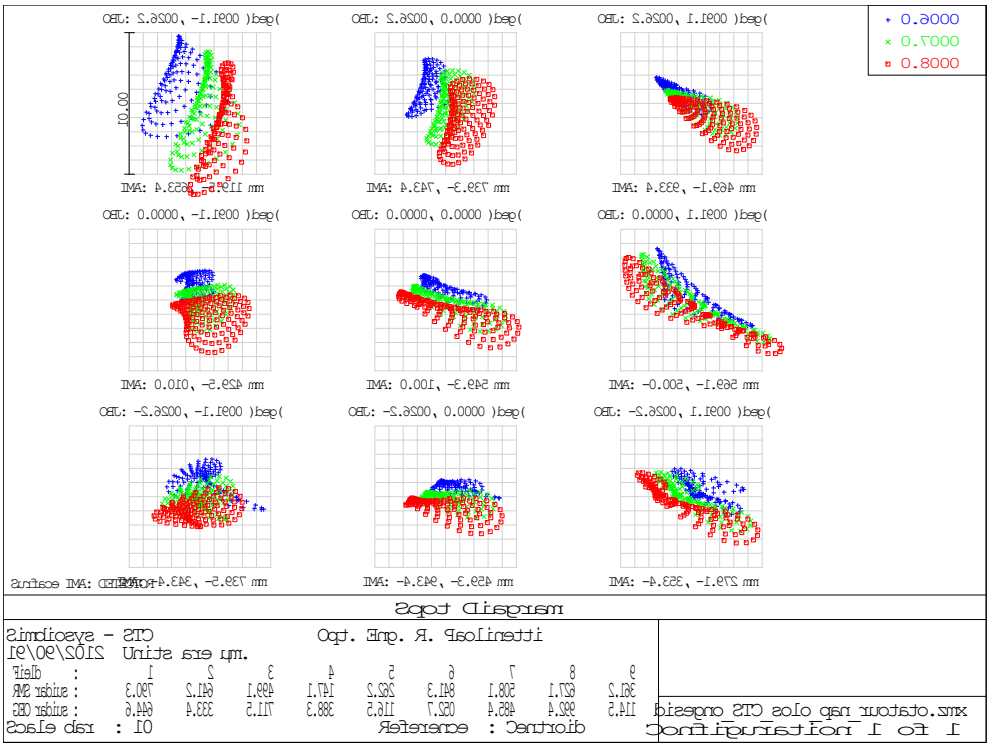

Figure 3-25: STC aligned with SVS. The spot rms radius is within pixel size of 10 µm.

3.4 Setup components

3.4.1 Optics

3.4.1.1 Cameras

The cameras selected for the STC FB are two AVT Stingray F-033B monochromatic cameras with pixel size of 9.9×9.9 μm^2 and a resolution of 640×480 pixels (Figure 3-26, Figure 3-27). The cameras can be controlled from a standard PC through a IEEE 1394b (Firewire 800) port.

Figure 3-26: Stingray F-033B monochromatic camera and sensor relative response vs wavelength curve.

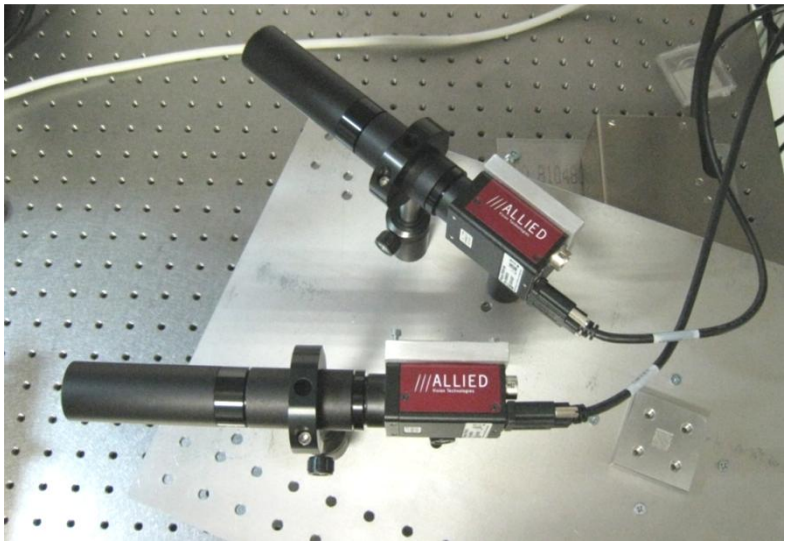

Figure 3-27: Stingray F-033B monochromatic cameras mounted over the STC FB rotating support plate with custom optics lens assembly.

3.4.1.2 Lenses

The optical system for each channel is given by the combination of two achromatic doublets with 25.4 mm diameter, selected in ray-trace analysis phase, described in 3.3, and mounted on a lens holder tube.

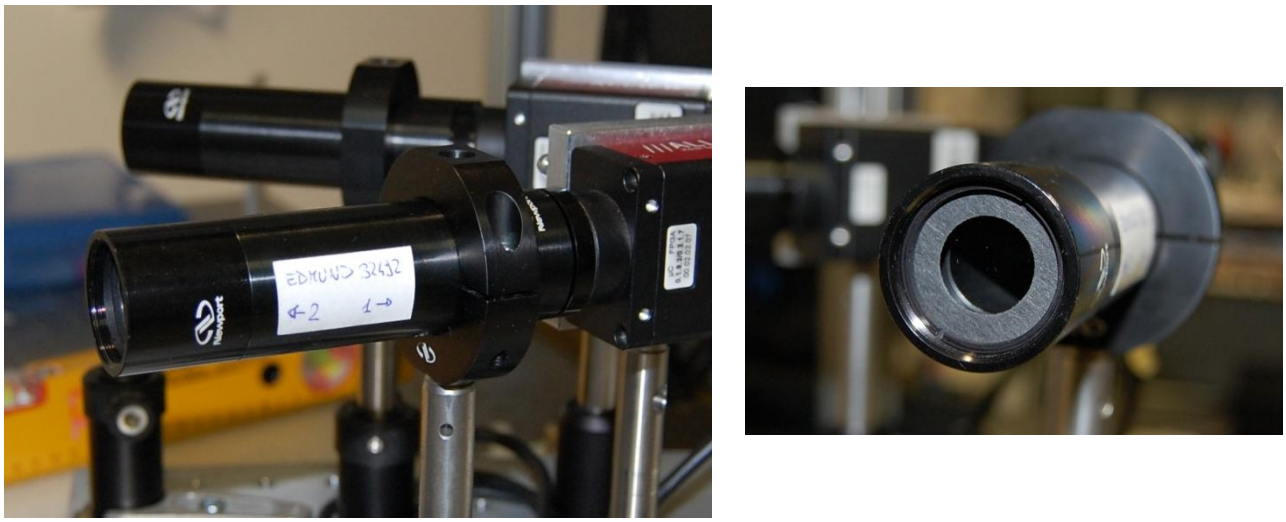

Figure 3-28: STC FB commercial optics assembled and aligned with F-033B cameras.

The collimator lens is a JML DBL21597 achromatic doublet with nominal focal length of 1000 mm mounted over the STC SVS optical bench by means of an ad-hoc lens holder.

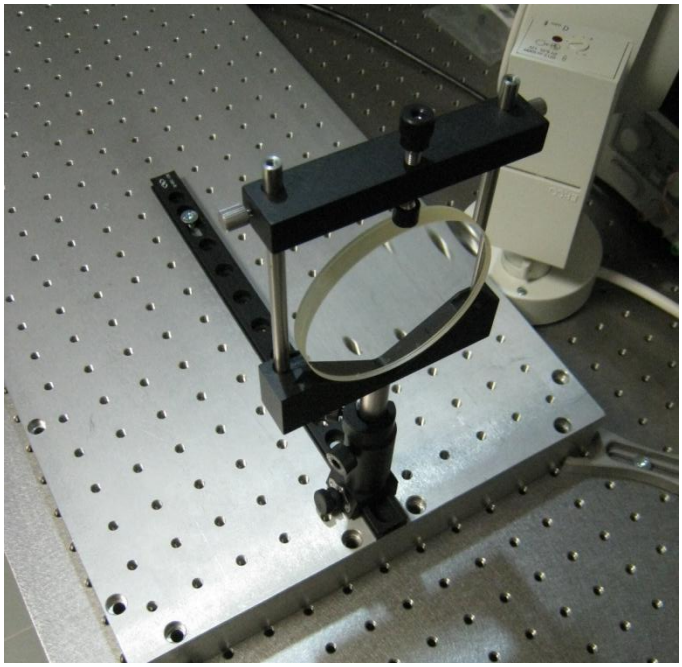

Figure 3-29: Collimator lens mounted over the STC SVS movable optical bench. The lens holder is mounted over a linear rail to facilitate the collimator lens focusing adjustment.

The optical elements of both the SVS and of the STC FB have been tested by means of interferometric analysis, in order to preliminary evaluate the optical performance of the individual components and to verify the behavior of the system with respect to the theoretical performance obtained with ray-trace analysis.

3.4.2 Rotation stages

The ROC and the RPV units are equipped with a Newport© RV-120-PEVB6 rotation stage with a guaranteed absolute accuracy of 0.01° and motion resolution of 0.001°.

The positioning error of the rotation stages could affect the accuracy of the stereo reconstruction, being responsible of the reproduction of the stereo geometry of the system. As an example, a positioning error of 0.005° of the RPV stage produces an image shift of about 1 pixel, that could affect calibration accuracy in stereo calibration phase. The uncertainty in extrinsic parameters estimation could be compensated anyway applying bundle adjustment algorithms to improve DTM accuracy.

The positioning accuracy of the rotation stages has been verified in setup alignment phase [29]; the rotation angle has been measured by a theodolite through auto-collimation on the reference cubes mounted over the rotation axes of the ROC and RPV. The positioning error has been defined as the difference between the desired angle and the measured angle. The standard deviations of the measurements resulted to be always below 1.7 arcsec, corresponding to a maximum positioning error of about 0.0014 deg.

The rotation stage is controlled by a Newport ESP301 Motor controller that provides both motion control and motor power supply. The controller can be managed using the front panel or by remote through a PC using a standard USB or RS232 connection.

3.4.3 Light source

The light source is an intensity adjustable halogen lamp with narrow spot, mounted over a custom curve rail system illustrated in Figure 3-30.

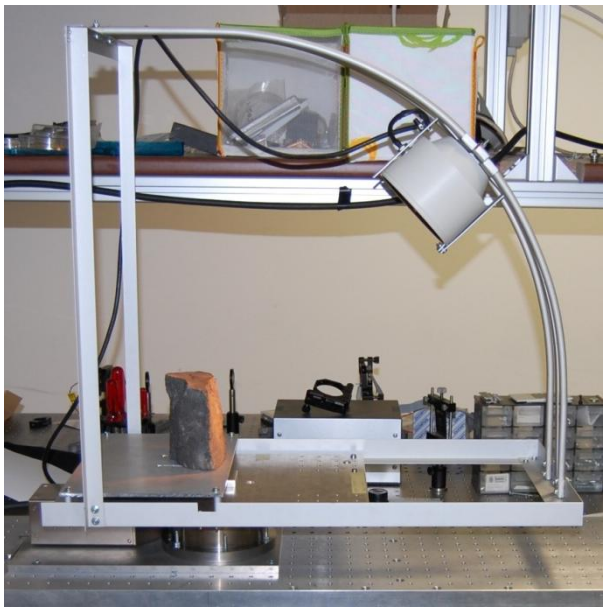

Figure 3-30: STC SVS light source mounted over the custom curve rail system. The lamp support is fixed to the target support plate, providing the same light incidence angle for both left and right (or forward and backward) images of stereo couples.

The curve support has been designed to reproduce all the possible light incidence angles between 0° and 90°, referring to possible Sun rays incidence angles w.r.t. the Mercury surface when the SC is at periherm. As illustrated in Figure 3-31, we can refer to the optical bench as the SC orbital plane when inclination is 90°: considering a reference frame fixed to Mercury, the Sun describes an orbit which is perpendicular to the SC orbit plane. As a consequence the rail system for lamp support has been designed to be perpendicular to the rotation plane of the target support.

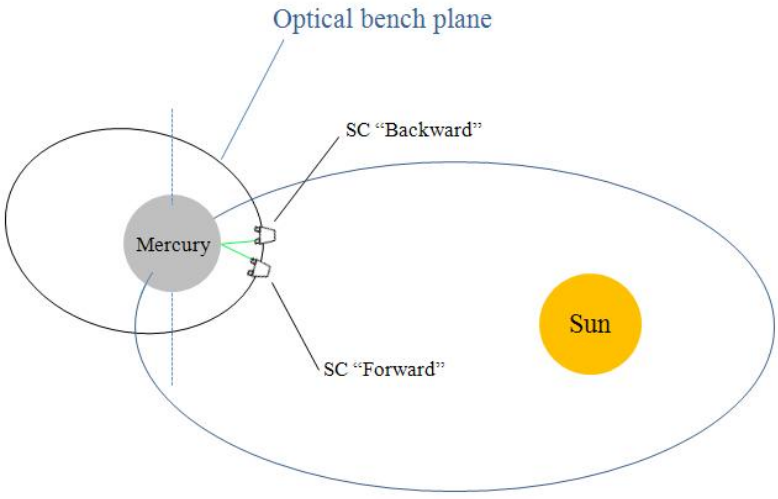

Figure 3-31: Illustration of the SC orbit and planet orbit around the Sun. When the instrument is working indoor with SVS the SC orbital plane corresponds to the optical bench plane.

Figure 3-32 shows a set of images of the same area of a Basalt stone, acquired in lab with the STC FB at three different light support angles.

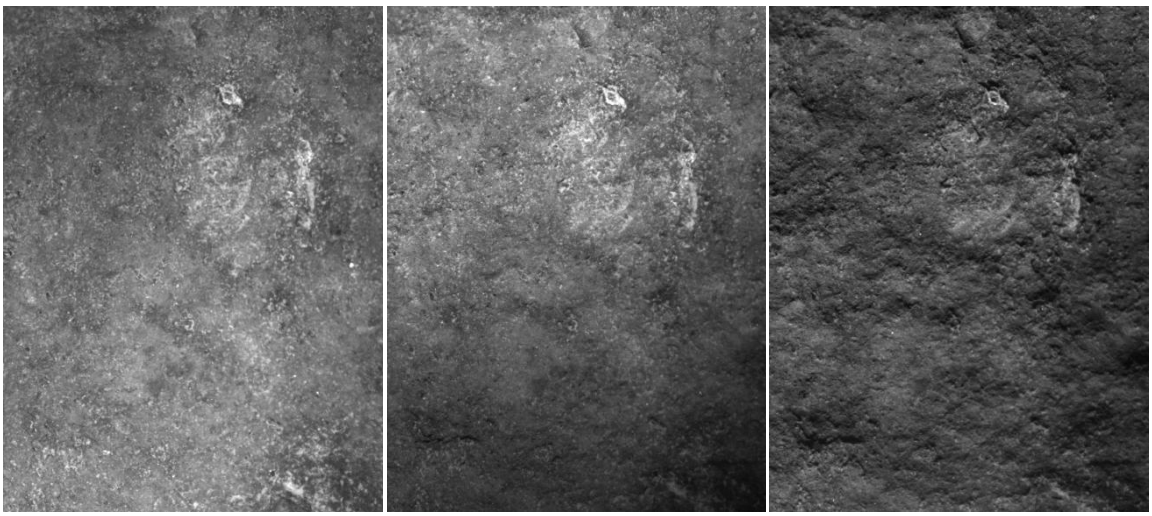

a. b. c.

Figure 3-32: Image of the same area of Basalt stone sample obtained from STC SVS with ST FB at three different light support angles: (a) 0°, (b) 30° and (c) 60°.

3.4.4 Targets

The target selected for the 3D reconstruction test consists in a set Anorthosite, Basalt stones and concrete samples with different morphologic and reflective properties. The rock samples of Basalt and Anorthosite considered for the stereo validation tests (see Figure 3-33 and Figure 3-34) have been chosen because of the characteristics of their albedo function, which should resemble the one of the rocks we expect to observe on the Mercury surface.

The concrete sample is provided with a series of markers which have been used to facilitate the alignment process between the stereo DTM and the laser scanner measure.

Figure 3-33: Basalt stone sample.

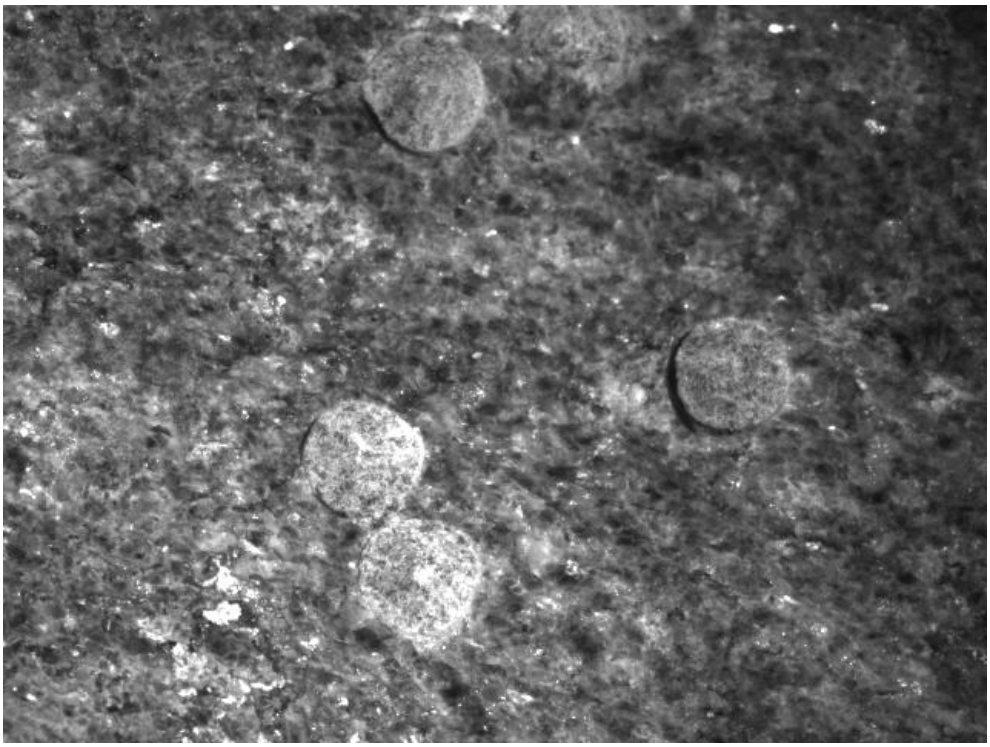

Figure 3-34: Anorthosite stone sample.

Figure 3-35: Concrete sample.

3.4.4.1 Target altitude map

In order to check the consistency of the stereo reconstruction, the stereo DTM has to be compared with a reference DTM of the rock samples. This has been provided by scanning by a CAM2® FaroArm Platinum (see Figure 3-36), a portable Coordinate Measurement Machine (CMM) with a Z axis accuracy of 0.02 mm.

The data collected by the instrument are in the form of a cloud of points convertible in a mesh of equidistant points on a XY grid. The rock samples have been measured several times, so to obtain different grids of the same surface: the measures obtained have been then merged together to return a surface with a larger number of measured points. Finally, the reference surface (see Figure 3-38) has been produced by interpolation on a grid with point spacing of 0.05 mm, i.e. about half of the image resolution (105 μm/pix, see Table 3-1).

Figure 3-36: CAM2® FaroArm Platinum laser scanner. Coordinate Measurement Machine (CMM) with a Z axis accuracy of 0.02 mm.

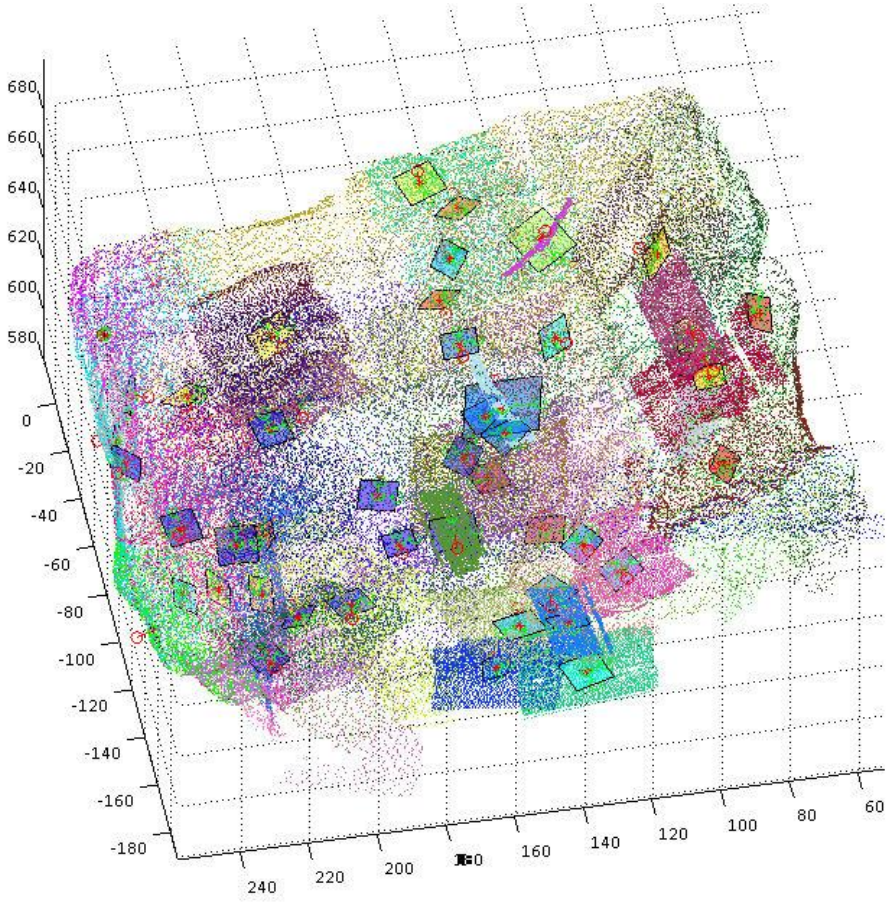

Figure 3-37: 3D plot of the grid of points obtained with laser scanner from Anorthosite stone sample.

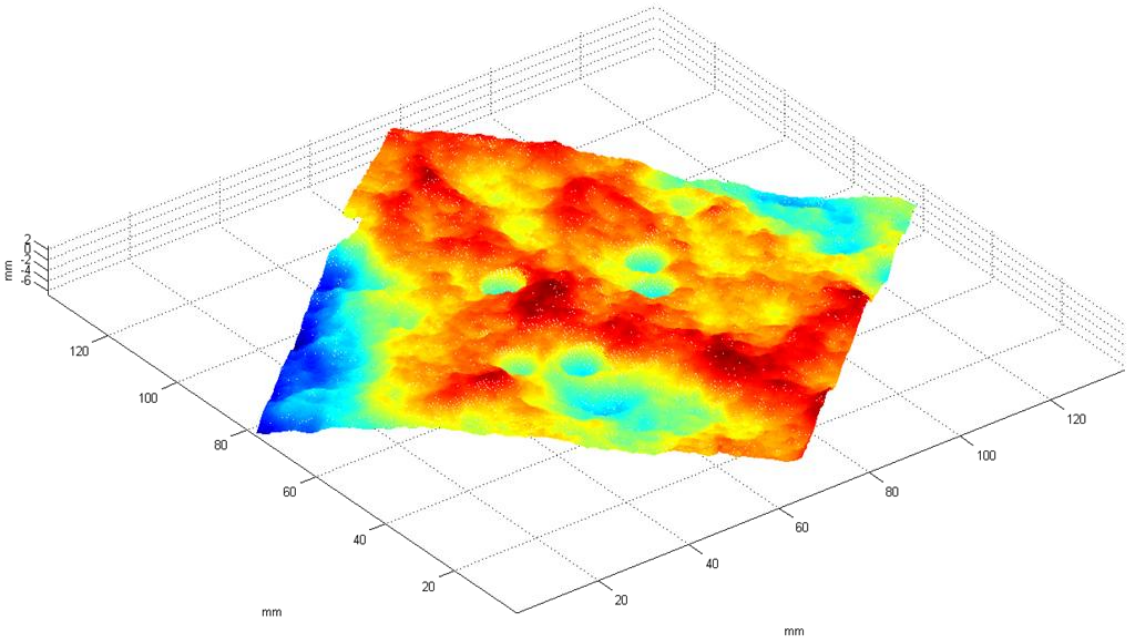

Figure 3-38: 3D plot of the grid of points obtained with laser scanner from Anorthosite stone sample after measure overlapping.

3.5 Assembling and alignment

All the setup components have been assembled and aligned over the optical bench in order to satisfy the following conditions[29]:

- Rotation axes are perpendicular w.r.t. the optical bench plane,
- The collimator optical axis intersects the two rotation axes of the rotation stages and it is parallel w.r.t. the horizontal plane,
- Collimator focus is positioned over the target plate rotation axis,
- STC FB Forward and Backward optical channels axes can be aligned with the collimator optical axis by a STC FB ROC rotation.

The alignment operations have been performed with the support of: a laser beam, used as reference, a high accuracy theodolite and the reference cubes mounted over the two rotation stages.

3.6 Operation modes

The STC Stereo Validation Setup has been designed to operate both with STC FB and with STC FM. This section describes how the setup has to be configured in the two different operation modes.

3.6.1 Configuration with STC functional Breadboard

In this working configuration the STC SVS support plate is positioned over the optical bench and aligned with the STC FB as showed in Figure 3-39. The setup is controlled by a workstation which manages the rotation stages controller and the fire-wire cameras controller through a custom designed software application.

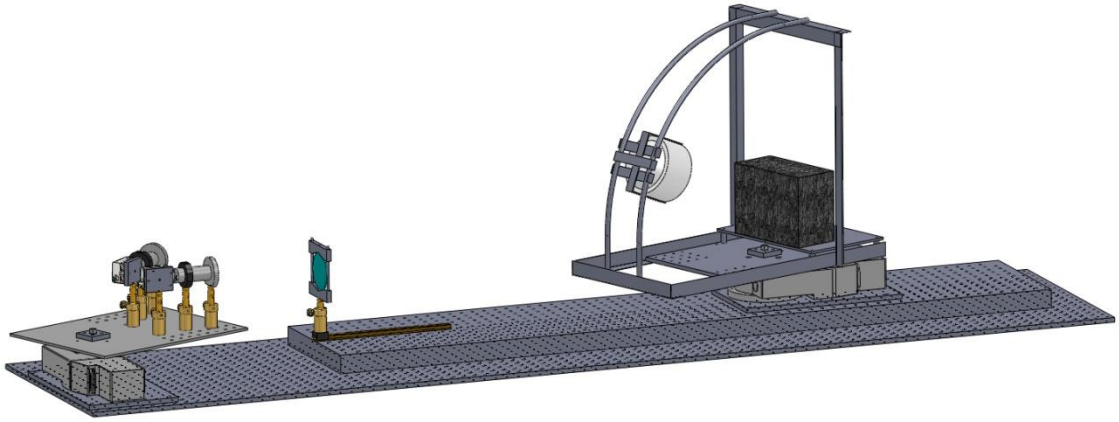

Figure 3-39: SVS aligned with STC Functional Breadboard over optical bench.

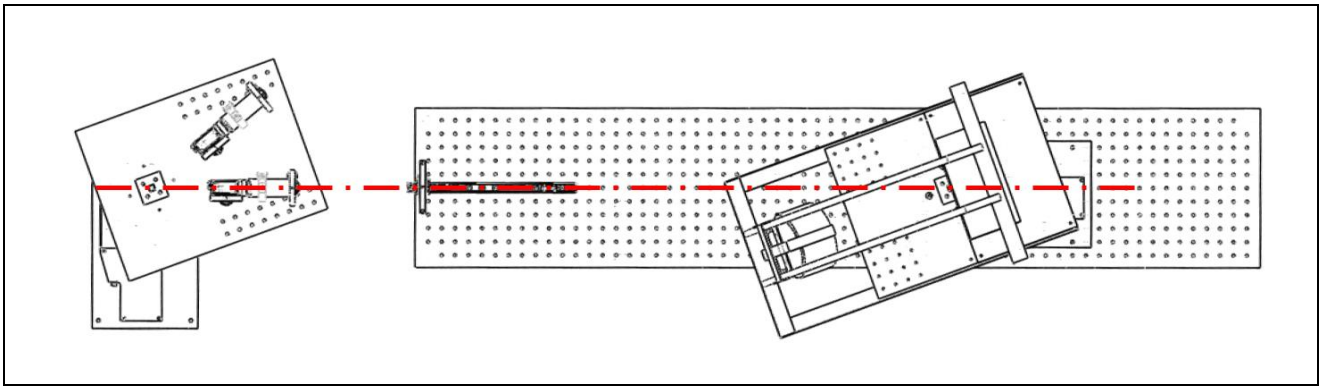

Figure 3-40: Stereo Validation Setup aligned with STC FB in Backward channel configuration, top view. The two elements are aligned such that the optical axis of the Backward looking channel coincide with collimator lens optical axis and intersect the two rotation axis.

In Figure 3-40 a top view of the SVS aligned with the STC FB is illustrated. The red dotted line represents the direction of the optical axis of the system configured in Backward channel mode, crossing both the RPV and the ROC rotation axes.

3.6.2 Configuration with STC FM

The integration of the SVS with STC FM will be performed within the Selex ES S.p.A. (SE) facility, where the instrument has been assembled, integrated and will be calibrated. The SVS will be aligned with the STC FM, which is hosted in a custom TVC, designed for the SIMBIO-SYS calibration activities. The TVC has been designed such that the rotation axis of the rotation stage intersects the crossing point of the two STC sub-channels chief rays. In order to provide the alignment of the STC SVS optical elements with the optical sub-channels of the STC FM a custom adjustable support has been foreseen (see Figure 3-41). The rotation stage controller will be integrated with the SE OGSE system, which will control the whole experimental sequence by means of custom experiment control software.

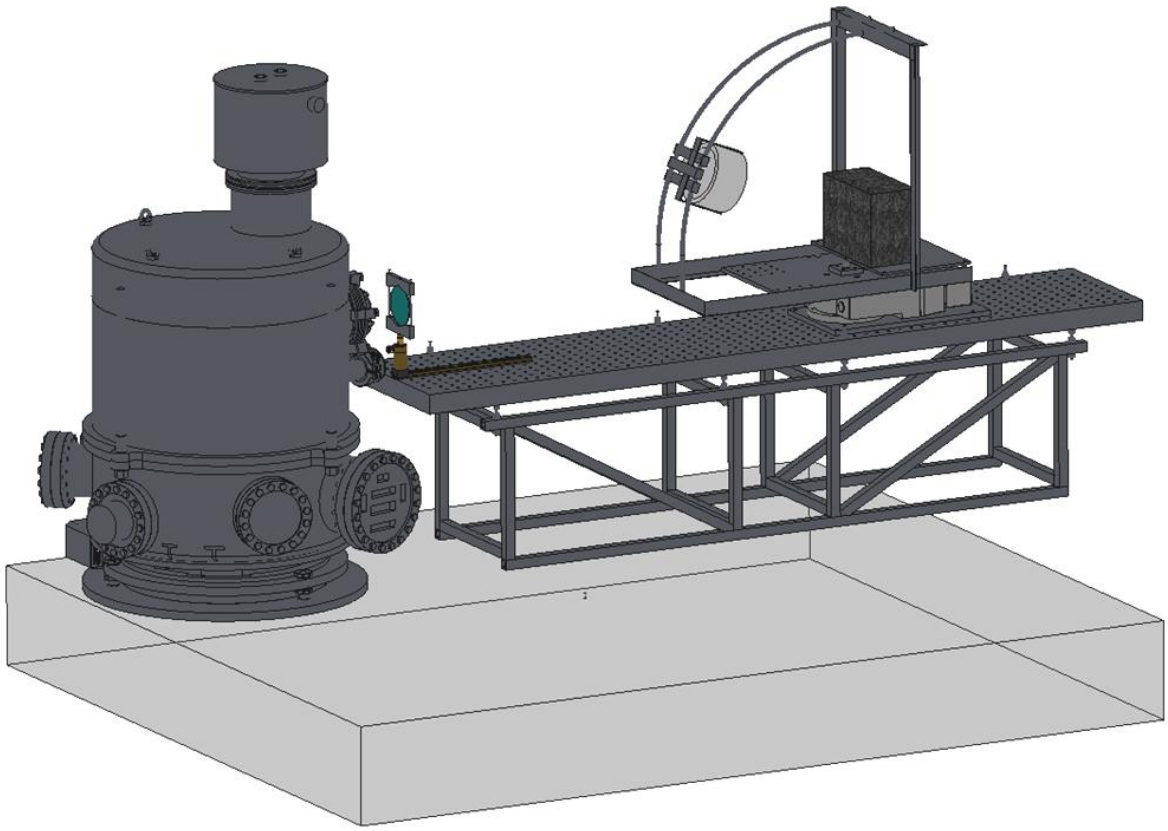

Figure 3-41: SVS aligned with STC-VIHI TVC containing the STC FM. The SVS is mounted over a custom height-adjustable support to provide the alignment between collimator lens optical axis and TVC viewports.

Figure 3-42 shows a top view of the SVS aligned with one of the two STC FM sub-channels. The dotted red lines perpendicular to the TVC viewport and crossing the SVS RPV rotation axis, represents the chief ray of the active optical sub-channel.

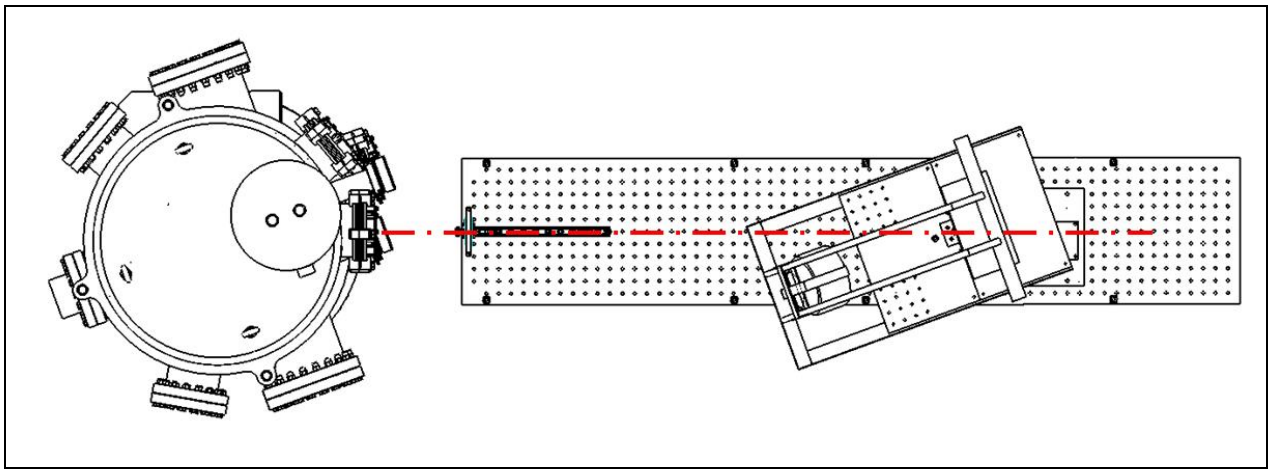

Figure 3-42: STC TVC aligned with SVS in Forward channel configuration, top view. The TVC and SVS must be aligned such that STC Forward channel optical axis is aligned with SVS collimator optical axis and intersecting SVS rotation stage rotation axis.

4. Numerical model of the experimental setup

4.1 Introduction

The intrinsic parameters necessary for the tridimensional reconstruction of the target surface are generally evaluated with camera calibration. Classical algorithms available have been implemented for general purpose optical systems equipped with cheap cameras and simple optical systems. The main idea for stereo validation activity is to apply these calibration techniques for the calibration of the setup. The latter anyway, presents an a-typical optical design, characterized by a long focal length, by the presence of the collimator lens and by elements working off-axis in STC FM test case. A simulation activity has been foreseen with the aim of preliminary verify the performance of classical calibration procedures applied to the stereo validation setup test case.

The simulation of the calibration process, applied both in case of SVS applied to STC FB and to STC instrument, is composed of two main steps:

- numerical simulation of the optical system, to generate synthetic calibration data.
- simulation of camera calibration procedure.

The performance of camera calibration is finally evaluated in terms of re-projection error, as described in 2.3, and by calibration residual analysis.

The numerical simulation of the calibration data has been provided using ray-trace software: the 3D coordinates of a calibration pattern have been projected through the ray-trace model of the setup, providing a set of simulated calibration images.

The block diagram in Figure 4-1 illustrates the process adopted to preliminary evaluate the camera calibration process.

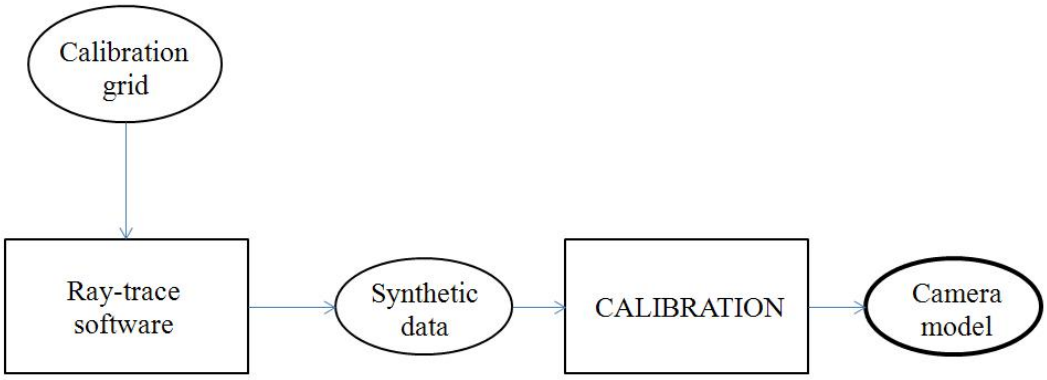

Figure 4-1 Simulation of calibration data by means of ray-trace model of the optical system. A calibration target is provided as input for the ray-trace model of the optical system, the output is the image plane coordinates (mm) of the calibration target features, which are used as input for a calibration software.

The simulation process described above does not take into account the noise introduced by the real imaging systems, due to the pixel sampling which is partially compensated by the sub-pixel accuracy of the feature detection process which characterize the classical camera calibration process. In order to provide a simulation with a more realistic data set, a random noise with normal distribution has been added to the ray-trace data. The noise distribution properties have been selected in order to emulate the corner detection process accuracy provided by the available calibration software [23]. In Figure 4-2 a scheme of synthetic data generation process with the addition of random noise is provided.

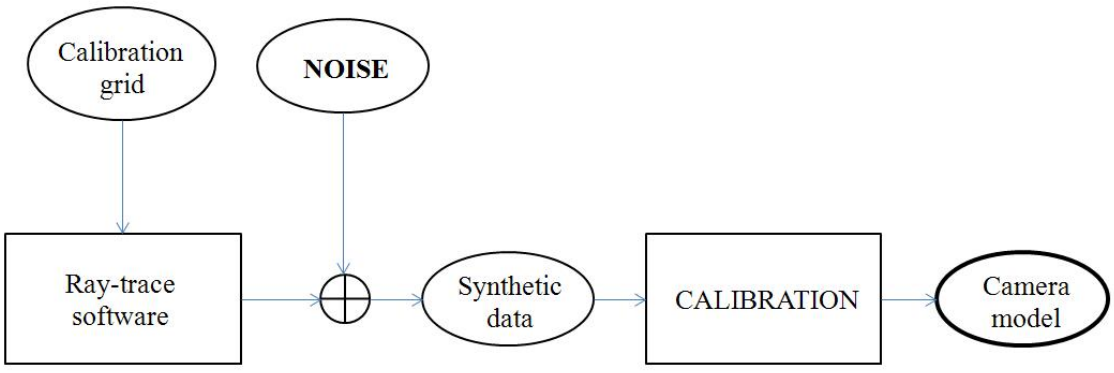

Figure 4-2 Synthetic image generation process. The ray-trace output data has been added with random noise with Gaussian distribution with zero mean. Several standard deviation levels have been chosen in order to simulate different noise conditions.

4.1.1 Calibration software

The synthetic data generated with ray-trace technique have been used as input for the Camera Calibration Toolbox software [26], which provides an implementation of the Zhang's algorithm described in 2.3.

The calibration toolbox has been customized in order to operate with the ray-trace generated data. The outputs of calibration procedure, concerning camera intrinsic parameters, are summarized in the following table:

Parameter	**Name**	**Unit**	**Description**
fc	Focal length	pixel	Focal length along x and y direction (2x1 vector)
cc	Camera center	pixel	Principal point coordinates in pixel (2x1 vector)
alpha_c	Skew coefficient	scalar	Angle between x and y pixel axes
kc	Distortion vector	scalar	5x1 vector with Radial and tangential distortion coefficients: kc(1,2,5) elements correspond to the 2^{nd}, 4^{th} and 6^{th} order radial distortion coefficients, kc(3,4) elements are the two tangential distortion coefficients, as defined in 2.1.2.

Table 4-1: Definition of the calibration software output concerning camera intrinsic parameters.

Moreover, for each image of the calibration pattern, an estimation of the camera extrinsic parameters is provided w.r.t. a reference frame which is univocally defined over the calibration pattern. As specified in 2.3 each estimated parameter is provided with an associated uncertainty.

4.2 Numerical model of the setup with STC functional breadboard

The first step in the numerical simulation of calibration process is to consider the STC SVS configured with STC FB. The results obtained will be compared with the results obtained in laboratory, illustrated in §5, providing a preliminary validation of the synthetic data generation process.

4.2.1 Camera model

The main idea for the simulation of camera calibration process is to consider the two optical heads of the STC FB combined with the collimator lens as two new optical units, with a focal length which is the result of the combination of the focal lengths of the STC FB optical channels (95mm), the focal length of the collimator lens (1000mm) and the distance between this two elements (at least 250mm). The stereo imaging system is thus composed by two optical units with an estimated equivalent focal length of about 135mm.

The following paragraphs will describe the results obtained by simulating single camera calibration data, and using them as input for a standard explicit camera calibration software.

4.2.2 Simulation of calibration data with ray-tracing software

In order to provide a set of synthetic calibration data, the ray-trace model adopted in optical design phase has been considered. A calibration pattern, represented by a set of 3D point coordinates specified on a user defined reference frame have been projected to the image plane through the model of the optical system, simulating the light rays path.

The so obtained calibration pattern image coordinates represent the chessboard corners coordinates, that in real calibration procedure are extracted by real calibration images. Since the calibration is computed using a set of target images, obtained orienting the target in different ways over the camera f.o.v., the calibration pattern attitude has been arbitrarily changed for each chessboard synthetic image (the operation is possible by modifying a set of attitude parameters which define the ray-trace software surface in which the virtual calibration pattern is defined).

The dimension of the calibration grid used for input has been chosen to provide a sufficient coverage of the f.o.v.. Considering a target area of about 70 by 50 mm at about 1000 mm from collimator lens, a grid of 9 by 8 points spaced by 3 mm in both directions has been considered as a suitable chessboard for calibration process, covering a target area of 24 by 21 mm.

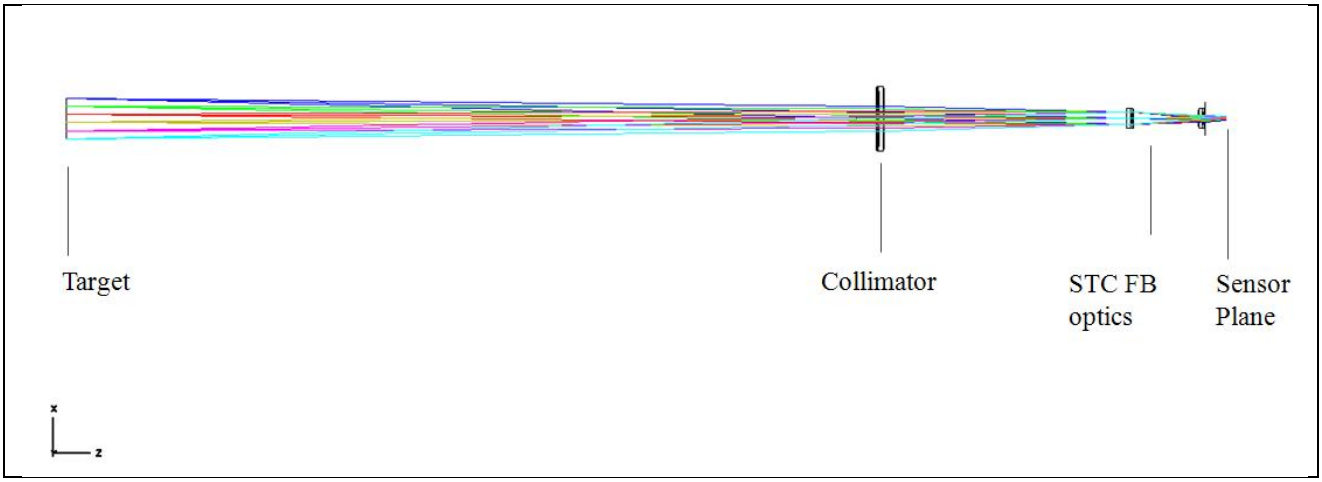

Figure 4-3: Optical layout of the STC FB aligned with STC Stereo Validation Setup. From the left the optical components are illustrated: Target source, collimator lens, STC FB optics and image plane.

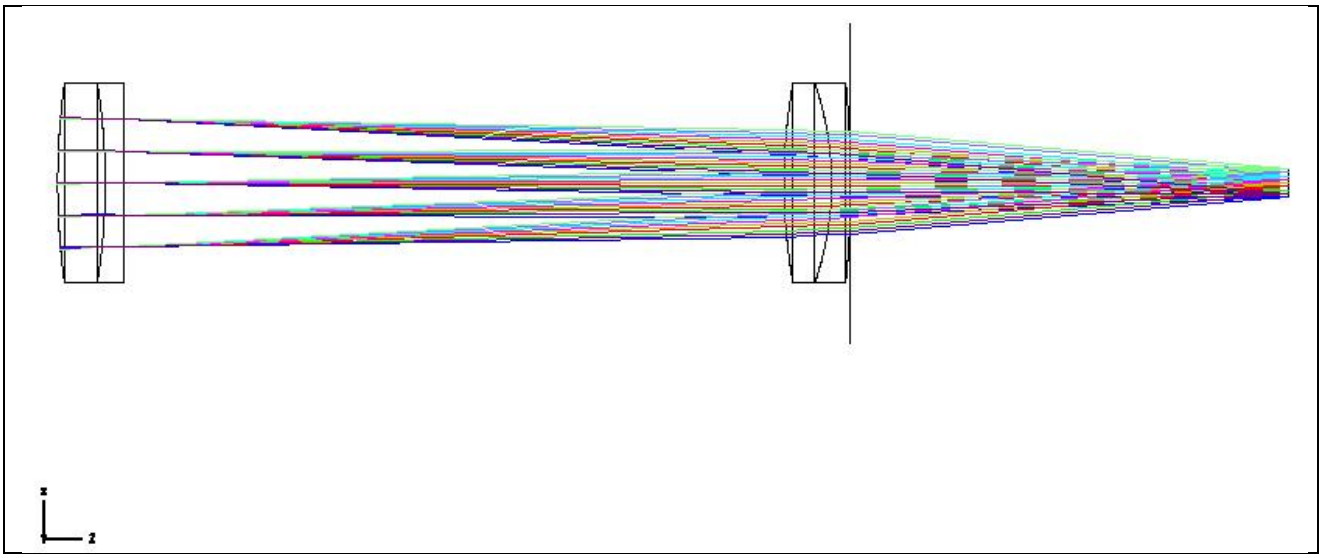

Figure 4-4: Optical layout of the STC FB aligned with STC Stereo Validation Setup: detailed view of the STC FB optical components.

A set of 20 different calibration pattern poses has been projected through the ray-trace model of the system, providing 20 synthetic target images.

The conversion of each image plane point $p = [i, j]^T$ to image pixel coordinates has been performed according to the following relation:

$$\begin{bmatrix} u \\ v \\ 1 \end{bmatrix} = \begin{bmatrix} 1/p_x & 0 & cc_x \\ 0 & 1/p_y & cc_y \\ 0 & 0 & 1 \end{bmatrix} \begin{bmatrix} i \\ j \\ 1 \end{bmatrix} \quad 4.1$$

In which p_x and p_y represent the pixel size along x and y direction, respectively, and cc_x, cc_y represent the pixel coordinates of the camera center.

Without loss of generality, for this preliminary analysis the pixels have been assumed to be perfectly square (with $p_x = p_y$), and the camera center to be positioned exactly in center of the sensor array.

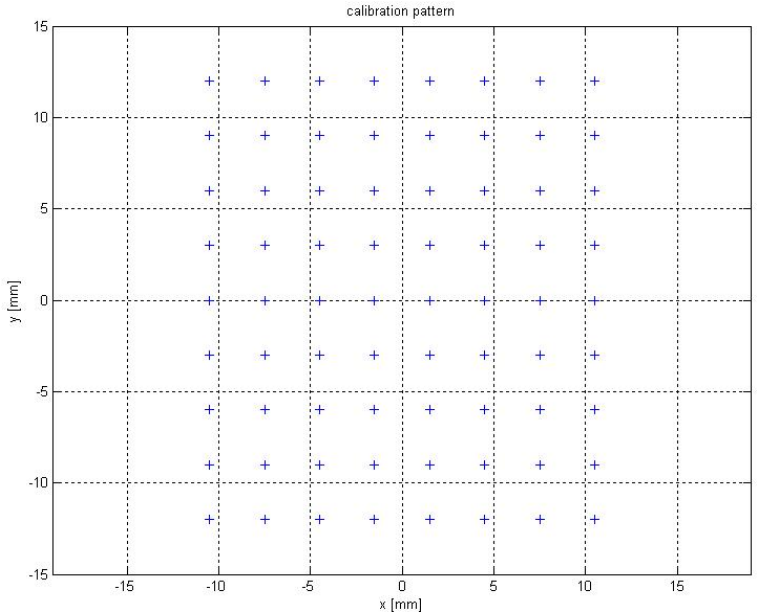

Figure 4-5: Plot of planar calibration pattern. The blue crosses represent the coordinates of the calibration pattern features in an arbitrary 3D reference frame. The *Z* axis is not represented being the *Z* coordinate value of each point equal to 0. As a convention in ray-trace software, the *x* and *y* coordinates represent the position of a point on a surface which is normal to the optical axis of the optical system, and, if no tilt nor de-centering parameters are set, centered at *(0,0)*.

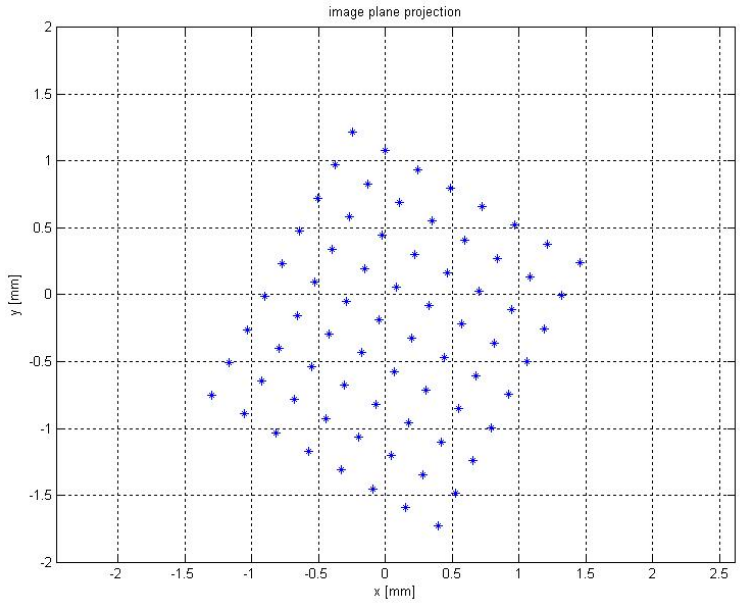

Figure 4-6: Ray-trace projection of a calibration pattern pose to image plane. The ray-trace surface containing the calibration pattern have been tilted and de-centered to simulate a calibration pattern arbitrary positioning. The sensor plane coordinates are expressed in mm.

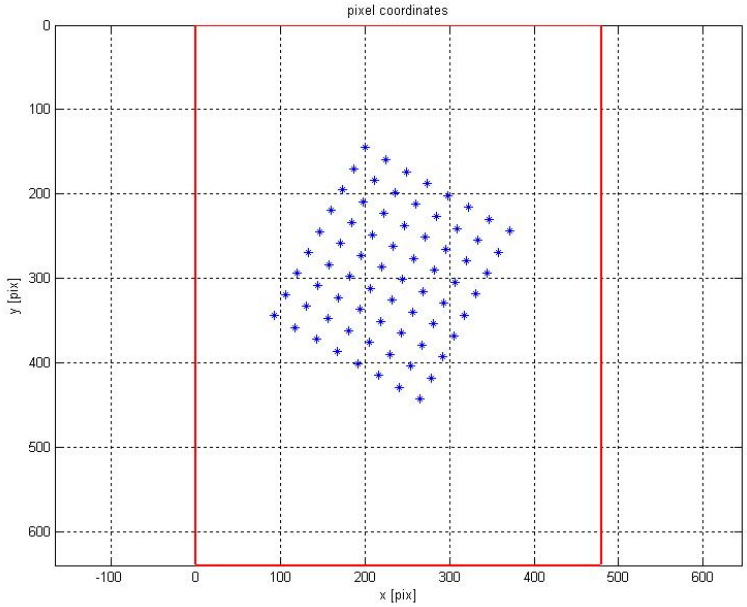

Figure 4-7: Image plane projection of a calibration pattern pose converted in pixel coordinates. The red lines represent the theoretical boundaries of the STC FB camera's image frame.

4.2.3 Calibration: Simulation results

The synthetic data from SVS with STC FB ray-trace model have been analyzed as supplied by ray-trace software at first, and then with the addition of a random noise vector, whose amplitude has been selected in order to simulate the noise introduced by corner extraction process. In the next sub-sessions the results of the two tests are reported[3].

4.2.3.1 Noiseless data

The calibration test with a set of 20 simulated images, without the addition of image sampling or noise effects, lead to the following result:

Parameter	**Estimated Value**
Focal length	136.67 ± 0.0007 mm
Camera center [*x*, *y*]	[240.01 320.01] ± [0.014 0.012] pixel
Distortion vector	[0.3333 0 0 0 0] ± [0.00023 0 0 0 0]
Error standard deviation [*x*, *y*]	4.32×10^{-6} 6.41×10^{-6}

Table 4-2 Calibration results of STC stereo validation setup with STC FB ray-trace model.

[3] both skew and aspect ratio effects have not been evaluated in these analysis, since the conversion from physical image-plane coordinates obtained with ray-trace software to pixel units is performed assuming perfectly square pixel with 9.9 µm side, referring to the nominal pixel size of the FB cameras detectors.

The focal length estimated value is close to the nominal paraxial focal length value expected from the ray-trace software analysis, which is equal to 135.7 mm.

The camera center estimated value is positioned exactly at image plane center as expected, since both in ray-trace model and in ray-trace to image pixel conversion the optics and the sensor plane have assumed to be perfectly centered and aligned.

For what concerns distortion contribution, a 2nd order radial distortion component is detected with relatively high accuracy.

The very low values of re-projection error, with magnitude order of 10^{-6} pixel, underline that the camera model computed by means of calibration procedure describes with very high accuracy the imaging system modeled by means of ray-tracing software.

Observing the distribution of the re-projection error in Figure 4-8, we can notice that the 3-σ curve is within $1.5x10^{-5}$ pixel.

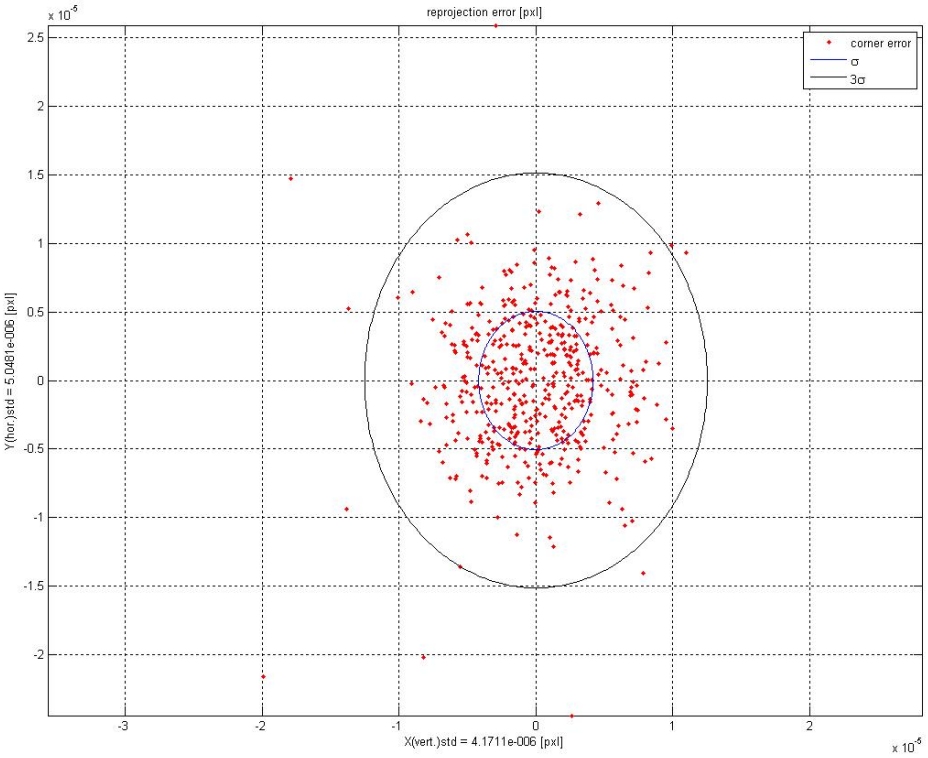

Figure 4-8: Simulation of calibration process with STC FB: re-projection error. The 3-σ curve is within $1.5x10^{-5}$ pixel.

4.2.3.2 Noisy data

As described in 4.1, to provide a simulation of calibration process with a data set closer to the experimental calibration data, a random noise has been added to pixel coordinates as illustrated in the scheme at Figure 4-2.

The pixel coordinates have been added with a normal distribution noise with zero mean and a standard deviation of 0.04 pixel, meaning a 99% of the values in the interval between -0.12 and 0.12 pixel, which is comparable to the accuracy of the corner extraction process (0.1 pixel, [23]). Finally, the noise addition and the calibration process have been repeated several times (500) in order to perform a Monte Carlo analysis of the calibration procedure and to verify the stability of the calibration parameters extracted w.r.t. variability of input noise.

The results obtained lead to the following considerations:

- Focal length: the estimated value presents a significant dependence on the input noise. The standard deviation of the obtained values exceeds the mean value of estimated focal length uncertainty.
- Camera center: the estimation of camera center is not possible by means of calibration procedure with noisy data. The center of the image sensor can anyway assumed to be a good approximation for camera center because of the geometry of the optical system, with long focal and narrow angle.
- Distortion coefficients: distortion coefficients cannot be estimated by means of calibration process, since their contribution on re-projection error is not appreciable.

Despite the reduction of the parameter set estimable by means of calibration process (focal length and extrinsic parameters), the pinhole camera can be still considered as an accurate model for the optical system, since the re-projection error curve is within the uncertainty of 0.15 pixel, as showed in Figure 4-9.

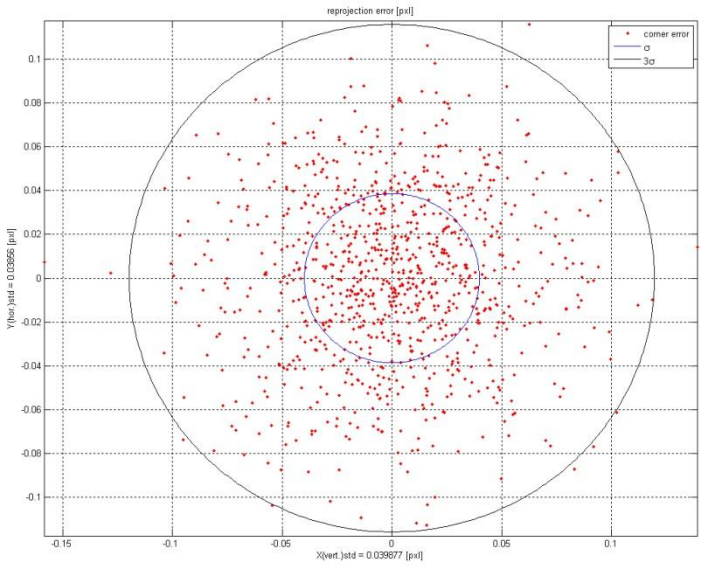

Figure 4-9: Calibration with simulated data added with Gaussian noise, with zero mean and $\sigma^2 = 0.04$. Plot of re-projection error: the 3-σ curve is within 0.15 pixel.

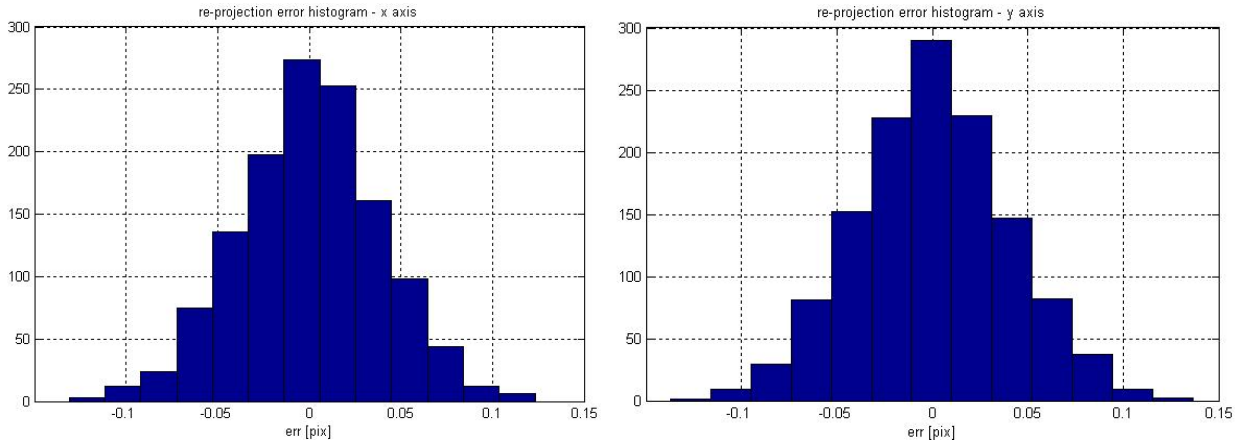

Figure 4-10: SVS with STC FB. Histogram of re-projection error obtained with simulated data added with Gaussian noise. The two histograms represent the distribution of re-projection error along horizontal and vertical direction respectively, in pixel. The two distributions can be compared to a Normal distribution with zero mean and $\sigma^2 \approx 0.04$ pixel.

From the Monte Carlo analysis, as we can see from Table 4-3, the calibration process results to be stable in terms of re-projection error, which presents a mean amplitude of 0.039 pixel, comparable to the σ^2 value of the input noise.

Parameter	**Mean value**	**Standard deviation**
Focal length [mm]	136.37	0.90
Focal length error [mm]	2.57	0.052
Re-projection error [pixel]	[0.0392 0.0391]	$[0.8189\ \ 0.8145]\times10^{-3}$

Table 4-3: Simulation of calibration process with STC FB ray-trace model. Results of the Monte Carlo analysis of the calibration procedure. The input data have been added with Gaussian noise with zero mean and $\sigma^2 = 0.04$.

The plot of Figure 4-11 shows the focal length values obtained over the 500 calibration tests: the distribution of the estimated values can be associated to a Gaussian distribution (see histogram of Figure 4-12), with mean value equal to 136.37 mm and standard deviation of 0.9 mm.

The mean value of the estimated error on focal length is 2.57 mm, while the re-projection standard deviation value is always close to 0.04 pixel.

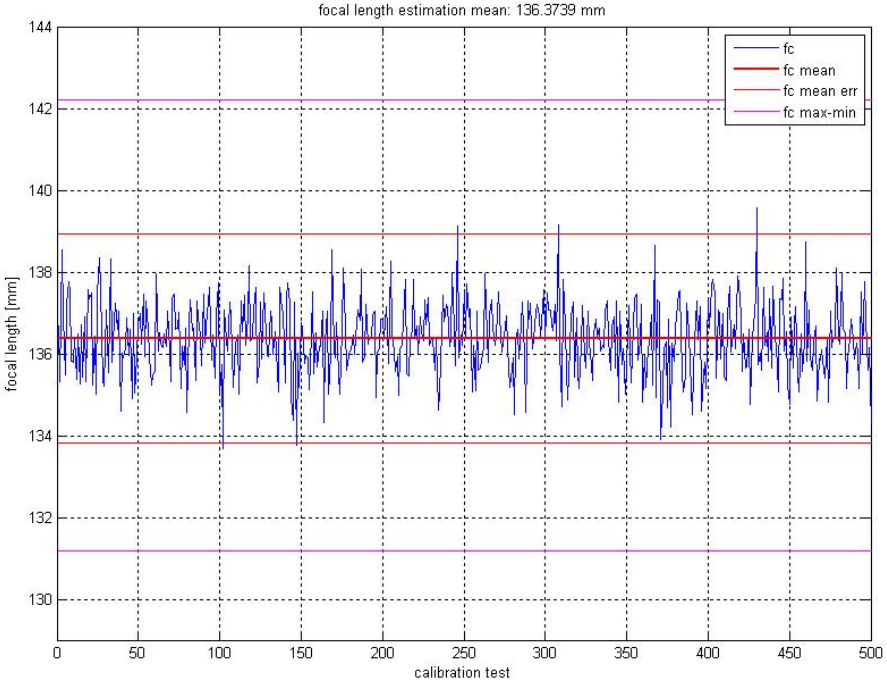

Figure 4-11 Calibration with synthetic data added with Gaussian noise with zero mean and $\sigma^2 = 0.04$. Estimated focal length over 500 calibration tests. On each test the additional noise is generated as a random vector with normal distribution. The thick central red line represents the mean value estimated. The thin red lines represent the mean focal length added and subtracted with the mean estimated uncertainty on the focal length and the magenta lines represent the maximum and minimum values reachable for focal length within uncertainty over the 500 tests.

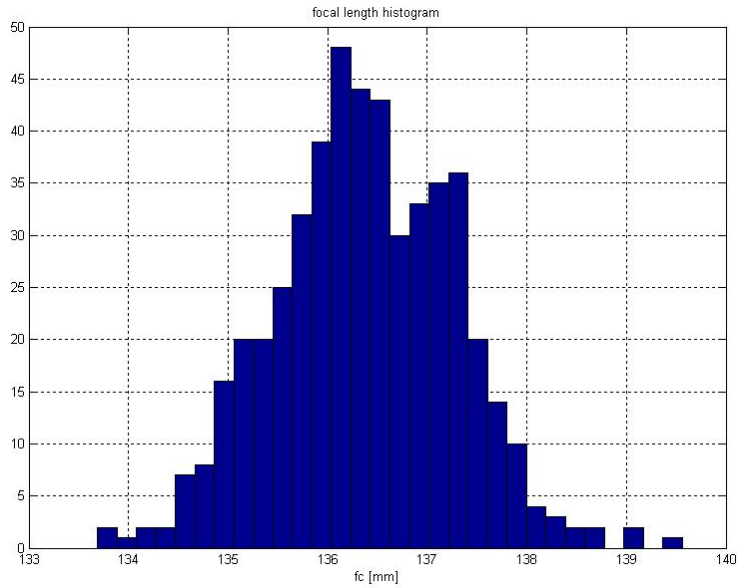

Figure 4-12 Histogram of the estimated focal length. The distribution of the estimated values (in mm) is comparable with a Gaussian distribution.

4.3 Numerical model of the setup with STC FM

After simulation of calibration procedure of the SVS aligned with STC FB channels, the same process has been applied to analyze the test case of SVS aligned with STC instrument.

4.3.1 Camera model

The setup has been considered as composed of two optical channels, obtained by the combination of the collimator lens of the Stereo Validation Setup with the panchromatic optical channels of the STC instrument.

Similarly to the STC FB case, the focal length of the whole optical system depends on the combination between the focal length of the STC instrument, which as from requirements equals to 95mm, the collimator focal length, which is about 1000mm, and the relative distance between the two optical elements. The estimated value for the equivalent paraxial focal length is about 168.9 mm considering the collimator lens positioned at 295mm from the last optical element of STC (see distance "*d*" in Figure 4-13).

4.3.2 Simulation of calibration data with ray-tracing software

The simulation of the calibration data has been performed referring to the ray-trace software model of the STC optical channels, implemented in STC optical design phase [14]. The calibration target

adopted is the same described in 4.2.2, since the f.o.v. of the STC is almost close to the one of the STC FB.

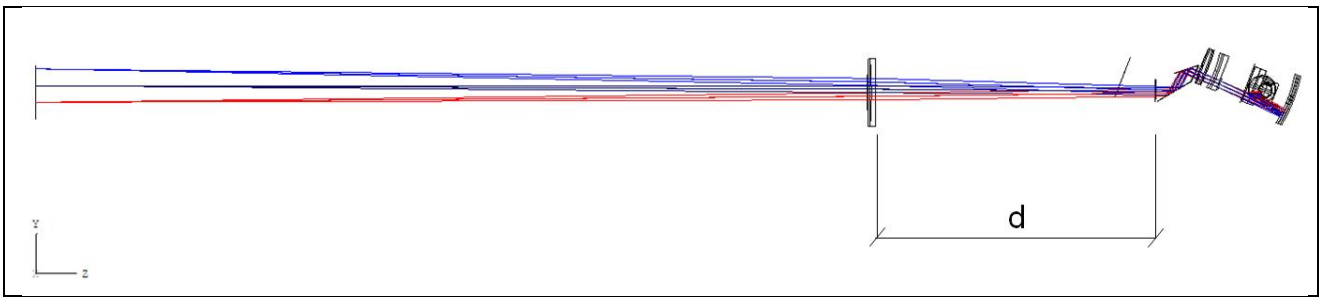

Figure 4-13: Layout of the ray-trace model of the STC (on the right) aligned with collimator lens of the SVS.

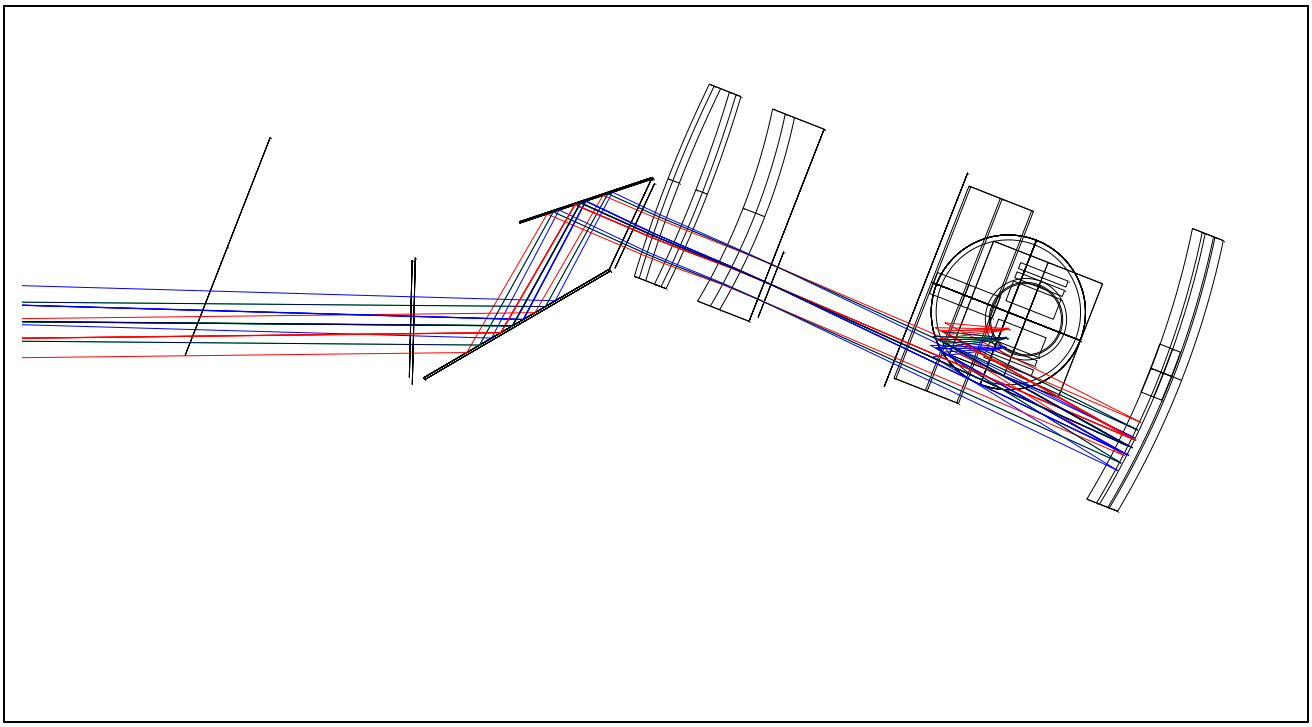

Figure 4-14: Detailed view of the optical layout of the STC ray-trace model adopted to generate synthetic calibration data.

The configuration illustrated in Figure 4-13 and Figure 4-14, has been adopted to project the coordinates of the calibration target features in 20 different target poses, obtaining a set of 20 simulated calibration images.

4.3.3 Simulation results

As done in the previous analysis the calibration procedure has been simulated and analyzed both in case of noiseless corner coordinates and in case of corner coordinates added with a Gaussian noise with distribution comparable with Harris corner extraction accuracy (mean = 0, $\sigma^2 = 0.04$)[4].

4.3.3.1 Noiseless data

The calibration test has been performed over a set of 20 images applying different settings in order to evaluate separately the contribution of both radial and tangential distortion evaluation on re-projection error. Table 4-4 shows the calibration results with central point estimation and distortion estimation disabled (the central point is positioned at the center of the panchromatic filter).

Parameter	**Estimated Value**
Focal length	167.89 ± 2.67 mm
Camera center [*x*, *y*]	[439.5 197.5] pixel
Distortion vector	[0 0 0 0 0]
Error standard deviation [*x*, *y*]	[0.0207 0.0206] pixel

Table 4-4: Calibration results of STC stereo validation setup with STC ray-trace model. Distortion estimation and camera center estimation disabled.

It can be noticed a higher re-projection error standard deviation w.r.t. the corresponding STC FB simulated case, together with an higher focal length estimation uncertainty. Figure 4-15 shows the re-projection residuals for this specific calibration test.

[4] As in STC FB simulation case, the skew parameter and aspect ratio are not considered, since the conversion from physical image-plane coordinates obtained with ray-trace software to pixel units is performed assuming perfectly square pixel with 10 μm side, referring to the nominal pixel size of the STC detector.

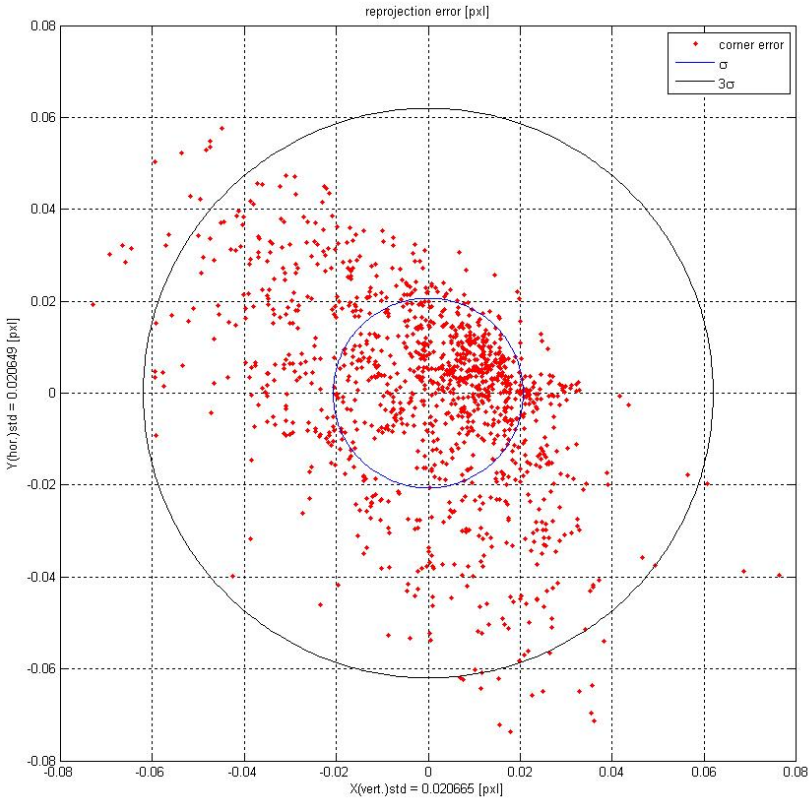

Figure 4-15: Simulation of calibration process with STC: re-projection error with central point and distortion estimation disabled. The 3-σ curve is near 0.06 pixel.

The calibration test has been repeated on the same data set enabling camera center estimation, in order to separately evaluate its contribution to the reduction of calibration error. In Table 4-5 the results of calibration procedure with camera center estimation are reported:

Parameter	**Estimated Value**
Focal length	165.97 ± 2.08 mm
Camera center [*x*, *y*]	[3.4219 422.5683] pixel
Distortion vector	[0 0 0 0 0]
Error standard deviation [*x*, *y*]	[0.0186 0.0149] pixel

Table 4-5: Calibration results of STC stereo validation setup with STC ray-trace model. Camera center estimation enabled, distortion estimation disabled.

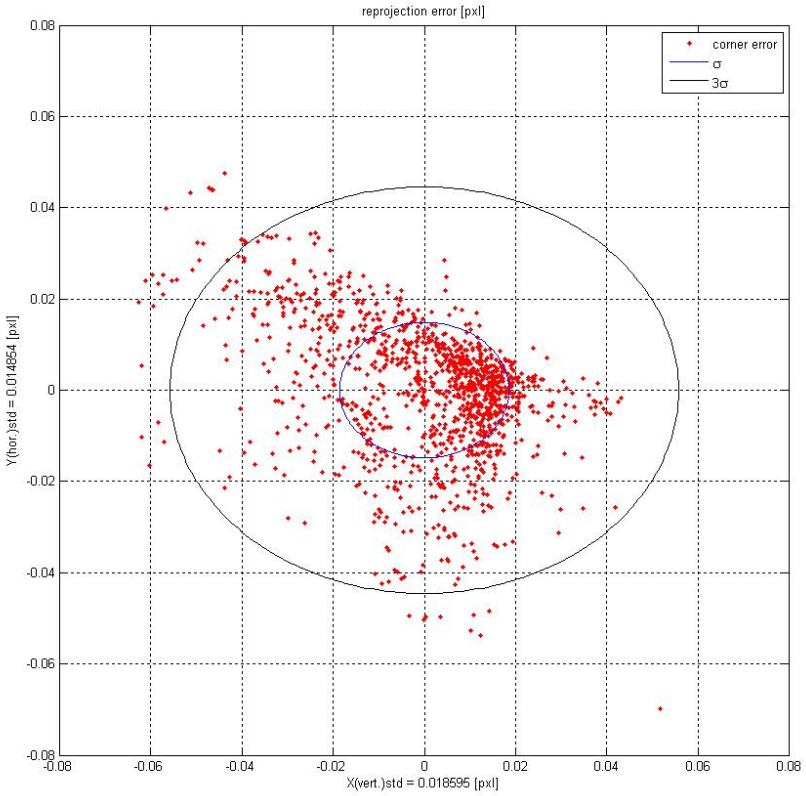

Figure 4-16: Simulation of calibration process with STC: re-projection error with central point estimation enabled and distortion estimation disabled. The 3-σ curve is below 0.06 pixel in horizontal direction and below 0.05 pixel in vertical direction.

The estimation of camera center involves a slight reduction both on focal length uncertainty estimation and on re-projection error standard deviation, as we can observe from Table 4-5 and Figure 4-16.

The estimated value for camera center evidences that the center of projection of the equivalent pinhole model is shifted with respect to the panchromatic filter in the direction of STC sensor central point, probably due to the off-axis STC optics design, as we can see in Figure 4-17.

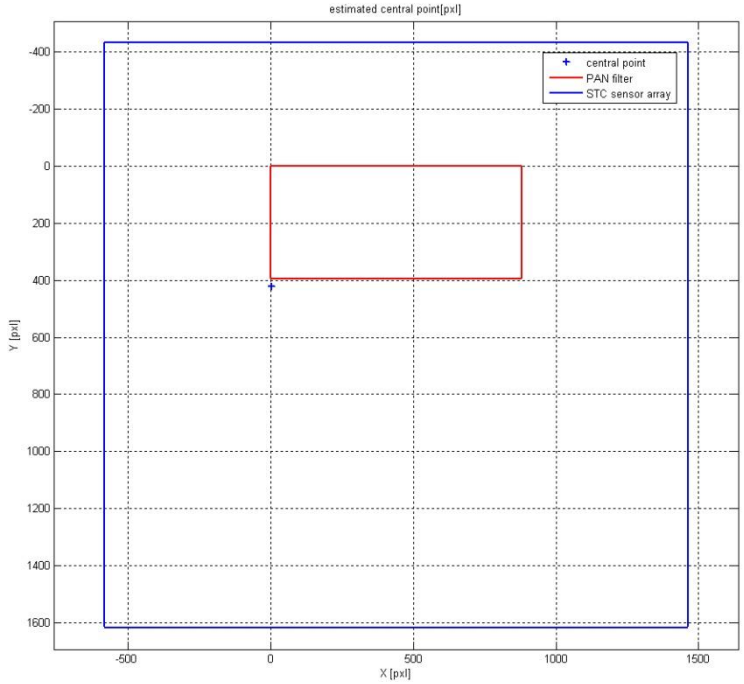

Figure 4-17: Simulation of calibration process with STC: estimated central point with distortion estimation disabled. The area delimited by red line represents STC PAN filter area, the blue line represents the STC sensor array area.

The impact of radial and tangential distortion compensation have been evaluated separately in order to analyze the impact of both components. In Table 4-6 are reported the calibration results with estimation of 2nd and 4th order radial distortion components:

Parameter	**Estimated Value**
Focal length	167.15 ± 2.05 mm
Camera center [*x*, *y*]	[-118.8019 487.6462] pixel
Distortion vector	[-0.3983 66.6 0 0 0] ± [0.0830 15.1 0 0 0]
Error standard deviation[*x*, *y*]	[0.0169 0.0145] pixel

Table 4-6: Calibration results of STC stereo validation setup with STC ray-trace model. Camera center estimation enabled, 2nd and 4th radial distortion estimation enabled.

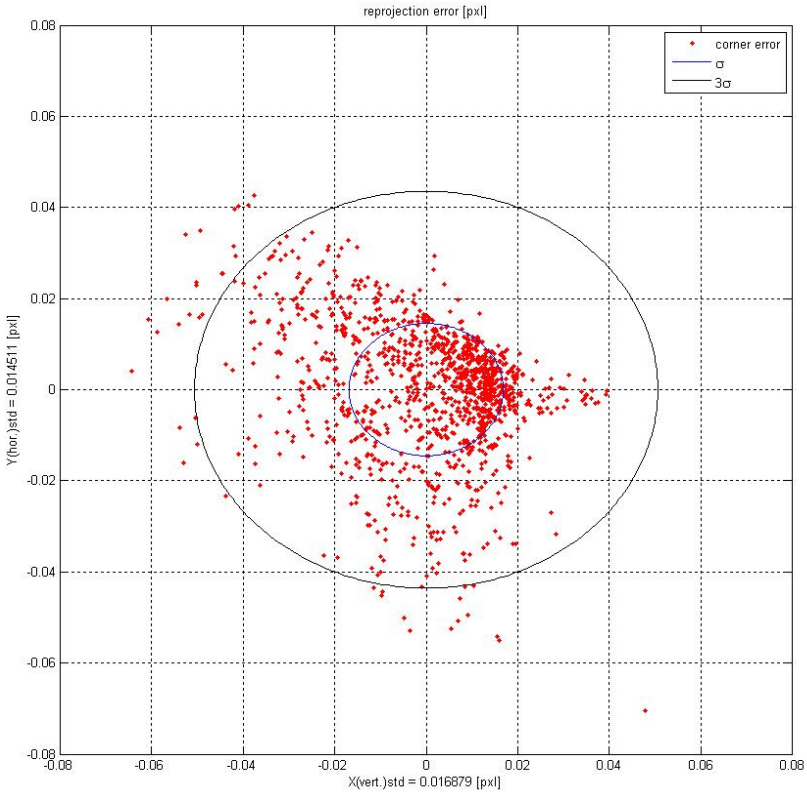

Figure 4-18: Simulation of calibration process with STC: re-projection error with central point estimation enabled and 2nd and 4th radial distortion estimation enabled. The 3-σ curve is close to 0.05 pixel in horizontal direction and below 0.05 pixel in vertical direction.

The compensation of 2nd and 4th order radial distortion does not provide significant improvements in terms of re-projection error, with an improvement of about 0.01 pixel along the horizontal direction. The 6th order radial distortion component is not detected by calibration software.

Finally, Table 4-7 and Figure 4-19,Figure 4-20 show the calibration results with the addition of tangential distortion estimation:

Parameter	**Estimated Value**
Focal length	168.05 ± 1.92 mm
Camera center [*x*, *y*]	[-352.3 272.0] pixel
Distortion vector	[0.53 0 0 -0.031 0] ± [0.099 0 0 0.0041 0]
Error standard deviation [*x*, *y*]	[0.01633 0.01303] pixel

Table 4-7: Calibration results of STC stereo validation setup with STC ray-trace model. Camera center estimation enabled, 2nd and 4th radial distortion estimation enabled.

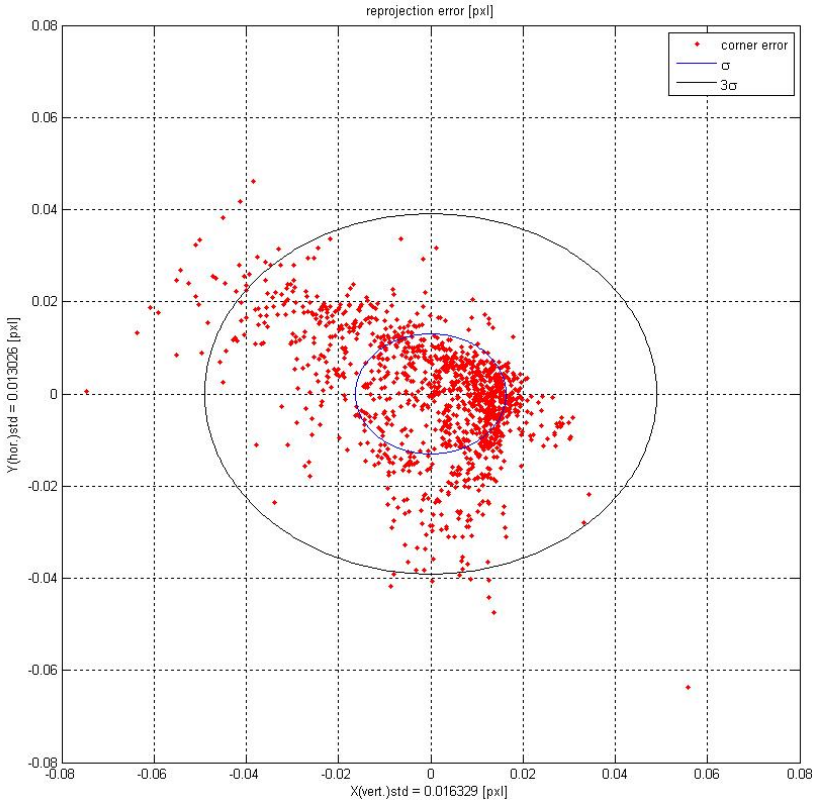

Figure 4-19: Simulation of calibration process with STC: re-projection error with central point, radial and tangential distortion estimation enabled. The 3-σ curve is close to 0.05 pixel in horizontal direction and below 0.04 pixel in vertical direction.

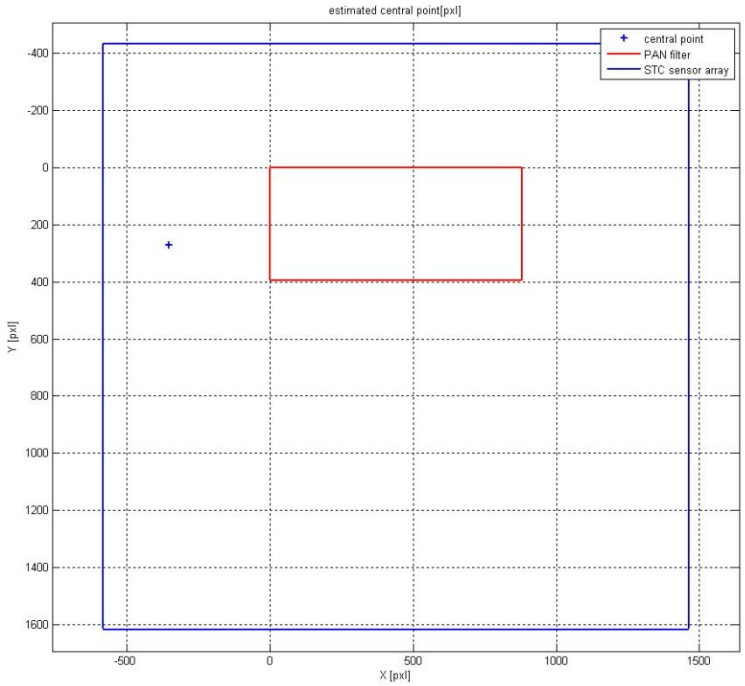

Figure 4-20: Simulation of calibration process with STC: estimated central point with distortion estimation enabled. The area delimited by red line represents STC PAN filter area, the blue line represents the STC sensor array area.

The radial distortion coefficients values are subjected to a substantial change w.r.t. the previous test case due to the introduction of tangential distortion component estimation, which leads anyway to a negligible reduction of re-projection error.

The introduction of distortion estimation involves also a change in camera center estimated value (see Figure 4-20 and Table 4-7), moving its position towards the left-side of the Panchromatic filter area.

The overall results of the calibration test with classical camera calibration procedure show a sensitive worsening of the calibration algorithm performance w.r.t. STC FB test case, due to the more complex geometry of optical system, which can be only partially described by a classical distortion model. The re-projection error standard deviation is anyway of the magnitude order of 0.01 pixels which can still be considered a good result if compared with the guaranteed accuracy in corner extraction process and generally in feature extraction process.

4.3.3.2 Noisy data

As in STC FB case, the calibration data obtained with ray-trace projection have been added with normal distribution noise with zero mean and a standard deviation of 0.04 pixel following the scheme indicated in Figure 4-2.

In Table 4-8, the results of calibration procedure with both optical center and distortion vector estimation disabled. The re-projection error standard deviation is very close to the one of noise vector which has been added to corner coordinates.

Parameter	**Estimated Value**
Focal length	166.82 ± 5.76 mm
Camera center [*x*, *y*]	[439.5 197.5] pixel
Distortion vector	[0 0 0 0 0]
Error standard deviation [*x*, *y*]	[0.0454 0.0449] pixel

Table 4-8: Calibration results of STC stereo validation setup with STC ray-trace model, added with zero mean and σ^2=0.04. Camera center estimation disabled, distortion estimation disabled.

The same noise-affected data have been used to perform a calibration test enabling camera center estimation. This involves a weak reduction of re-projection error, with magnitude order of 0.01 pixels, as shown in Table 4-9.

Parameter	**Estimated Value**
Focal length	164.68 ± 5.23 mm
Camera center [*x*, *y*]	[-41.48 454.30] pixel
Distortion vector	[0 0 0 0 0]
Error standard deviation [*x*, *y*]	[0.0440 0.0419] pixel

Table 4-9: Calibration results of STC stereo validation setup with STC ray-trace model, added with zero mean and σ^2=0.04. Camera center estimation enabled, distortion estimation disabled.

Table 4-10 and Figure 4-21 Figure 4-23 show the results obtained on the same calibration data by introducing distortion vector estimation. We can notice that distortion estimation does not provide significant improvements in re-projection error: the distortion contribution is in fact partially covered by the additional input noise.

Parameter	**Estimated Value**
Focal length	163.97 ± 5.23 mm
Camera center [*x*, *y*]	[-336.68 440.90] pixel
Distortion vector	[0.24418 0 0 -0.01843 0] ± [0.17836 0 0 0.00791 0]
Error standard deviation [*x*, *y*]	[0.04309 0.04179] pixel

Table 4-10: Calibration results of STC stereo validation setup with STC ray-trace model, added with zero mean and σ^2=0.04. Camera center estimation enabled, distortion estimation disabled.

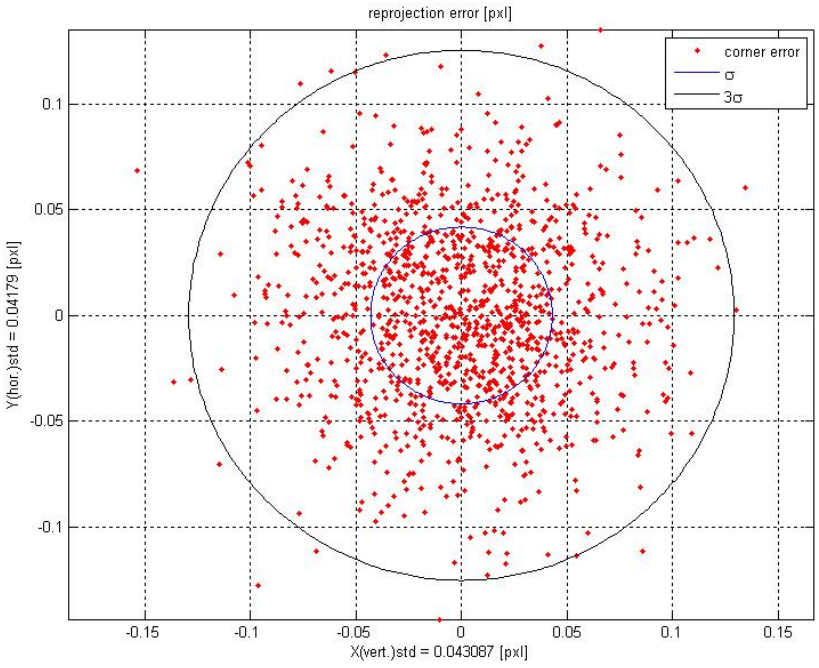

Figure 4-21: Simulation of calibration process with STC. Gaussian noise (mean = 0, σ^2=0.04) has been added to the calibration data: re-projection error with central point, radial and tangential distortion estimation enabled. The 3-σ curve is close to 0.12 pixel.

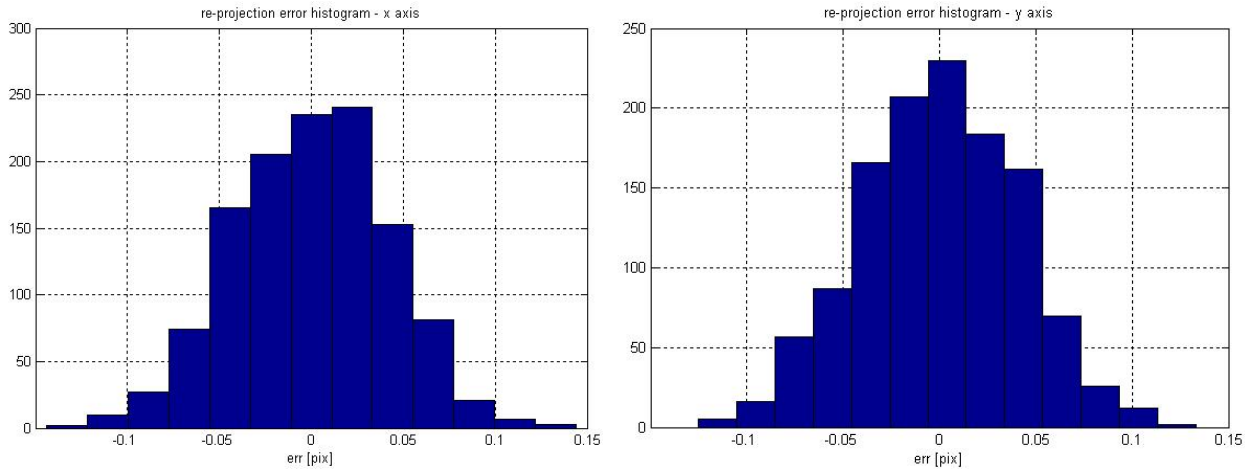

Figure 4-22: : SVS with STC. Histograms of re-projection error obtained adding Gaussian noise (mean = 0, σ^2=0.04) to the simulated calibration data. The two histograms represent the distribution of re-projection error along horizontal and vertical direction respectively, in pixel. The two distributions can be compared to a Normal distribution with zero mean and $\sigma^2 \approx 0.04$ pixel.

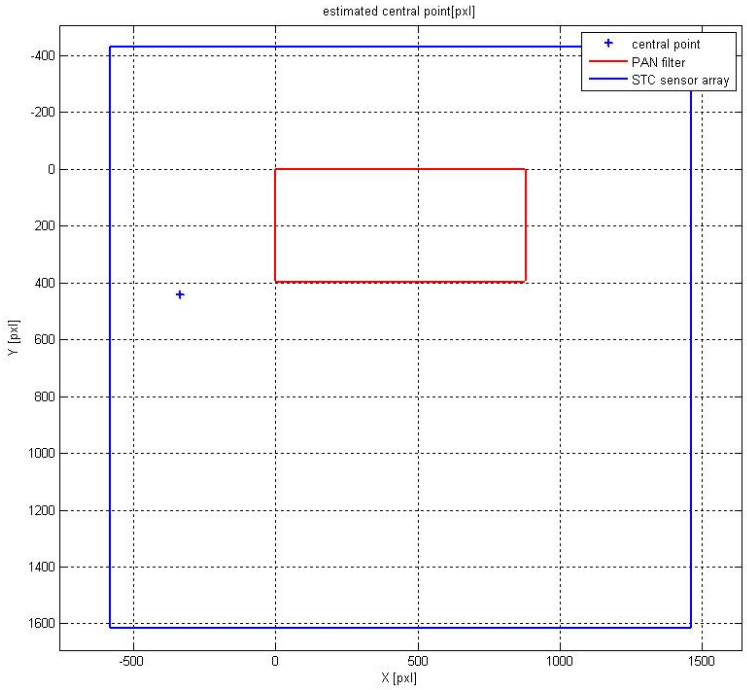

Figure 4-23: Simulation of calibration process with STC. Gaussian noise (mean = 0, σ^2=0.04) has been added to the calibration data: estimated central point position. The area delimited by red line represents STC PAN filter area, the blue line represents the STC sensor array area.

From the results obtained, we can conclude that the pinhole camera model adopted in classical camera calibration algorithms provide a sufficiently accurate analytical model of the optical system also in the test case of SVS applied to STC instrument, being the re-projection error distribution comparable with the distribution of noise introduced by feature extraction process.

Monte Carlo analysis have been performed in order to analyze calibration process repeatability and stability w.r.t. input noise variability: Table 4-11 reports the obtained results.

Parameter	**Mean value**	**Standard deviation**
Focal length [mm]	168.09	1.85
Focal length error [mm]	5.56	0.16
Camera center [pixel]	[-97.55 266.37]	[53.17 18.48]
Distortion vector	[0.6761 0 0 -0.0223 0]	[0.1292 0 0 0.0053 0]
Distortion vector error	[0.3977 0 0 0.0123 0]	[0.0336 0 0 0.0007 0]
Re-projection error [pixel]	[0.0429 0.0417]	[0.9137 0.8673]×10^{-3}

Table 4-11: Simulation of calibration process with STC ray-trace model. Results of calibration procedure Monte Carlo analysis. Gaussian noise (mean = 0, σ^2=0.04) has been added to the calibration data.

The focal length estimated values (see Figure 4-24Figure 4-25) present a distribution comparable with a normal distribution with 168.09 mm mean and a standard deviation of 1.85 mm (see Figure 4-25). The uncertainty over the focal length value is much higher w.r.t. STC FB case, with a mean value of 5.56 mm.

Despite of focal length value variability the calibration results in terms of re-projection error are stable, with a mean value of 0.0429 pixel and 0.0417 pixel along horizontal and vertical direction respectively, with a standard deviation of about $9 \cdot 10^{-4}$ pixel in both directions.

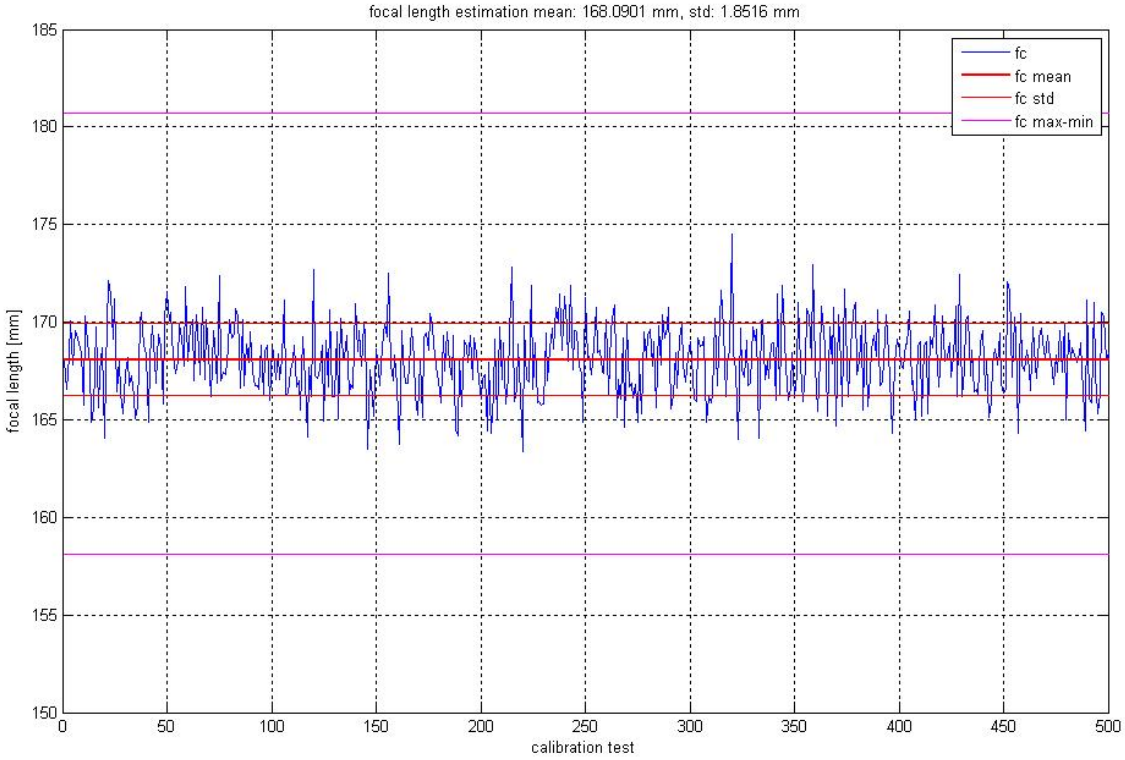

Figure 4-24: Simulation of calibration process with STC ray-trace model. Monte Carlo analysis of calibration procedure with ray-trace data added with Gaussian noise with zero mean and $\sigma^2 = 0.04$. Estimated focal length value over 500 calibration tests. The thick central red line represents the mean estimated value. The thin red lines represent the mean focal length added and subtracted with the mean value of estimated uncertainty on the focal length, and the magenta lines represent the maximum and minimum values reachable for focal length within uncertainty over the 500 tests.

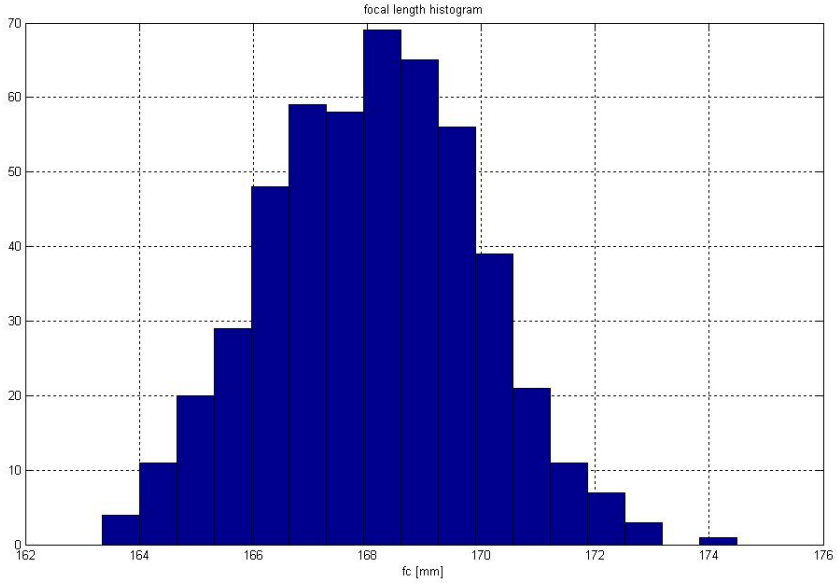

Figure 4-25: Histogram of the estimated focal length. The distribution of the estimated values (in mm) is comparable with a Gaussian distribution.

The camera center estimated values are concentrated within an area centered at the image coordinate [-97.55 266.37] pixel, which is outside the panchromatic filter area (see Figure 4-26), as in noiseless data test case.

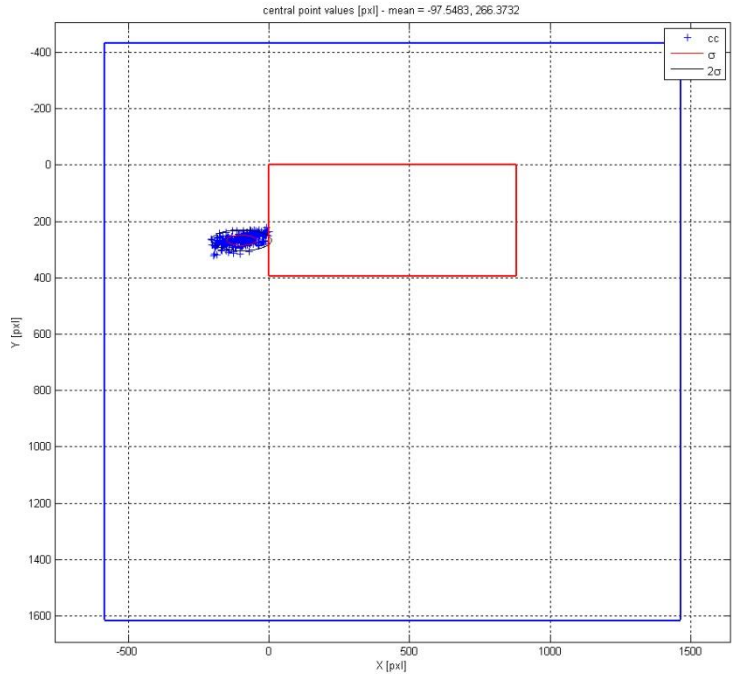

Figure 4-26: Simulation of calibration process with STC ray-trace model. Monte Carlo analysis of calibration procedure with ray-trace data added with Gaussian noise with zero mean and $\sigma^2 = 0.04$. Distribution of estimated camera centers over image plane. The red area represents the STC panchromatic filter area.

Concerning distortion vector evaluation, the Monte Carlo analysis shows that the values obtained are stable w.r.t. to data input noise. However, the uncertainties associated to the distortion coefficient underline that the distortion contribution in calibration process with noise affected data is almost negligible.

5. STC experimental setup: test activity

5.1 Introduction

This chapter will describe the experimental activity for the calibration of the Stereo Validation Setup aligned with the STC Functional Breadboard.

After setup components realization, integration and alignment [29], sets of images of several calibration targets have been acquired in order to perform camera calibration of both STC FB optical channels.

The results of experimental camera calibration activity will be compared with the results obtained with the numerical simulation described in §4, in order to get a validation of the setup numerical model and of the calibration data simulation procedure.

5.2 Calibration software

As specified in 4.1.1, the calibration process of the SVS with STC FB is based on the open source implementation of the Zhang camera calibration algorithm provided by the Camera Calibration Toolbox software [26]. In addition, the software extension for stereo camera calibration has been applied to this specific test case to perform a preliminary evaluation of the extrinsic parameters of the stereo imaging system.

Usually, the calibration of a stereo imaging system is performed by two main calibration steps: the single camera calibration, which performs separately an estimation of the intrinsic parameters of the two cameras, and the stereo camera calibration, in which the simultaneous projection of the calibration target towards the two image planes allows the computation of the mutual camera orientation parameters. The next two sub-sections will describe the procedures adopted to perform the single channel and the stereo calibration respectively.

5.2.1 Single camera calibration procedure

Each imaging channel of the STC FB has been calibrated separately with standard Zhang calibration procedure with the following steps:

Sequence step no	Operation
1	Optical channel alignment with STC SVS by means of STC FB rotation stage (ROC).
2	Calibration target arbitrary positioning within target field of view
3	Image frame acquisition

Table 5-1 Single camera calibration steps with STC SVS.

Steps 2 and 3 have been repeated several times to get a sufficiently large set of images (at least 50). The operation have been repeated both on Forward Channel and Backward Channel of the STC FB.

5.2.2 Stereo camera calibration procedure

After single camera calibration procedure refinement, the stereo calibration procedure has been performed in order to evaluate the extrinsic parameters which characterize the equivalent pinhole model of the stereo rig.

The stereo calibration procedure applied to STC SVS is resumed by the following steps:

Sequence step no	Operation
1	Target positioning with arbitrary pose within f.o.v.
2	FWD channel alignment with STC SVS (ROC: +20 deg)
3	Target rotation stage positioning in FWD configuration (RPV: +20 deg)
4	FWD Image acquisition
5	BWD channel alignment with STC SVS (ROC: -20 deg)
6	Target rotation stage positioning in BWD configuration (RPV: -20 deg)
7	BWD Image acquisition

Table 5-2 Stereo calibration procedure steps with STC SVS.

The sequence steps 1 to 7 have been repeated several times in order to get a sufficiently large set of stereo couples (at least 50). Both target and STC FB rotation stages have been rotated in order to reproduce the Forward and Backward observing configurations as described in 3.2.3[5].

In order to generate stereo couples of the calibration target, the calibration pattern between sequence steps 2 to 7 is maintained in a given position by a clamping support which is connected to the target support plate (see Figure 5-1), allowing the acquisition of a couple of Backward and Forward image of the target in exactly the same pose. The target clamping support is an adjustable arm which allows 6 d.o.f. movements for the calibration pattern within the SVS f.o.v..

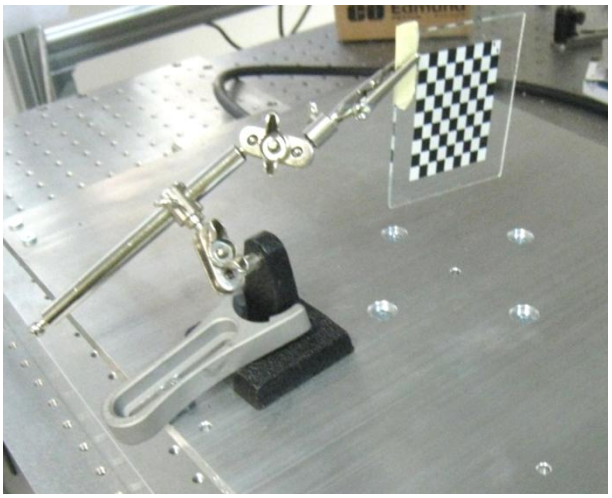

Figure 5-1: Calibration target clamping support.

Several tests have been performed in order to check stereo calibration repeatability and to get sufficient confidence with calibration procedure.

5.3 **Calibration target**

The calibration pattern commonly used is a planar chessboard, which guarantees sub-pixel accuracy in the edge detection process adopted to extract the image corner coordinates. In order to guarantee a sufficient accuracy in corner detection a print resolution of at least 1200 dpi for the target chessboard has been estimated. Considering a mean pixel footprint of 105µm, a print

[5] The rotation stage moves and target positioning sequence has been optimized w.r.t. the one described above, in order to reduce acquisition time required for the stereo couples acquisition process.

resolution of at least 5 points per pixel side has been foreseen as reasonable value to provide chessboard images with a suitable print quality.

Several solutions for the support (glass, plastic material, photographic paper etc.; see Figure 5-2 to Figure 5-5) have been tested in order to find the one which guarantees the best performance.

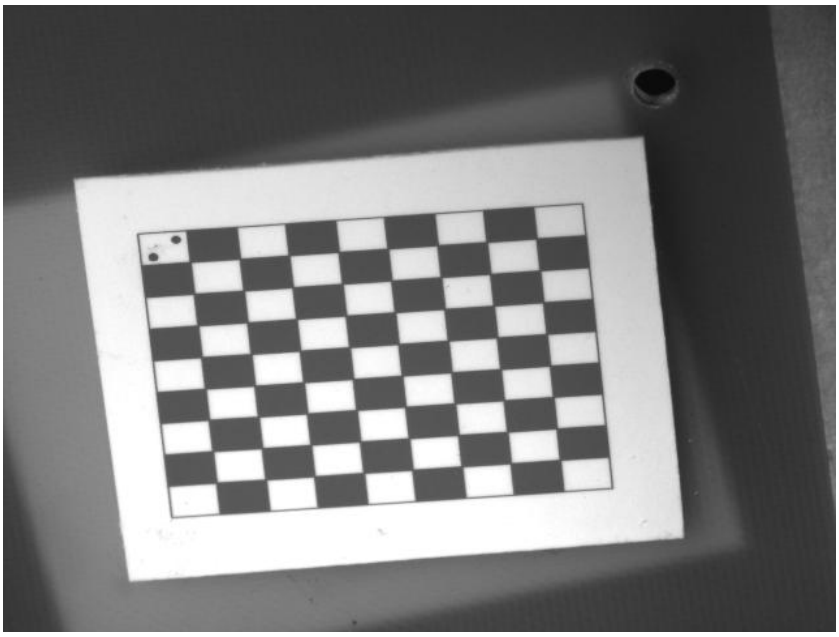

Figure 5-2 Calibration chessboard: Glossy paper print support.

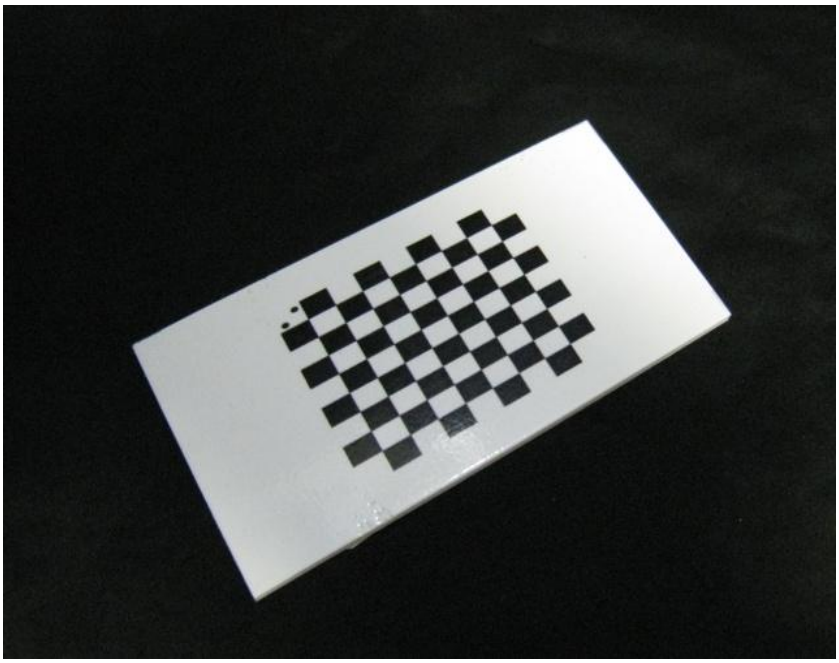

Figure 5-3 Calibration chessboard: Rigid plastic support.

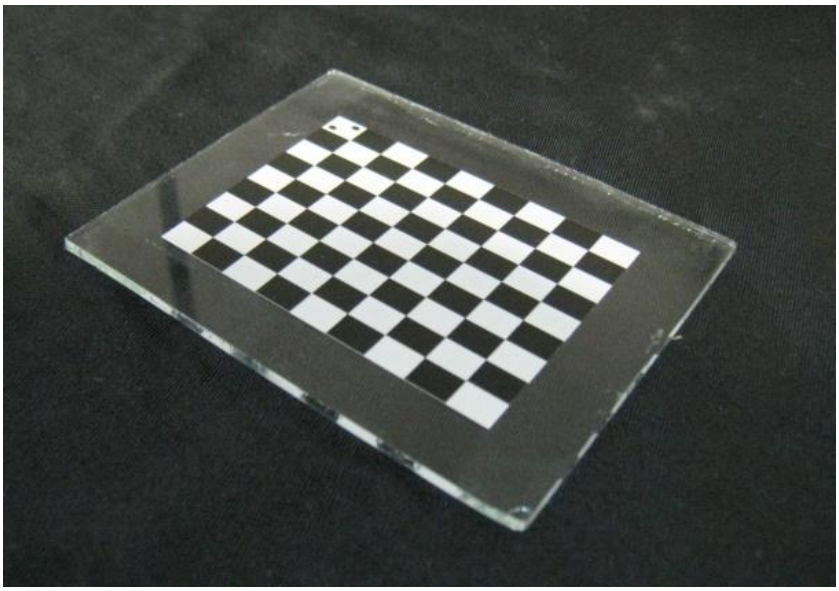

Figure 5-4 Calibration chessboard: Glass print support.

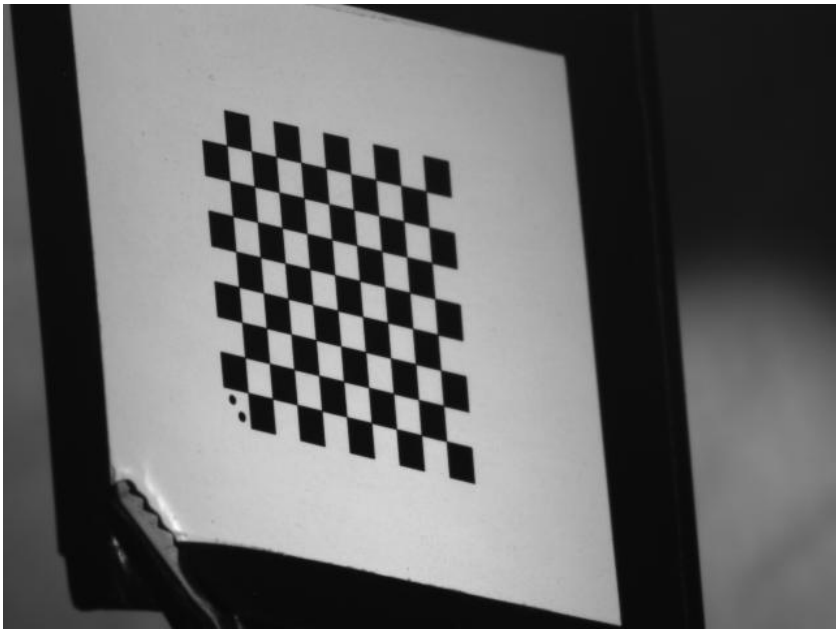

Figure 5-5 Calibration chessboard: Matte hi-res paper print support.

The performance of the selected targets have been evaluated in terms of calibration re-projection error. From the Monte Carlo analysis described in §4, we can observe in fact that the re-projection error is stable w.r.t. to the variability of input noise, leading to the hypothesis that significant variations of such parameter between different calibration tests, performed over different target print supports, can be only attributed to the different material reflective properties.

The tests results reported in Table 5-3 show that the best calibration performance is obtained with the high resolution Matte Paper target.

Print support	Re-p. error standard deviation [pixel]
Glossy Paper	0.11765
Plastic	0.17284
Glass	0.14539
Matte Hi-res Paper	0.05242

Table 5-3 Re-projection error with different chessboard print supports.

The amount of calibration images needed to perform calibration tests has been estimated in order to get a best compromise between duration of calibration procedure sequence and the reachable accuracy in parameter estimation. The graph in Figure 5-6 represents the standard deviation of re-projection error (both in horizontal and vertical direction) at the varying of the number of calibration images, obtained by a calibration test of the STC FB Forward channel: it can be noticed that despite a slight increase up to about 30 images, the value is almost stable above about 40 calibration images.

Concerning camera parameters estimation, in Figure 5-7 the focal length variation and its relative estimated accuracy vs the number of input images are reported. It can be noticed that the estimated value for the focal length presents a variation of about 4mm within the considered range of image numbers, accompanied by an increase of focal length estimation accuracy, from about ±3 mm to less than ±1.5 mm.

From the results we can conclude that, to get an estimation of camera parameters with best accuracy, a suitable set of calibration images must range between 50 and 70 target pictures.

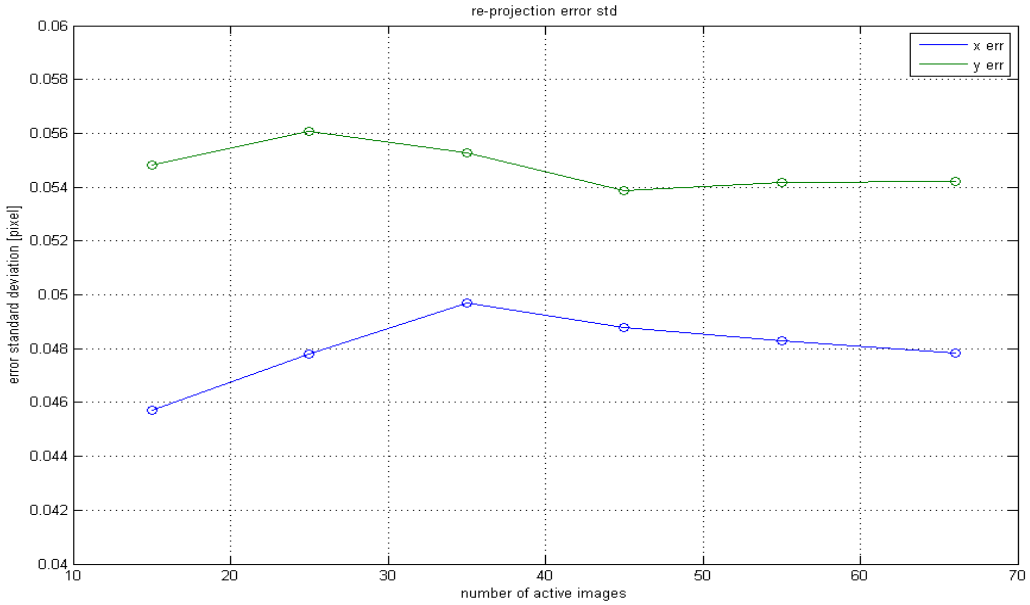

Figure 5-6: STC SVS with STC FB Forward channel camera calibration: re-projection error standard deviation VS number of calibration images.

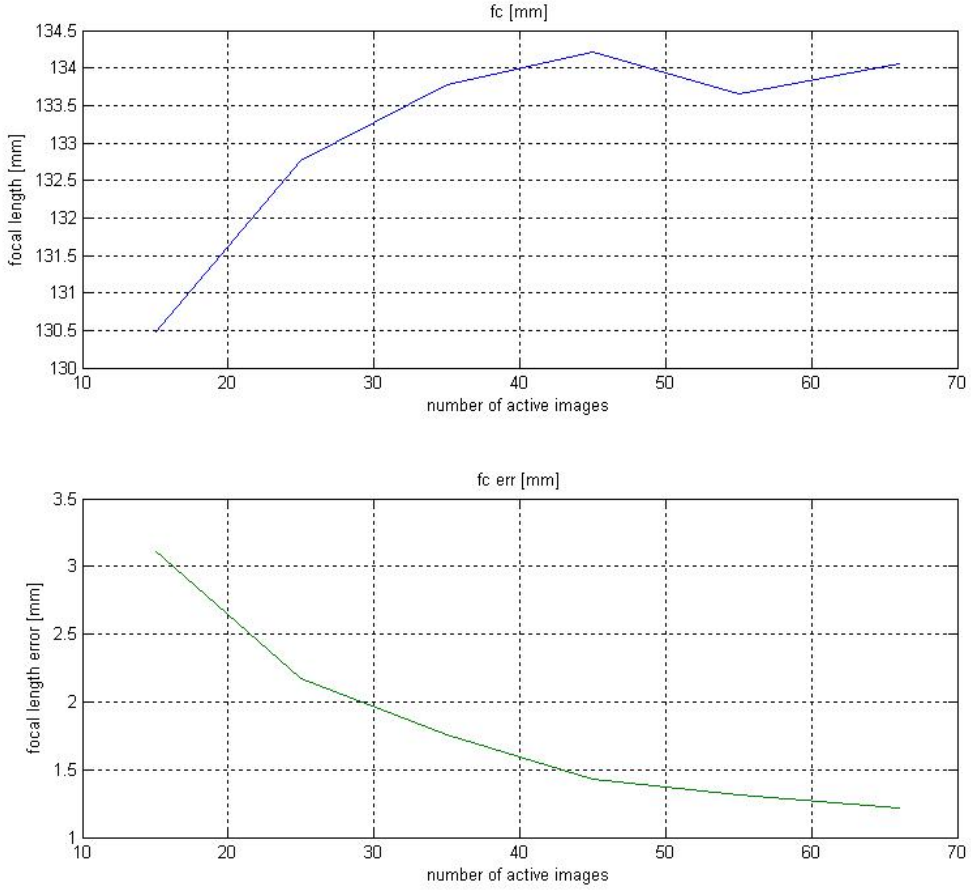

Figure 5-7 STC SVS with STC FB – FWD Channel a) Estimated focal length versus number of calibration images. b) estimated focal length uncertainty versus number of calibration images.

5.4 Camera calibration test with STC functional breadboard

In this section the results of the experimental activity for the calibration of the STC SVS configured with STC FB are reported. The Forward and Backward looking channels have been calibrated several times in order to evaluate calibration process repeatability. The calibration tests evidenced the following aspects:

- The camera center coordinates cannot be estimated accurately by the Zhang calibration algorithm for this specific application: because of the system geometry, with a long focal length and very narrow field of view, the corner coordinates doesn't provide enough information to get a camera center estimation. Anyway, as a good approximation, the camera center can be assumed to be at the center of image plane.
- The optical distortion contribution in terms of radial and tangential distortion coefficients is not evaluable. According to the results obtained by ray-trace simulation, the optical system is working close to optical axis, with a very narrow field of view. As a consequence the contribution of radial and tangential distortion is lower than the noise introduced in feature coordinates by the imaging system.
- The focal length along the *x* and *y* image frame axis assume the same values within the estimated uncertainties, so the camera pixel must be assumed to have the same height and width.
- The skew factor resulted to be negligible in both cameras: the pixel can be assumed to be squared for each evaluated CMOS.

The set of parameters extracted by means of single camera calibration process has been reduced to the following:

- Focal length, expressed in pixel units.
- Camera extrinsic parameters: position of calibration chessboard w.r.t. camera reference frame. The camera extrinsic parameters are provided in the following structure:
    - Rotation vector *Omc*: rotation, in radians, w.r.t. *X*, *Y*, and *Z* axis.
    - Translation vector *Tc*: 3D vector, in pixel units.

All the evaluated parameters are provided with an estimated error, as specified in 2.3.

5.4.1 Forward Channel calibration

The forward looking channel has been tested in-lab several times, in the following table are reported the measured focal length.

"Forward" camera			
Calibration test no	**Re-projection error [x, y] [pixel]**	**Focal length [mm]**	**Focal length error [mm]**
1	[0.045 0.051]	134.24	1.44
2	[0.048 0.053]	136.86	1.61
3	[0.047 0.055]	136.29	1.76
4	[0.050 0.055]	135.30	1.70
5	[0.048 0.055]	134.55	1.82
6	[0.048 0.054]	134.11	1.24

Table 5-4: SVS with STC FB Forward channel: results of several calibration tests.

The first column reports the calibration test number, the second column shows the re-projection error, the third and fourth columns report the estimated focal length for the whole optical system and the relative estimated uncertainty in millimeters respectively, considering a sensor's pixel size of 9.9μm.

The results of the different calibration sessions evidenced that the estimated value for focal length is stable within the estimated uncertainties, as evidenced in Figure 5-8, with a mean focal length value equal to 135.22 mm. The obtained value is compatible with preliminary numerical analysis of the optical system, according with the simulations performed in §4.

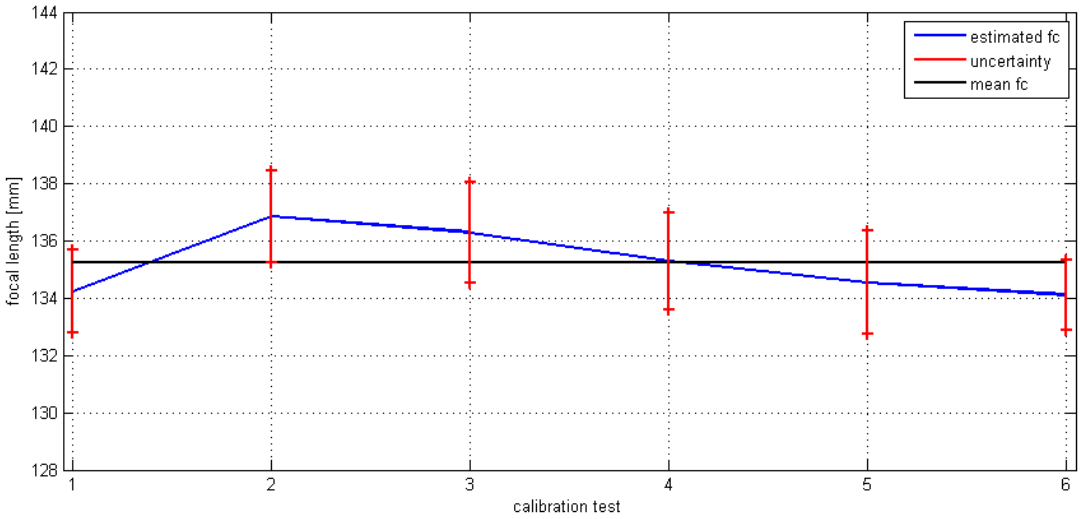

Figure 5-8 STC SVS with STC FB: FWD channel focal length estimation – the estimated mean value for focal length is always within the uncertainty bar of every single test.

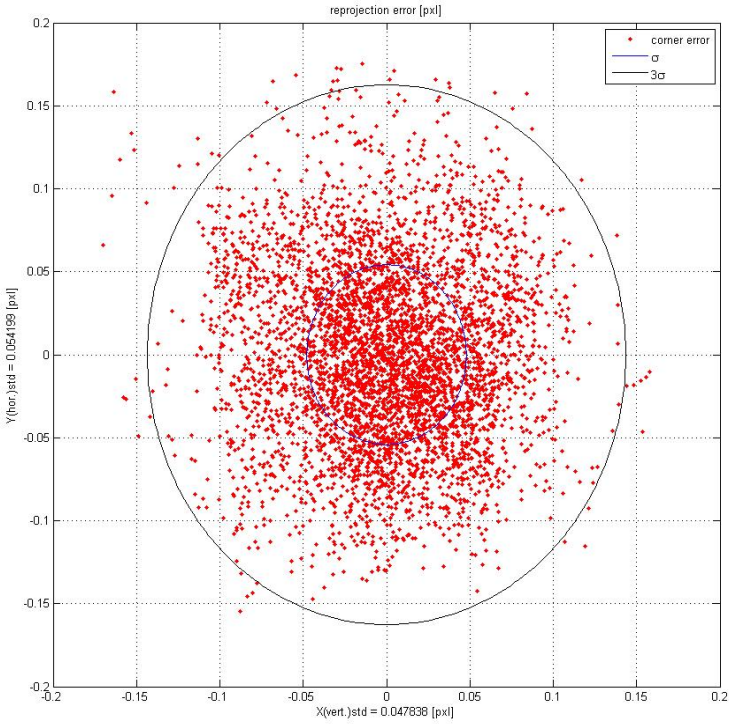

Figure 5-9 Re-projection error – calibration test no 6: the red points coordinates represent the distance between extracted corner coordinates and back-projected model coordinates along x and y directions for each image, using the computed equivalent pin-hole model. The 1-σ curve (blue line) is close to 0.05 pixel along both directions.

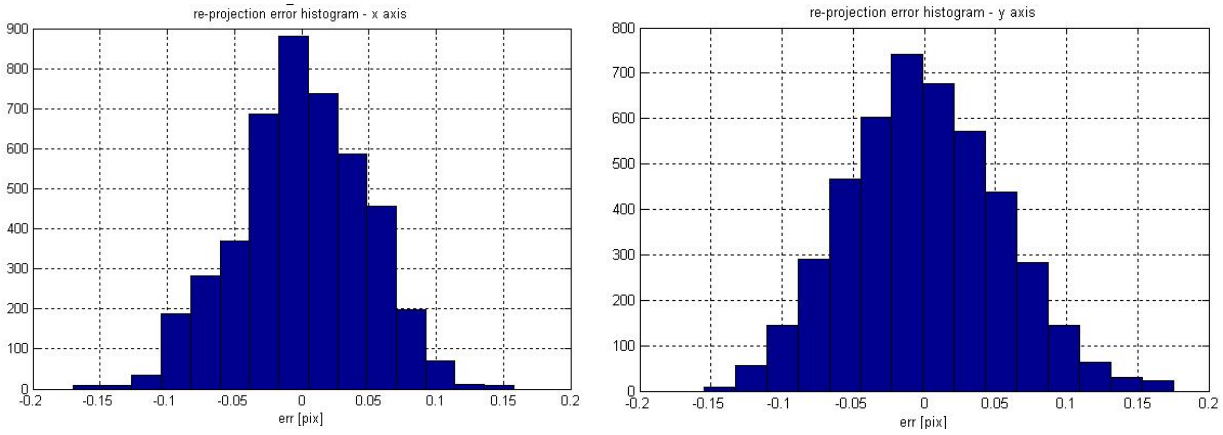

Figure 5-10: Forward channel - Re-projection error histograms – calibration test no 6. The two histograms represent the distribution of re-projection error along horizontal and vertical direction respectively, in pixel. The two distributions can be compared to a Normal distribution with zero mean and $\sigma^2 \approx 0.05$ pixel.

Figure 5-9 shows the re-projection error obtained in one of the calibration tests. Each red point represents the distance, expressed in pixel, between the extracted feature coordinate from calibration image and the back-projection of its corresponding chessboard model corner with the

estimated extrinsic and intrinsic camera parameters. It can be noticed that the 1-σ curve of re-projection error is close to 0.05 pixel along both directions, while the 3-σ curve, containing the 99.8% of the back projected points, is near to 0.15 pixel.

The obtained results underline that the equivalent pinhole model obtained describes with sufficient accuracy the analyzed optical channel.

5.4.2 Backward Channel calibration

The same calibration test has been performed several times on the STC SVS aligned with the Backward channel of the STC FB. Table 5-5 reports the re-projection error and the focal length values obtained.

"Backward" camera			
Calibration test no	**Re-projection error [x, y] [pixel]**	**Focal length [mm]**	**Focal length error [mm]**
1	[0.057 0.048]	135.87	1.69
2	[0.052 0.047]	135.54	1.66
3	[0.046 0.055]	136.77	1.82
4	[0.046 0.057]	136.34	2.08
5	[0.049 0.053]	135.25	1.78
6	[0.047 0.057]	135.74	1.40

Table 5-5 SVS with STC FB Forward channel: results of several calibration tests.

The results of different calibration sessions evidenced that the extracted value for focal length is stable within estimated uncertainties, as evidenced in Figure 5-11, with a mean estimated value equal to 135.92 mm, which is, as in Forward channel case, in accordance with the preliminary numerical analysis of the optical system.

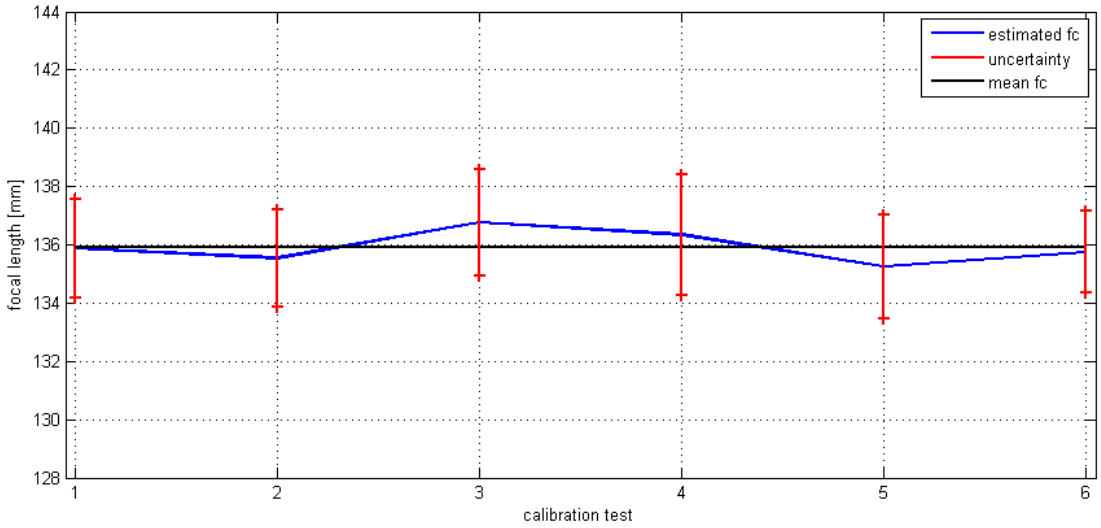

Figure 5-11 STC SVS with STC FB: Backward channel focal length estimation – the estimated mean value for focal length is always within the uncertainty bar of every single test.

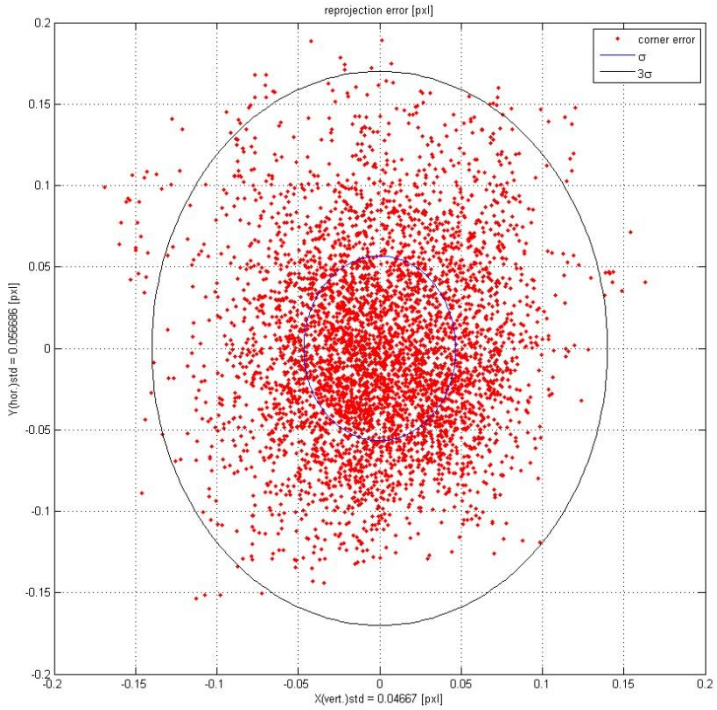

Figure 5-12 Re-projection error – calibration test no 6: the red points coordinates represent the distance between extracted corner coordinates and back-projected model coordinates along x and y directions for each image, using the computed equivalent pin-hole model. The 1-σ curve (blue line) is close to 0.05 pixel along both directions.

As in Forward channel case, the number of calibration images provided as input for calibration algorithm has been evaluated in order to get the best match between test data and calibration accuracy. Figure 5-12 shows the distribution of re-projection error for one of the performed

calibration test. The calibration error standard deviation is close to 0.05 pixel in both horizontal and vertical direction.

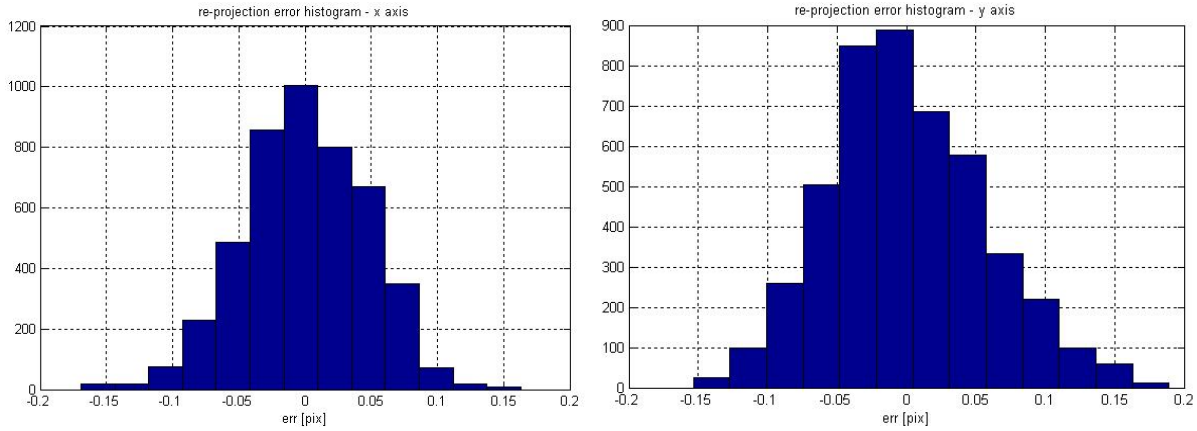

Figure 5-13: Forward channel - Re-projection error histogram – calibration test no 6. The two histograms represent the distribution of re-projection error along horizontal and vertical direction respectively, in pixel. The two distributions can be compared to a Normal distribution with zero mean and $\sigma^2 \approx 0.05$ pixel.

5.5 **Stereo Camera calibration**

A preliminary evaluation of extrinsic parameters of the SVS with STC FB has been performed using the stereo extension of the calibration software (see 5.2). As specified in 2.3, the orientation parameters are computed in terms of a rotation and a translation which define the position and orientation of the right camera reference frame (the "Backward" camera in SVS) expressed w.r.t. left camera ("Forward" camera in SVS) reference frame. The position and orientation of the reference frames axes for this particular application are shown in Figure 5-14.

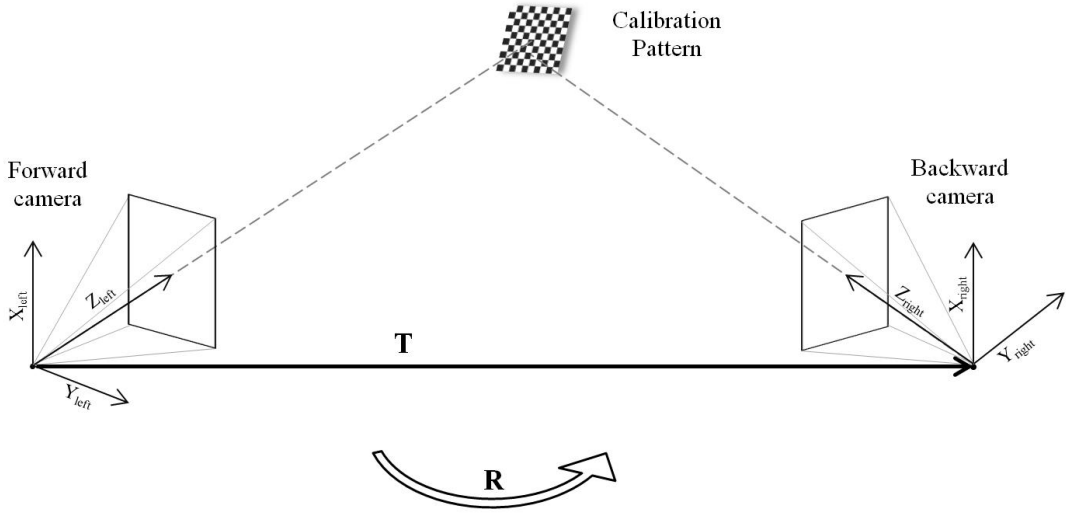

Figure 5-14: SVS pinhole model. Illustration of cameras disposition and reference frames axis orientation.

The calibration test has been repeated with two different stereo image sets, the results are reported in the two columns of Table 5-6. It can be noticed that the re-projection error, which in stereo calibration is given as the combination of error both in *x* and *y* directions, significantly decrease increasing the number of calibration stereo images.

Parameter		**Test 1**	**Test 2**
R [rad]	R_x	0,68919 ± 0,0010	0,68958 ± 0,0003
	R_y	0,00498 ± 0,0003	0,00295 ± 0,0001
	R_z	0,00835 ± 0,0003	0,00493 ± 0,0001
T [mm]	T_x	2,16 ± 0,44	1,42 ± 0,11
	T_y	911,49 ± 1,07	915,91 ± 0,31
	T_z	321,02 ± 0,93	307,13 ± 0,27
Baseline [mm]		966,37 ± 1,48	966,03 ± 0,43
Images no		43	65
Error [pixel]		0,3467	0,1620

Table 5-6: SVS with STC FB – stereo calibration results of two calibration tests.

The values extracted for rotation and translation from Forward to Backward camera reference frame give a self-consistent set of parameters (within uncertainties): the parameters resulting from different calibrations may differ significantly as their computation is limited to corners coordinates accuracy[6]. However, the two baseline values extracted by the two translation vectors are very close considering parameters uncertainties.

The maximum likelihood optimization code of stereo calibration software can be set to perform a global optimization of the optical system, refining both extrinsic and intrinsic cameras parameters. In this particular application, due to the particular system geometry characterized by long focal values and narrow angles, the intrinsic parameters optimization didn't provide appreciable improvements in terms of calibration error.

Figure 5-15 shows the distribution of re-projection error in both directions for the stereo calibration test no 2: the two error components presented a standard deviation value of 0.13 and 0.18 pixel respectively.

[6] The setup alignment conditions have been preserved during the whole calibration tests: the differences in parameters values is only imputable to calibration algorithm accuracy and to optical system properties. Each set of so computed parameters can be used as initial input for any stereo imaging pipeline, and they can be subsequently refined by means of bundle adjustment process.

a.

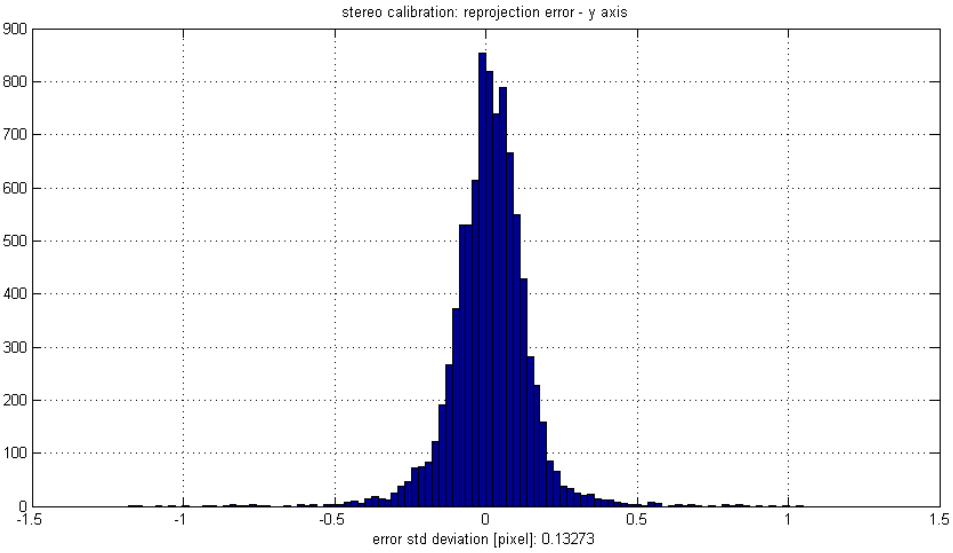

b.

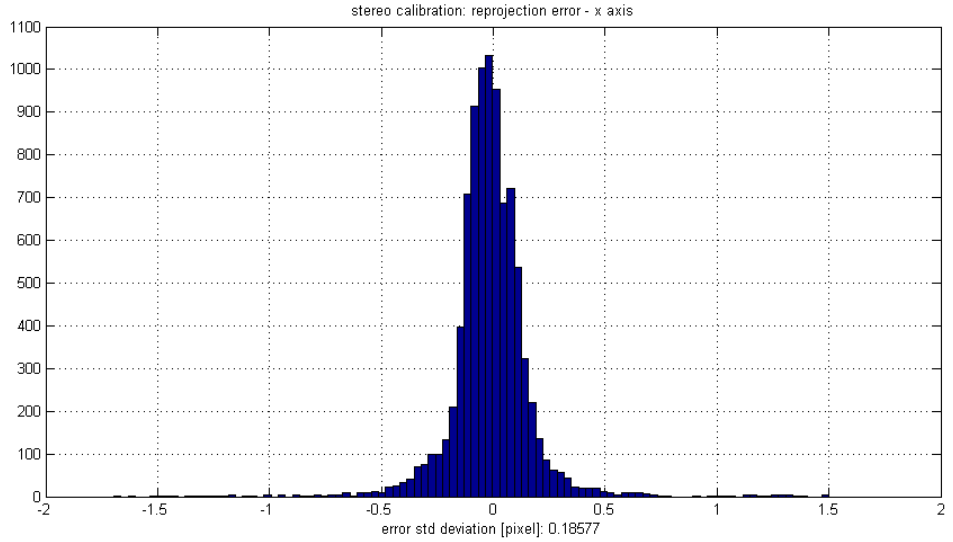

Figure 5-15: SVS with STC FB – stereo calibration re-projection error. Histograms of re-projection error along x axis (a) and y axis (b). The two distribution present a standard deviation value of 0.13 and 0.18 pixel respectively.

The next figures show an example of stereo couple of calibration target images before stereo rectification (Figure 5-16a) and after stereo rectification (Figure 5-16b), computed over the extrinsic parameter set estimated in stereo calibration test no 2.

a.

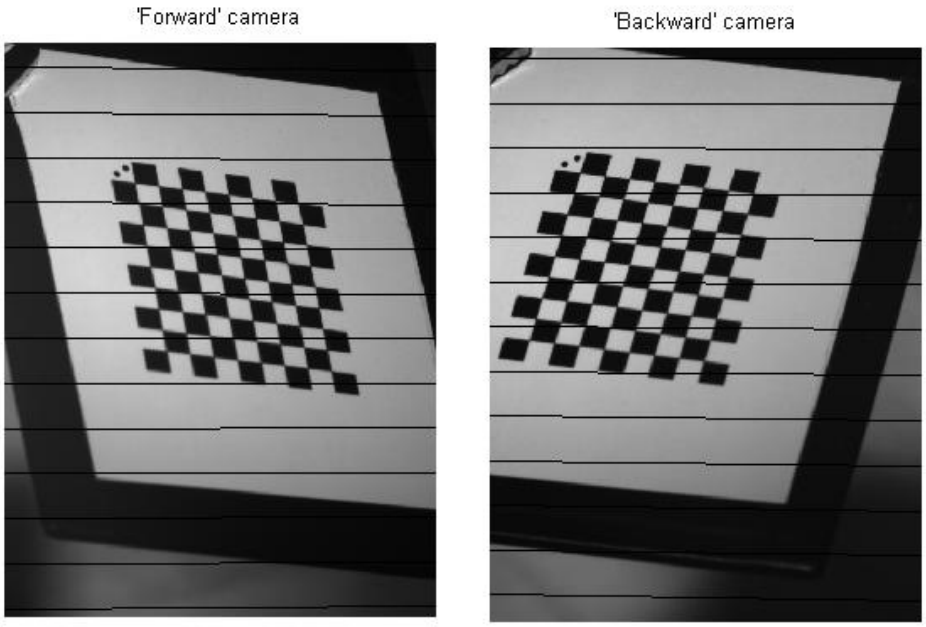

b.

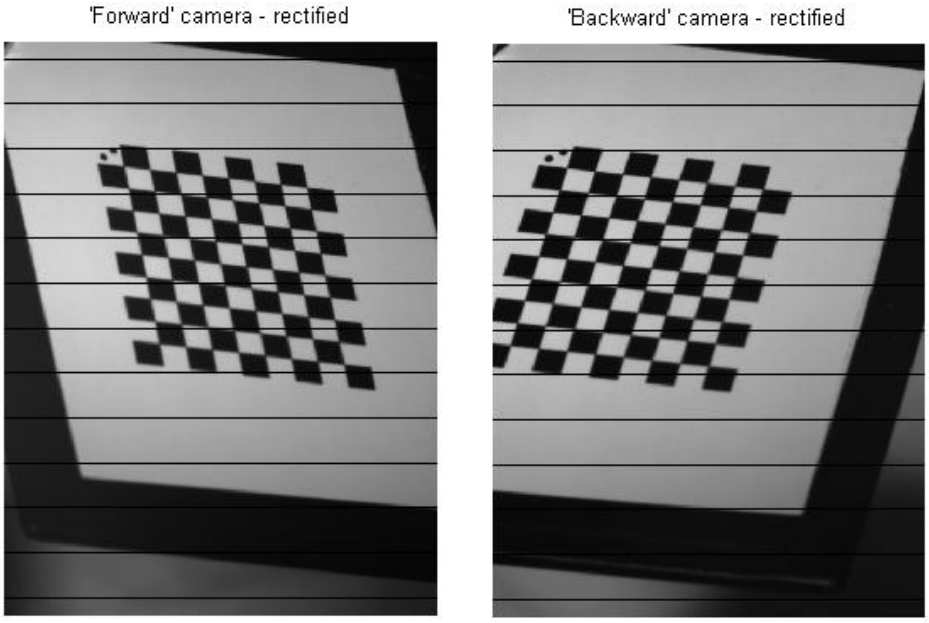

Figure 5-16: Stereo couple of calibration target images with epipolar lines, in black, before stereo rectification (a) and after stereo rectification (b).

5.5.1 Target surface 3D reconstruction test

As a 3D reconstruction preliminary test, the stereo calibration data have been applied to perform a stereo reconstruction of calibration target surface. The calibration target surface has been assumed to be a nearly planar target.

The 3D coordinates of the chessboard corners have been triangulated with least squares method, and the obtained surfaces have been compared with a reference plane. Figure 5-17 shows the

surface reconstruction obtained from a stereo couple acquired during the second stereo calibration test: the bottom blue colored surface and the top brown surface represent the constraint for vertical accuracy, which is equal to 170 µm (see 3.2.4). As we can observe the 3D reconstruction of the planar target fulfills the vertical accuracy requirement.

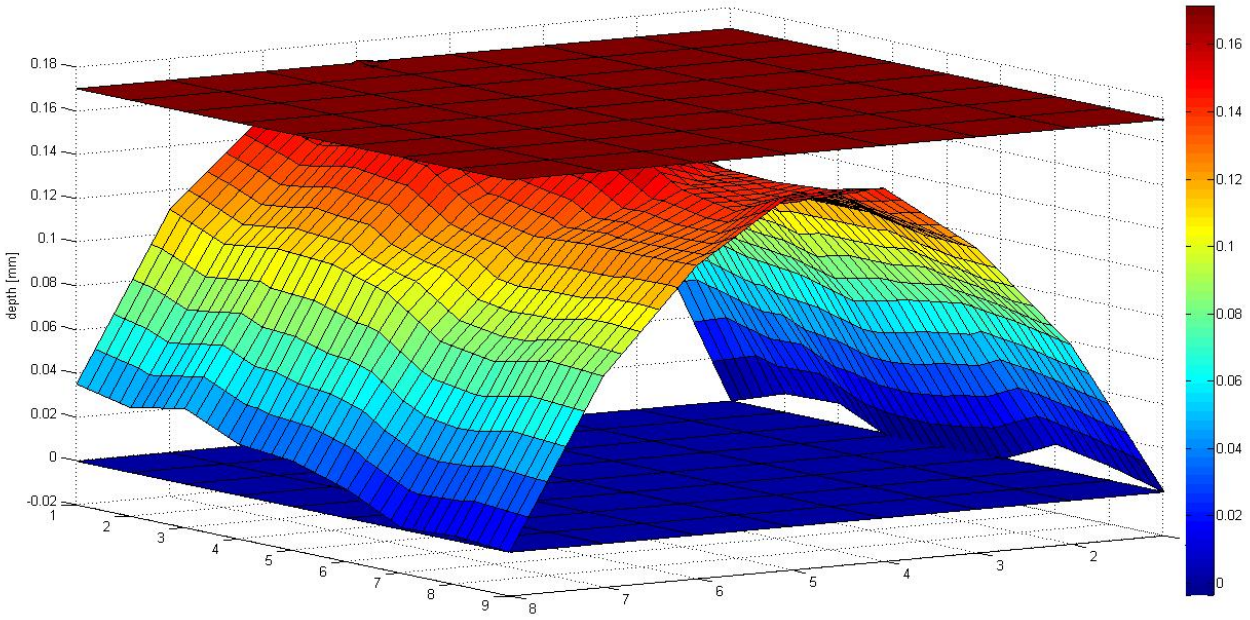

Figure 5-17: 3D stereo reconstruction of calibration pattern. The 3D surface is the result of the interpolation of the 3D data obtained from triangulation. The bottom and top planes are placed at 0 and 170µm respectively, representing the vertical accuracy requirement for the stereo validation activity.

Table 5-7 reports the results of 10 different chessboard reconstruction tests, obtained by 10 different chessboard poses stereo couples. The first three column report the estimated chessboard rotation w.r.t. left (Forward) camera reference frame (Figure 5-14). The 10 poses here analyzed have been obtained by 2 deg rotations of the target rotation stage, according with the estimated R_x data of the first column. The error in chessboard reconstruction has been computed as the standard deviation of the distance of each chessboard point from a reference plane, obtained computing the mean depth of all chessboard points.

Chessboard rotation [deg] – left camera reference frame			Chessboard error std [mm]
Rx	**Ry**	**Rz**	
27,61	2,64	-4,58	0,0551
25,61	2,60	-4,61	0,0558
23,61	2,55	-4,67	0,0558
21,61	2,50	-4,73	0,0571
19,62	2,45	-4,80	0,0566
17,63	2,39	-4,85	0,0565
15,64	2,33	-4,90	0,0560
13,66	2,27	-4,96	0,0556
11,66	2,20	-5,01	0,0548
9,67	2,14	-5,07	0,0530

Table 5-7: 3D reconstruction error of calibration target.

From the results we can observe that the standard deviation of 3D points error is within the vertical accuracy requirement, and that the amount of error is stable w.r.t. target attitude.

5.6 Stereo validation preliminary results

The calibration data, together with stereo couples of images of the stone samples have been provided as input to a stereo reconstruction pipeline based on the Dense Matcher [27] software, developed at the University of Parma. Figure 5-18 and Figure 5-19 illustrate the results of the comparison between obtained DTMs and the laser scanning for two of the stone samples analyzed. The grey surfaces represent the laser scanner data, while the color map represents the distance of the stereo DTM points from the corresponding laser scanner reference: violet to cyan tones represent error ranging from -0.9 to -0.1 mm, while the dark green to yellow tones represent distances ranging from 0.1 to 0.9 mm. The barrel distortion visible in Figure 5-17 have been corrected by re-computing extrinsic parameters with bundle adjustment technique [25][28].

Sample	RMS (mm)	# points	% of inliers
Anorthosite	0.125	193457	94.4
Basalt_1	0.072	207025	99.8
Basalt_2	0.091	66421	97.3
Concrete	0.060	164200	99.9

Table 5-8: Stereo validation activity with STC FB results.

Table 5-8 shows the results obtained with the different stone samples: once aligned, the RMS value of the distance between the two DTMs has been computed rejecting the points which presented a distance greater than 0.5 mm from reference. The percentage of inlier points is then the percentage of points from the total computed from the matching algorithm which are within this threshold. The number of detected points and inliers percentage is largely dependent on target surface texturing and reflective properties and on the matching algorithm settings.

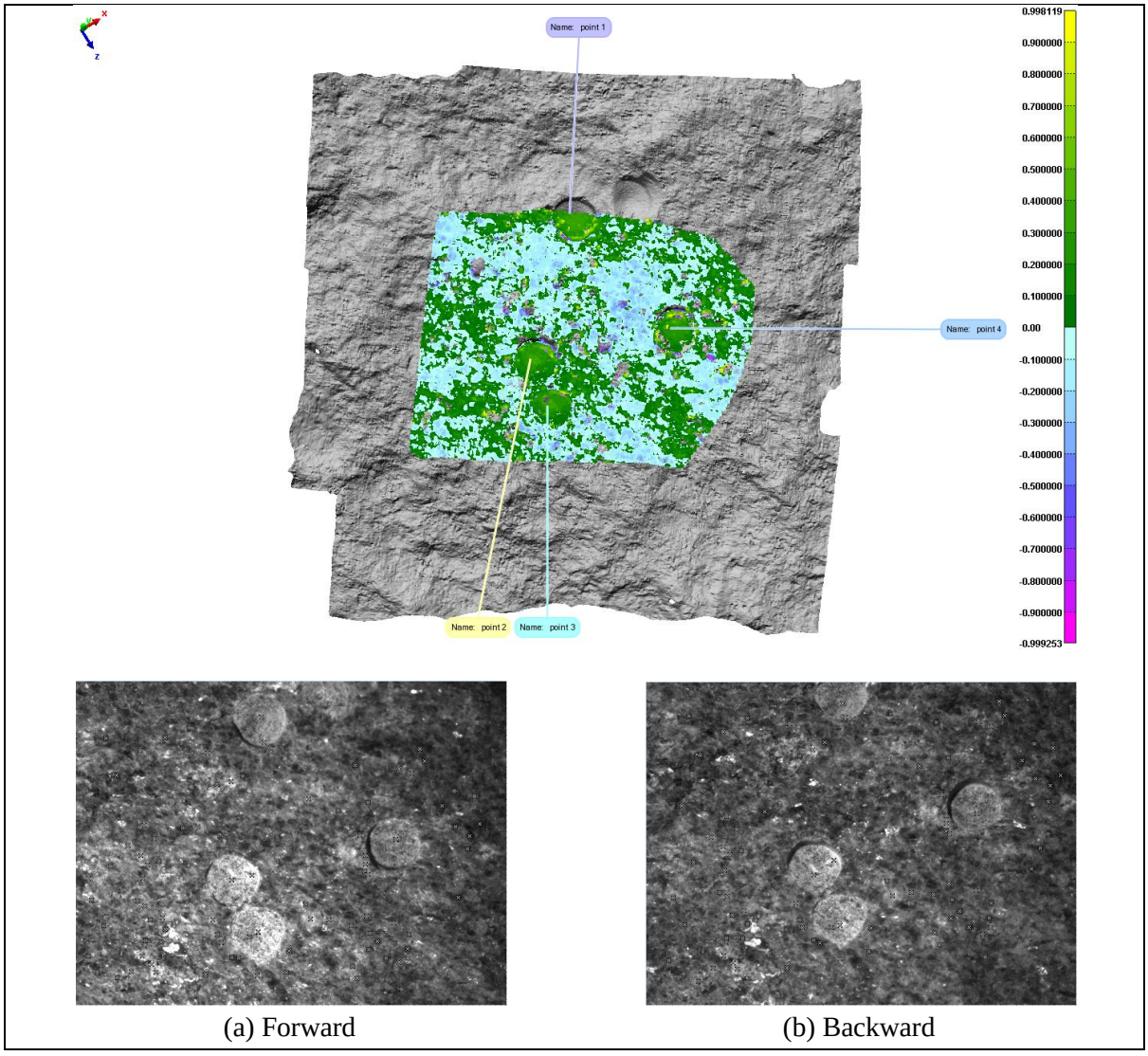

(a) Forward (b) Backward

Figure 5-18: ANORTHOSITE stone sample DTM color-coded error map compared with reference laser scanner DTM. DTM obtained from (a) Forward channel and (b) Backward channel images with +20 deg light incidence angle.

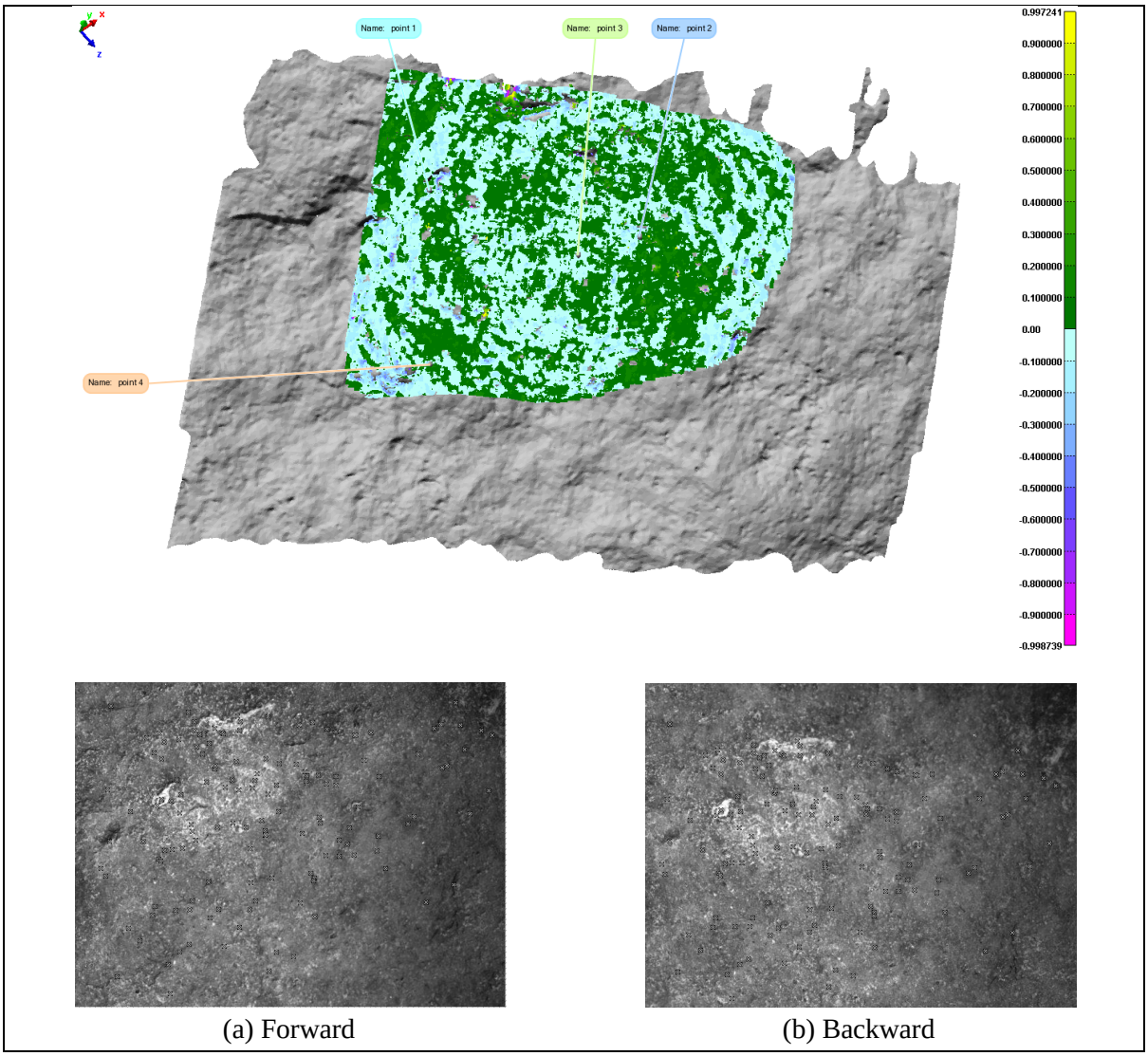

(a) Forward (b) Backward

Figure 5-19: BASALT_1 stone sample DTM color-coded error map compared with reference laser scanner DTM. DTM obtained from (a) Forward channel and (b) Backward channel images with +20 deg light incidence angle.

FIGURE shows the results obtained with a concrete sample, which lead to the best results with an RMS value equal to 60 µm. In this figure the violet to cyan tones represent error ranging from -0.2 to 0 mm, while the dark green to yellow tones represent distances ranging from 0 to 0.2 mm.

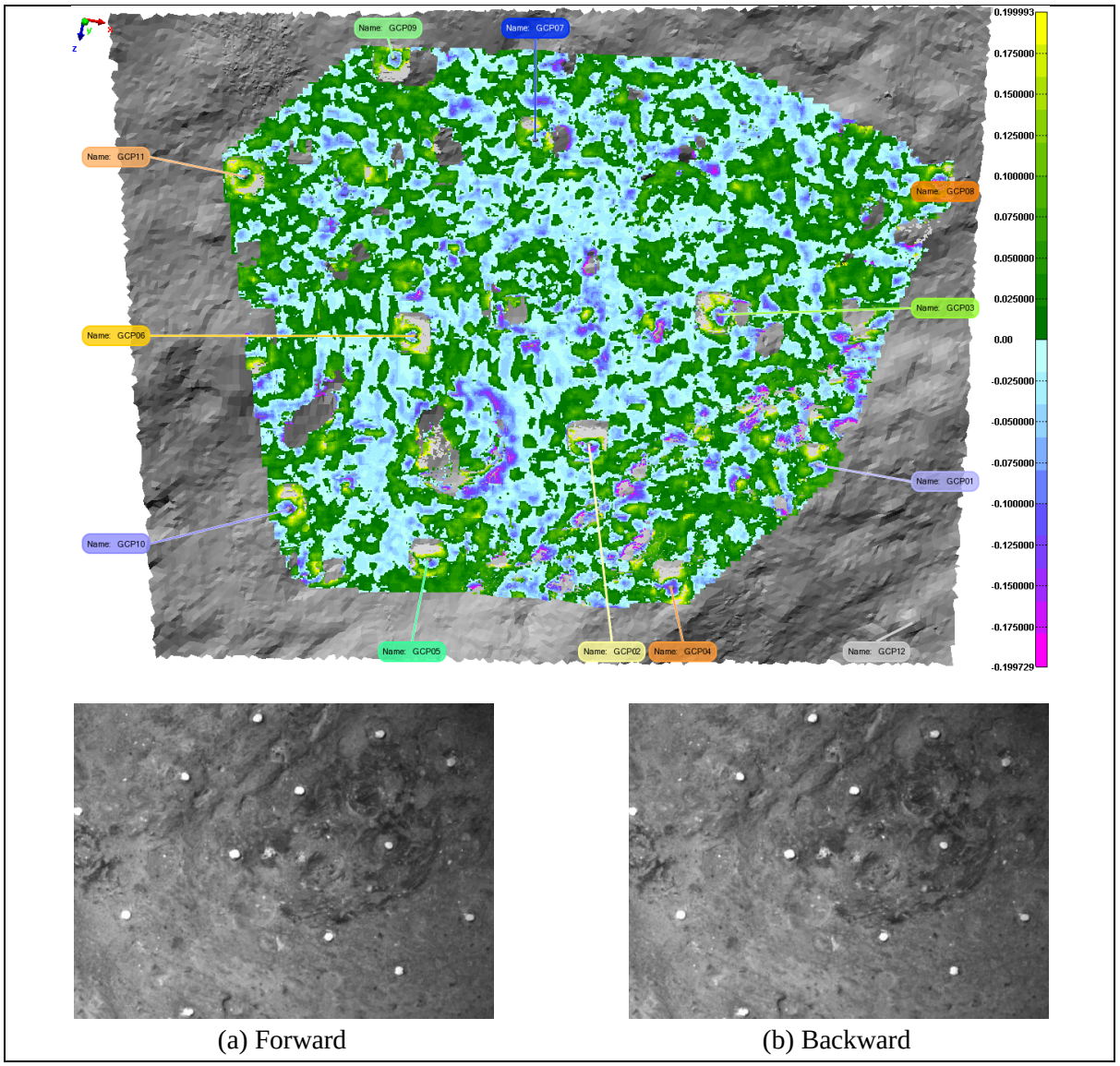

(a) Forward (b) Backward

Figure 5-20: Concrete stone sample DTM color-coded error map compared with reference laser scanner DTM. DTM obtained from (a) Forward channel and (b) Backward channel images with +20 deg light incidence angle.

5.7 Conclusions

From the results obtained with the experimental activity with the functional model of STC we can conclude that the calibration procedure provides an evaluation of the optical system parameters with a suitable accuracy for this particular application. The oscillation of the estimated values through the different calibration tests is compatible with the variability observed in numerical simulation phase at §4, due to the variability of input noise. For what concerns calibration process we can conclude that the results validate the procedure developed for the numerical simulation of the calibration process.

The preliminary results obtained from the comparison of the stereo reconstruction of the stone samples with the relative reference measures present RMS values that are compatible with the accuracy requirements defined in §3.

Conclusions

The main goal of this work was the development of numerical and experimental methods for the validation of the stereo performance of the SIMBIO-SYS STC onboard BepiColombo mission.

The STC instrument is a stereo camera with two sub-channels oriented at ±20 deg with respect to Nadir direction. STC telescope design is innovative: it's composed of two optical sub-channels with a common sensor and it will acquire images with the push frame concept, instead of the most common push-broom mode.

A verification of the 3D reconstruction ability of the STC camera before launch is needed. Unfortunately it is not possible to foresee calibration activities with the flight model of the camera placed outside or mounted on an airplane; thus an indoor pre-flight verification of the stereo instrument performance had to be planned. A stereo validation set-up (SVS) has to be developed to reproduce indoor at a finite distance the geometry of the acquisition on the Mercury's surface. The additional optical and mechanical components of the SVS allows the reproduction of the observing geometry in at least one point of the spacecraft trajectory. The collimator lens of the SVS brings the focusing distance of STC from the 400 km of the in-orbit situation to the about one meter of the laboratory one. The reduction of the focusing distance involves a downscaling of the stereo reconstruction problem: the resolution and vertical accuracy requirements have been scaled with the same proportion which relates the on-flight baseline and the in-lab baseline.

The basic concept for the stereo validation set-up is to perform a tridimensional reconstruction of a target, which replicates in scale the morphologic and radiometric properties of the Mercury surface. The target has to be known with a much better accuracy than the one that can be reached with the stereo reconstruction process, so that the reconstruction ability of the STC can be evaluated. The comparison between the stereo DTM of the target obtained with STC using the SVS and the reference target measure, done with the laser scanner, will provide information about the STC stereo reconstruction accuracy.

In order to provide a preliminary verification of the stereo validation setup performance and to define the stereo validation procedure before integration with STC FM, a functional model of the STC has been realized. STC functional model replicates the instrument main optical and geometrical features using mainly commercial hardware.

The stereo validation activity can be resumed in three main phases:

- Setup calibration: the reconstruction of depth information from stereo images of an observed surface requires the characterization of the imaging system in terms of camera calibration process. Several images of a calibration pattern have been acquired with the two sub-channels of the setup. The images have been processed with a classical camera calibration algorithm, which provided an estimation the intrinsic parameters, defining the camera model of the two cameras, and a preliminary estimation of the extrinsic parameters of the imaging system;
- Target stereo reconstruction: the calibration parameters together with stereo couples of images of the stone samples have been provided as input for a stereo reconstruction pipeline, based on dense stereo matching classical algorithms;
- Evaluation of DTM accuracy: the stereo reconstruction of the target is aligned with the laser scanner digital map, computing the distance between each point of the stereo DTM with the closest point of the reference measure. The accuracy of the stereo reconstruction is quantified as the standard deviation of the distances between the two surfaces.

The results obtained from the comparison between the obtained DTM and the reference laser scanner measurement lead to encouraging results which completely fulfill the requirements, with a best RMS value of reconstruction error equal to 60 μm.

Before experimental activity, a numerical simulation of the setup based on the ray-trace model of the optical system has been performed to simulate the calibration process: this activity allowed the preliminary test of the calibration procedure, evaluating the performance of classical camera calibration algorithms with statistical methods. For the simulation activity it was considered the case of stereo validation both with the functional model the STC and with the STC FM. The results of numerical analysis provided useful information, in particular concerning the possibility of adopting the classical pinhole model to describe the optical system, also in case of a complex optical design such as for the STC FM case, and the evaluation of optical distortion contribution, which in both cases resulted to be negligible if compared with the input noise.

The results obtained from experimental activity with the functional model of STC compared with the simulations results validated the numerical method developed, providing important information for the application of the calibration process to the flight model of the instruments.

From the results we can conclude that:

- The developed stereo validation method can be applied for the evaluation of reconstruction capabilities of stereo telescopes.

- The preliminary results with the functional model of STC show that the observing geometry of the STC instrument is compatible with the vertical accuracy requirement, considering observations at periherm.

The stereo validation activity will be completed within April 2013 with the integration of the stereo validation setup with the flight model of the STC. Thanks to the flexibility of the setup, the work done and the acquired knowledge anyway open the door to several new possible investigation subjects: from the testing of novel stereo reconstruction methods performance on mission-like data, to the evaluation of the impact of light incidence on the reconstruction of tridimensional structures, to the test of different observing geometries or different optical design.

References

[1] Davies M. E. et al., *"Atlas of Mercury"*, NASA SP-423, 1976.

[2] Cook A. C. and Robinson M. S., "*Mariner 10 stereo image coverage of Mercury"*, JGR, Vol. 105 (4), 9429-9443, 2000.

[3] Slavin J. A., Owen J. C. J., Connerney J. E. P. and Christon S. P., *"Mariner 10 observations of field aligned currents at Mercury"*, Planetary and Space Science, Vol. 45 (1), 133-141, 1997.

[4] Solomon, S.C., McNutt, R.L., Gold, R.E., Acuna, M.H., Baker, D.N., Boyton, W.V., Chapman, C.R., Cheng, A.F., Gloeckler, G.,Head, J.W., Krimigis, S.M., McClintock, W.E., Murchie, S.L., Peale, S.J., Philips, R.J.,Robinson, M.S., Slavin, J.A., Smith, D.E., Strom, R.G., Trombka, J.I., Zuber, M.T., 2001. *"The MESSENGER mission to Mercury: scientific objectives and implementation."* Planet.SpaceSci.49,1445–1465.

[5] Anselmi A., Scoon G. E. N., *"BepiColombo, ESA's Mercury Cornerstone mission"*, Planetary and Space Science, Volume 49, Issue 14-15, p. 1409-1420, 2001.

[6] Benkhoff J., van Casteren J., Hayakawa H., Fujimoto M., Laakso H., Novara M., Ferri P., Middleton H. R., Ziethe R., *"BepiColombo—Comprehensive exploration of Mercury: Mission overview and science goals"*, Planetary and Space Science, Volume 58, Issues 1–2, Pages 2-20, ISSN 0032-0633, 10.1016/j.pss.2009.09.020, January 2010.

[7] BepiColombo Project Team, *"Experiment Interface Document – Part A"*, BepiColombo, BC-EST-RS-01140, issue 1, rev.0, 2008.

[8] H. Hayakawa, Y. Kasaba, H. Yamakawa, H. Ogawa and T. Mukai, *"The BepiColombo/MMO model payload and operation plan"*, Advance in Space Research, vol. 33, pp. 2142-2146, 2004.

[9] E. Flamini, F. Capaccioni, L. Colangeli, G. Cremonese, A. Doressoundiram, J.L. Josset, Y. Langevin, S. Debei, M.T. Capria, M.C. De Sanctis, L. Marinangeli , M. Massironi, E. Mazzotta Epifani, G. Naletto, P. Palumbo, P. Eng, J.F. Roig, A. Caporali, V. Da Deppo, S. Erard, C. Federico, O. Forni, M. Sgavetti, G. Filacchione, L. Giacomini, G. Marra, E. Martellato, M. Zusi, M. Cosi, C. Bettanini, L. Calamai, M. Zaccariotto, L. Tommasi, M. Dami, J. Ficai Veltroni, F. Poulet, Y. Hello and The SIMBIO-SYS Team, *"SIMBIO-SYS: The spectrometer and imagers integrated observatory system for the BepiColombo planetary orbiter"*, Planet. Space Sci., vol. 58, pp. 125-143, 2010.

[10] G. Marra, L. Colangeli, E. Mazzotta Epifani, P. Palumbo, S. Debei, E. Flamini and G. Naletto, *"The optical design and preliminary optomechanical tolerances of the high resolution imaging channel for the BepiColombo mission to Mercury"*, Proc. SPIE 6273, 6273-28, 2006.

[11] V. Da Deppo, G. Naletto, G. Cremonese, and L. Calamai, *"Optical design of the single-detector planetary stereo camera for the BepiColombo European Space Agency mission to Mercury"*, App. Opt., vol. 49(15), pp. 2910-2919, 2010.

[12] F. Capaccioni, M.C. De Sanctis, G. Piccioni, E. Flamini, S. Debei and SYMBIOSYS International Team, *"VIHI: the Visible and Infrared Hyperspectral Imager channel of the SIMBIO-SYS instrument for the BepiColombo mission to Mercury"*, AAS/Division for Planetary Sciences Meeting Abstracts, vol. 37, 2005.

[13] Cremonese G., Fantinel D., Giro E., Capria M.T., Da Deppo V., Naletto G., Forlani G., Massironi M., Giacomini L., Sgavetti M., Simioni E., Bettanini C., Debei S., Zaccariotto M., Borin P., Marinangeli L., Flamini E., *"The stereo camera on the BepiColombo ESA/JAXA mission: a novel approach"*, Advances in Geosciences, 15, 305 (2009).

[14] Da Deppo V., Naletto G., Cremonese G., Calamai L., *"Optical design of the single-detector planetary stereo camera for the BepiColombo European Space Agency mission to Mercury"*, Appl. Opt. 49, pp. 2910-2919 (2010).

[15] Da Deppo V., Naletto G., Cremonese G., Calamai L., Paolinetti R., Debei S., Flamini E., *"Optical Design performance of the stereo channel for SIMBIOSYS onboard the BepiColombo ESA mission"*, Proceedings of the International Conference on Space Optics (ICSO2010), Rhodes Greece, 1981911 (2010).

[16] Seitz, S.M., Curless, B., Diebel, J., Scharstein, D., Szeliski, R., , *"A Comparison and Evaluation of Multi-View Stereo Reconstruction Algorithms,"* Computer Vision and Pattern Recognition, 2006 IEEE Computer Society Conference on , vol.1, no., pp. 519-528, 17-22 June 2006.

[17] Hartley R., Zisserman A., *"MULTIPLE VIEW GEOMETRY IN COMPUTER VISION"*, CUP, Cambridge, UK, 2003.

[18] Scharstein D., and Szeliski R., *"A taxonomy and evaluation of dense two-frame stereo correspondence algorithms"*, IJCV, 47(1):7-12, 2002.

[19] Bay, H. et al., *"SURF: Speeded Up Robust Features"*, *CVIU* 110, No. 3, pp. 346—359 (2008).

[20] Briechle K., Hanebeck U. D., *"Template matching using fast normalized cross correlation"*, Proc. SPIE 4387, Optical Pattern Recognition XII, 95, March 20, 2001.

[21] Khaleghi, B., Shahabi, S.M.A., Bidabadi, A. , *"Performace Evaluation of Similarity Metrics for Stereo Corresponce Problem"*, Electrical and Computer Engineering, 2007. CCECE 2007. Canadian Conference on , vol., no., pp.1476-1478, 22-26 April 2007

[22] Zhang Z., *"A flexible new technique for camera calibration"*, IEEE Transactions on Pattern Analysis and Machine Intelligence, 22(11):1330-1334, 2000.

[23] Harris C., Stephens M.J.. *"A combined corner and edge detector"*. In Alvey Vision Conference, pages 147–152, 1988.

[24] J. More. *"The Levenberg-Marquardt algorithm, implementation and theory"*. In G. A. Watson, editor, Numerical Analysis, Lecture Notes in Mathematics 630. Springer-Verlag, 1977.

[25] Naletto G., Cesaro M., Da Deppo V., Albasini A., Cremonese G., Forlani G., Re C., Roncella R., Salemi G., Simioni E.. *"Innovative optical setup for testing a stereo camera for space applications."*, In: Space Telescopes and Instrumentation 2012: Optical, Infrared, and Millimeter Wave. vol. 8442, p. 84421M-1-84421M-12, SPIE, 2012.

[26] Bouguet J.-Y., *"Camera Calibration Toolbox for Matlab"*, Available online, http://www.vision.caltech.edu/bouguetj/calib doc (2010)

[27] Re C., Roncella R., Forlani G., Cremonese G., Naletto G., *"Evaluation of area-based image matching applied to DTM generation with Hirise images"*, Int. Arch. Of Photogrammetry, Reomote Sensing and Spatial Information Sciences, Vol XXXIX, Part IV/7, in press.

[28] Nister D., *"An efficient solution to the five-point relative pose problem"*, IEEE T, Pattern Anal, 26(6), 756-770 (2004).

[29] Albasini A., *"Setup sperimentale per la calibrazione stereo di STC/SIMBIOSYS per la missione BepiColombo"*, bachelor degree thesis, Università degli studi di Padova, 2012.